LEVEL II

12

CALSPAN ADVANCED TECHNOLOGY CENTER

ADA096325

ADAPTIVE-WALL WIND-TUNNEL INVESTIGATIONS

J.C. Erickson, Jr., C.E. Wittliff, C. Padova and G.F. Homicz

February 1981

Calspan Report No. RK-6040-A-2

Contract No. N00014-77-C-0052
Task No. NR 061-199
FINAL TECHNICAL REPORT

DTIC

Prepared for:

OFFICE OF NAVAL RESEARCH
DEPARTMENT OF THE NAVY
ARLINGTON, VIRGINIA 22217

Approved for public release; distribution unlimited.

A DIVISION OF CALSPAN CORPORATION
ARLANDIA [illegible] BUFFALO, NEW YORK 14225

DISCLAIMER NOTICE

THIS DOCUMENT IS BEST QUALITY PRACTICABLE. THE COPY FURNISHED TO DTIC CONTAINED A SIGNIFICANT NUMBER OF PAGES WHICH DO NOT REPRODUCE LEGIBLY.

PREFACE

This is the final technical report summarizing the adaptive-wall wind-tunnel research carried out in the Aerodynamic Research Department of the Calspan Advanced Technology Center, Buffalo, NY, under Contract Number N00014-77-C-0052, Task No. NR 061-199, during the performance period from 1 November 1976 to 31 October 1980. The research was sponsored jointly by the Office of Naval Research, with Mr. Morton Cooper as technical monitor, and by the Air Force Office of Scientific Research, initially with Mr. Milton Rogers and later with Dr. James D. Wilson as technical monitors.

The late Mr. R. J. Vidal was principal investigator until May 1978 and was followed by Dr. J. C. Erickson, Jr. Dr. A. Ritter, Head of the Aerodynamic Research Department, had overall cognizance of the research. The authors of this final report are indebted to several other present and former Calspan ATC personnel who participated in various tasks of this research, namely P. A. Catlin, J. T. Curtis, D. C. Daughtry, J. Nemeth, Jr., J. P. Nenni, R. R. Phibbs and the late A. F. Gretch. The authors also wish to acknowledge the valuable contributions of Prof. W. R. Sears of the University of Arizona, who was a consultant to Calspan ATC on this research effort.

UNCLASSIFIED

SECURITY CLASSIFICATION OF THIS PAGE (When Data Entered)

(14) **REPORT DOCUMENTATION PAGE**

READ INSTRUCTIONS BEFORE COMPLETING FORM

CALSPAN-RK-6040-A-2	2. GOVT ACCESSION NO. AD-A096 325
3. RECIPIENT'S CATALOG NUMBER (9)	
4. TITLE (and Subtitle) (6) ADAPTIVE-WALL WIND-TUNNEL INVESTIGATIONS	5. TYPE OF REPORT & PERIOD COVERED Final Technical Report 1 Nov 76 - 11/01/76 to 10/31/80 31 Oct 80
	6. PERFORMING ORG. REPORT NUMBER RK-6040-A-2
7. AUTHOR(s) (10) S. G. Erickson [redacted] Jr., C. E. Wittliff [redacted] C. J. Padova [redacted] G. F. Homicz [redacted]	8. CONTRACT OR GRANT NUMBER(s) (15) N00014-77-C-0052
9. PERFORMING ORGANIZATION NAME AND ADDRESS Calspan Advanced Technology Center Aerodynamic Research Department P. O. Box 400, Buffalo, NY 14225	10. PROGRAM ELEMENT, PROJECT, TASK AREA & WORK UNIT NUMBERS NR 061-199
11. CONTROLLING OFFICE NAME AND ADDRESS Office of Naval Research Department of the Navy Arlington, Virginia 22217	12. REPORT DATE (11) FEB [redacted] 81
	13. NUMBER OF PAGES 80 (12) 82
14. MONITORING AGENCY NAME & ADDRESS (if different from Controlling Office)	15. SECURITY CLASS. (of this report) UNCLASSIFIED
	15a. DECLASSIFICATION/DOWNGRADING SCHEDULE

16. DISTRIBUTION STATEMENT (of this Report)

Approved for public release; distribution unlimited.

17. DISTRIBUTION STATEMENT (of the abstract entered in Block 20, if different from Report)

18. SUPPLEMENTARY NOTES

19. KEY WORDS (Continue on reverse side if necessary and identify by block number)

Wind Tunnels, Transonic Flow, Transonic Testing, Wind Tunnel Wall Interference, Adaptive-Wall Wind Tunnels, NACA 0012 Airfoil Section Data, Static-Pipe Measurement Techniques.

20. ABSTRACT (Continue on reverse side if necessary and identify by block number)

The results of a program of research on transonic wind tunnels with adaptive walls for eliminating wall interference are presented. A description is given of related experimental research performed at other laboratories using several alternative methods for controlling the flow. Features of the segmented-plenum, perforated-wall, two-dimensional test section of the Calspan One-Foot Tunnel and the associated instrumentation for measuring the flow disturbance quantities are reviewed and necessary modifications

(Continued on Reverse Side)

DD FORM 1 JAN 73 1473 EDITION OF 1 NOV 65 IS OBSOLETE

UNCLASSIFIED

SECURITY CLASSIFICATION OF THIS PAGE (When Data Entered)

410802

20. (Cont'd.)

made to the original experimental configuration are described. Details of adaptive-wall iteration experiments with a 4%-blockage NACA 0012 airfoil model are presented, particularly those at a free-stream Mach number of 0.9 and nominal angles of attack of 3°, 2° and 1°. In these experiments, regions of supercritical flow terminated by shock waves extended to the tunnel walls. The results of the experiments indicate that successful iterations toward interference-free flow conditions are achieved. For another phase of the research, conceptual design studies of a three-dimensional transonic adaptive-wall test section using the segmented-plenum, perforated-wall method of flow control are reported. Finally, numerical simulations of low-speed flow within the Calspan test section, including the interaction of the transpired boundary layer at the walls with the flow over the model, are described in AIAA Paper No. 81-0160, which is appended to the report.

TABLE OF CONTENTS

LIST OF FIGURES

LIST OF FIGURES (Cont'd.)

NOMENCLATURE

C_p	pressure coefficient on airfoil surface, $(p-p_\infty)/q_\infty$
c	airfoil chord
h	distance from tunnel centerline to control surface
M	Mach number
p	static pressure
q	dynamic pressure
Re_c	Reynolds number based on chord length, c
U_∞	free-stream velocity
u, v	perturbation velocity components in streamwise, normal directions, respectively
u[v], v[u]	u and v found from the exterior-flow functional-relationship evaluations, using v and u, respectively, as boundary conditions
x	streamwise coordinate with origin at the junction between plenum chambers 6 and 7, and 16 and 17, see Fig. 1
α	angle of attack
β	$\sqrt{1-M^2}$

Subscript

∞	free-stream conditions

Section 1
INTRODUCTION

The severity of transonic wind-tunnel wall interference and the inability of conventional procedures to correct the data because of the inherent nonlinearity of the flow again raised concern about ten years ago. At that time, there was a renewed importance attached to achievement of reliable experimental data on flight vehicle configurations, especially in transonic flow. Recognition of the deficiencies of existing techniques and procedures led Ferri and Baronti[1] and Sears[2], independently, to propose the concept of an adaptive-wall wind tunnel in which interference could be reduced greatly at least, if not eliminated for practical purposes.

The reduction of interference in an adaptive-wall wind tunnel is achieved by controlling the flow field in the vicinity of the tunnel walls. Measurement is made of the components of the disturbance velocity at discrete points along imaginary control surfaces, or interfaces, in the flow field within the tunnel. A theoretical representation for the flow field external to the control surfaces, including the boundary condition for unconfined flow, i.e., that all disturbances vanish at infinity, is used to determine if those measured velocity components satisfy functional relationships which are consistent with interference-free flow. If they do not, an iteration procedure provides a new approximation for the flow field at the interfaces, and the flow control in the vicinity of the walls is readjusted successively until the measured quantities are consistent with the boundary condition for unconfined flow. In this way, theory and experiment are combined to minimize wall interference. The concept of an adaptive wall-tunnel is discussed more completely in References 2 to 5.

A program of research has been in progress at Calspan since 1971 to develop and demonstrate the feasibility of the adaptive-wall concept. The concept was demonstrated theoretically in 1973 and 1974 by iterating idealized

---

[1] Ferri, A. and Baronti, P. "A Method for Transonic Wind Tunnel Corrections" AIAA Journal, Vol. 11, No. 1, pp. 63-66, January 1973.

[2] Sears, W.R. "Self-Correcting Wind Tunnels" (The Sixteenth Lanchester Memorial Lecture) Calspan Report No. RK-5070-A-2, July 1973; also the Aeronautical Journal, Vol. 78, No. 758/759, pp. 80-89, February/March 1974.

numerical simulations of the flow in two-dimensional adaptive-wall tunnels for incompressible[3] and transonic, supercritical-wall conditions[4]. Also in 1973, a two-dimensional adaptive-wall, transonic test section was designed, fabricated and installed in the circuit of the Calspan One-Foot Tunnel. The test section, which is described more fully in Section 3 and in Refs. 4 and 5, consists of perforated upper and lower walls with segmented plenum chambers. Each plenum has an individual pressure control to provide either suction or blowing. A model with an NACA 0012 airfoil section and a 6-inch chord was fabricated and tested[4,6] in the Calspan Eight-Foot Transonic Wind Tunnel to establish the airfoil characteristics in unconfined flow at a Reynolds number, Re_c, of 1.00×10^6 based on chord length, c. Aerodynamic data were obtained at free-stream Mach numbers, M , from 0.40 to 0.95 and angles-of-attack, , from -2° to 8°.

An experimental program[4,5] was carried out during 1974 and 1975 in the One-Foot Tunnel for flows which were supercritical at the model, but subcritical at the control surfaces and walls, i.e. for M 0.725. Initial experiments with the tunnel operated so as to simulate conventional perforated-wall tunnel operation displayed[4] significant wall interference for these free-stream conditions, since the solid blockage of the 6-inch chord model is 6%. Iteration at several flow conditions in this regime of operation indicated[4,5] satisfactory convergence to unconfined flow and elimination of the wall interference.

---

3 Erickson, J.C., Jr. and Nenni, J.P. "A Numerical Demonstration of the Establishment of Unconfined-Flow Conditions in a Self-Correcting Wind Tunnel" Calspan Report RK-5070-A-1, November 1973.

4 Vidal, R.J., Erickson, J.C., Jr. and Catlin, P.A. "Experiments with a Self-Correcting Wind Tunnel" AGARD-CP-174, October 1975; also Calspan Report No. RK-5070-A-4, October 1975.

5 Sears, W.R., Vidal, R.J., Erickson, J.C., Jr. and Ritter, A. "Interference-Free Wind-Tunnel Flows by Adaptive-Wall Technology" ICAS Paper No. 76-02, 10th Congress of the International Council of the Aeronautical Sciences, Ottawa, Canada, 3-8 October 1976; also Journal of Aircraft, Vol. 14, No. 11, pp. 1042-1050, November 1977.

6 Vidal, R.J., Catlin, P.A. and Chudyk, D.W. "Two-Dimensional Subsonic Experiments with an NACA 0012 Airfoil" Calspan Report No. RK-5070-A-3, December 1973.

The success achieved at these subcritical-wall conditions led to extension of the research effort to encompass tunnel operating conditions at higher Mach numbers for which shock waves generated by the model reach the control surfaces and walls. Moreover, consideration was given to a perforated-wall, segmented-plenum implementation of the adaptive-wall concept in three dimensions. This report summarizes the research performed to meet these objectives with joint sponsorship by the Office of Naval Research (ONR) and the Air Force Office of Scientific Research (AFOSR).

There have been three principal tasks in the investigation. First, experimental research was carried out in the two-dimensional test section of the One-Foot Tunnel. During 1976 and 1977, this task complemented and supplemented[7] the experiments performed[8] with sponsorship by the Arnold Engineering Development Center (AEDC). During 1980, additional experiments were carried out as a continuation of research accomplished[9] during 1978 and 1979 with further AEDC sponsorship. The second task, performed during 1978 and 1979, was the development of more realistic numerical simulations of an airfoil in a two-dimensional adaptive-wall test section, including the influence of tunnel-wall boundary layers. The third task was a preliminary investigation of the design requirements for three-dimensional adaptive-wall test sections, with particular attention given to the adaptability of the Calspan One-Foot Tunnel to meet these requirements. This task was performed during 1978 and 1979.

---

7 Vidal, R.J. and Erickson, J.C., Jr. "Experiments on Supercritical Flows in a Self-Correcting Wind Tunnel" AIAA Paper No. 78-788, AIAA 10th Aerodynamic Testing Conference, San Diego, California, 19-21 April 1978.

8 Vidal, R.J. and Erickson, J.C., Jr. "Research on Adaptive-Wall Wind Tunnels" AEDC Report No. AEDC-TR-78-36, November 1978.

9 Erickson, J.C., Jr., Wittliff, C.E. and Daughtry, D.C. "Further Investigations of Adaptive-Wall Wind Tunnels" AEDC Report No. AEDC-TR-80-34, October 1980.

For completeness and to place in perspective the progress on adaptive-wall wind tunnels, a brief survey of adaptive-wall experiments at other laboratories is given in Section 2. The adaptive-wall test section and airfoil models for the Calspan One-Foot Tunnel, including modifications that were made during the present investigation, are described in Section 3. Also described in this Section is the development of instrumentation and calibration techniques for measuring the streamwise disturbance velocity component, u , and the normal component, v. In Section 4, results of experimental iterations toward interference-free flow conditions with a 4%-blockage NACA 0012 airfoil model are presented for supercritical flow conditions at the walls. These experiments, which were performed during 1980 at $M_\infty = 0.9$ and $\alpha = 3°$, $2°$ and $1°$, have achieved reasonable success and have extended the applicability of the adaptive-wall concept to more severe transonic conditions than had been accomplished previously.

Appendix I contains a list of papers, reports and presentations that were prepared during this investigation. Appendix II contains a summary of the Calspan Design studies for a three-dimensional adaptive-wall test section. Finally, a copy is attached of AIAA Paper No. 81-0160 entitled, Numerical Simulations of a Segmented-Plenum, Perforated, Adaptive-Wall Wind Tunnel. This paper by J.C. Erickson, Jr. and G.F. Homicz was presented at the AIAA 19th Aerospace Sciences Meeting in St Louis on 12-15 January 1981, and describes the results of the work on the second task.

Section 2

SURVEY OF ADAPTIVE-WALL EXPERIMENTAL RESEARCH

There have been several different approaches to practical wall-control methods for adaptive-wall wind tunnels. To date, with exceptions to be noted, the experimental research has been carried out in two-dimensional flows. Two fundamentally different wall-control methods have been pursued, namely changing the shape of impermeable, flexible walls and using ventilated walls, either perforated or slotted, with segmented plenum chambers and/or porosity control. In this section, a brief survey is given of the experimental results that have been achieved elsewhere. There will be no discussion here of any theoretical efforts in support of the concept.

Impermeable, flexible-wall tunnels have been developed by three European groups, namely thosed led by Chevallier at ONERA/Chalais, Goodyer at the University of Southampton, and Ganzer at the Technical University of Berlin. In all of these implementations, the wall positions, with corrections for boundary-layer displacement, are used to determine the velocity component, v , normal to each control surface (the wall in this case) and static pressure measurements along the walls are used to determine the streamwise component, u .

Chevallier[10] achieved successful iteration to unconfined flow in 1975 with a 4.4%-blockage NACA 64A010 model for M_∞ up to 0.85. This tunnel configuration and associated techniques have been adapted[11] in a two-dimensional test section of 0.4 m x 0.4 m for the T2 Transonic Tunnel at ONERA/CERT at Toulouse.

---

10 Chevallier, J.P. "Soufflerie Transsonique a Parois-Adaptables" AGARD-CP-174, October 1975; also translated into English as European Space Agency Report ESA-TT-326, October 1976, available as NASA Accession No. N77-13085.

11 Poisson-Quinton, P. "Some New Approaches for Wind-Tunnel Testing Through the Use of Computers" AIAA Paper No. 79-0707, First Intersociety Atlantic Aeronautical Conference, Williamsburg, Virginia, 26-28 March 1979; also ONERA TP No. 1979-24.

Goodyer, et al. have obtained similar success, initially at low speeds[12] in 1975, and then at transonic speeds[13] in 1980. In these latter experiments, unconfined-flow conditions were achieved at $M_\infty = 0.89$ and $\alpha = 4°$ with an 8%-blockage NACA 0012-64 model. However, it should be noted that although shock waves extend to the walls, the exterior-flow calculation was based on subcritical-flow theory. Goodyer's configuration and techniques are being implemented[14] in a two-dimensional test section of 0.33 m x 0.33 m in the 0.3 m Transonic Cryogenic Tunnel at the NASA Langley Research Center.

Ganzer [15,16] achieved fully-automated iterative control of the walls for 8%-blockage models of NACA 0012 and supercritical CAST 7 airfoils up to $M_\infty = 0.82$ during 1979 and 1980. Again, subcritical exterior-flow calculations were performed. Ganzer also has carried out[16] preliminary experiments in the two-dimensional tunnel with a three-dimensional model, and the other groups plan[11,13] to do so as well. The objective in these experiments is to achieve partial control and then to use the measured wall pressures to compute residual corrections along the lines first

---

12 Goodyer, M.J. "A Low-Speed Self Streamlining Wind Tunnel" AGARD-CP-174, October 1975.

13 Goodyer, M.J. and Wolf, S.W.D. "The Development of a Self-Streamlining Flexible Walled Transonic Test Section" AIAA Paper No. 80-0440, AIAA 11th Aerodynamic Testing Conference, Colorado Springs, Colorado, 18-20 March 1980.

14 Ladson, C.L. "A New Airfoil Research Capability" in Advanced Technology Airfoil Research, Vol. 1, NASA CP-2045, Part 1, March 1979.

15 Ganzer, U. "Windkanale mit Adaptiven Wanden zur Beseitigung von Wandinterferenzen" Zeitschrift fur Flugwissenschaften und Weltraumforschung, Vol. 3, No. 2, pp. 129-133, 1979; also translated into English as NASA TM-75501, August 1979.

16 Ganzer, U. "Adaptable Wind Tunnel Walls for 2-D and 3-D Model Tests" ICAS Paper No. 23-3, 12th Congress of the International Council of the Aeronautical Sciences, Munich, Germany, 12-17 October 1980.

proposed by Kemp[17,18] and later treated by Capelier, et al.[19] and Murman[20]. Ganzer also describes[16] plans for building a three-dimensional flexible-wall test section.

Emphasis in the United States, namely at AEDC and NASA Ames Research Center besides Calspan, has been on ventilated adaptive-wall configurations. Also, although the complete adaptive-wall procedures were not used, Weeks[21] accomplished some wall control at the Air Force Flight Dynamics Laboratory in 1975 by slotted walls with contoured slots.

AEDC results,[22] published in 1979, describe experiments with two different wall configurations in the Aerodynamic Wind Tunnel (1T) up to M_∞ = 0.80 for an NACA 0012 model with 6%-blockage. One wall configuration has provisions for varying the hole angle of a perforated wall as a function of the streamwise direction by means of multiple rows of bored spheres connected by rods normal to the streamwise direction. The other wall configuration has variable-porosity walls formed by matched sliding plates that have inclined holes like those in the AEDC Aerodynamic Wind Tunnel (4T). These walls can be adjusted globally to give a porosity that is uniform on each wall, but may differ between the top and bottom walls. In each implementation, the top and bottom walls were both vented to a single plenum chamber, the pressure of which

---

17 Kemp, W.B., Jr. "Toward the Correctable-Interference Transonic Wind Tunnel" AIAA Paper No. 76-1794, AIAA 9th Aerodynamic Testing Conference, Arlington, Texas, 7-9 June 1976.

18 Kemp, W.B., Jr. "TWINTAN: A Program for Transonic Wall Interference Assessment in Two-Dimensional Wind Tunnels" NASA TM-81819, May 1980.

19 Capelier, C., Chevallier, J-P. and Bouniol, F. "A New Method for Correcting Wall Interference" La Recherche Aerospatiale, 1978, No. 1, January-February 1978, pp. 1-11; also translated into English as European Space Agency Report ESA-TT-491, August 1978, available as NASA Accession No. N79-11997.

20 Murman, E.M. "A Correction Method for Transonic Wind Tunnel Wall Interference" AIAA Paper No. 79-1533, AIAA 12th Fluid and Plasma Dynamics Conference, Williamsburg, Virginia, 24-26 July 1979.

21 Weeks, T.M. "Reduction of Transonic Slotted-Wall Interference by Means of Slat Contouring: Air Force AFFDL-TR-74-139, March 1975.

22 Kraft, E.M. and Parker, R.L., Jr. "Experiments for the Reduction of Wind Tunnel Wall Interferenced by Adaptive-Wall Technology" AEDC Report No. AEDC-TR-79-51, October 1979.

was adjustable in magnitude. In both experiments, u was measured by static pipes and v by aerodynamic probes. Both subsonic and transonic small-disturbance theory were used, as appropriate, to evaluate the functional relationships for unconfined flow. Sufficient control existed with both wall configurations to reduce the interference significantly, but complete iterations to unconfined flow were not achieved.

AEDC, in a paper published in 1980, also obtained significant reductions[23] in interference in three-dimensional flows for a wing/fuselage/horizontal-tail configuration in Aerodynamic Wind Tunnel (4T). In these experiments, global porosity variation on the top, bottom and side walls was used as with the two-dimensional variable-porosity walls, again with constant plenum pressure. A single translating probe was used to measure both u and v at a control surface of rectangular cross section that surrounded the model.

The NASA Ames Research Center adaptive-wall test section[24] has slotted top and bottom walls with ten independently-controlled plenum chambers behind each wall. Laser velocimetry is used to measure v at two different distances from the model and the corresponding functional-relationship evalutions were carried out by subsonic theory. Measured influence functions based on plenum pressure adjustment were used to determine control adjustments. Successful iteration to unconfined flow was reported in 1980 up to about $M_\infty = 0.8$ for an NACA 0012 airfoil model with 7%-blockage. The use of this two-dimensional tunnel for examining fully three-dimensional flows in the manner of the European experiments also has been suggested[24].

---

23 Parker, R.L., Jr. and Sickles, W.L. "Application of Adaptive Wall Techniques in a Three-Dimensional Wind Tunnel with Variable Wall Porosity" AIAA Paper No. 80-0157, AIAA 18th Aerospace Sciences Meeting, Pasadena, California, 14-16 January 1980.

24 Bodapati, S., Schairer, E. and Davis, S. "Adaptive-Wall Wind-Tunnel Development for Transonic Testing" AIAA Paper No. 80-0441, AIAA 11th Aerodynamic Testing Conference, Colorado Springs, Colorado, 18-20 March 1980.

Section 3

EXPERIMENTAL FACILITY AND INSTRUMENTATION

3.1 Test Section and Airfoil Models

The Calspan One-Foot Tunnel[4,5], shown schematically in Figure 1, is a closed-circuit, continuous flow facility. The two-dimensional adaptive-wall test section is 12-inches high, 10-inches wide and 56-inches long with perforated top and bottom walls of 22.5% open-area ratio. The plenum chambers behind the perforated walls have been divided into 18 segments, 10 on the top and 8 on the bottom, and each segment is connected to a pressure and a suction source through individual control valves. The pressure source is the tunnel stilling chamber, and the suction source is an auxiliary compressor discharging into the tunnel circuit in the diffuser. Six plenum chambers in the immediate vicinity of the model have provisions for a distributed porosity which can be varied linearly in the streamwise direction. This capability was not exercised in these experiments and a constant open-area ratio was used.

As mentioned in the Introduction, a model with an NACA 0012 airfoil section and a 6-inch chord (6% blockage in the One-Foot Tunnel) was fabricated and tested[4,6] in the Calspan Eight-Foot Transonic Wind Tunnel. This model is instrumented with a row of pressure orifices on both the upper and lower surfaces, and with a three-component force balance supporting a metric section on the tunnel centerline. An initial series of experiments with this airfoil model at higher Mach numbers had shown[7,8] that the available wall control was limited so that successful iteration to unconfined flow could not be achieved. This recurring inability to achieve full control of the flow field at all plenum sections led to an analysis of the flow in the auxiliary suction system and the test section[7,8].

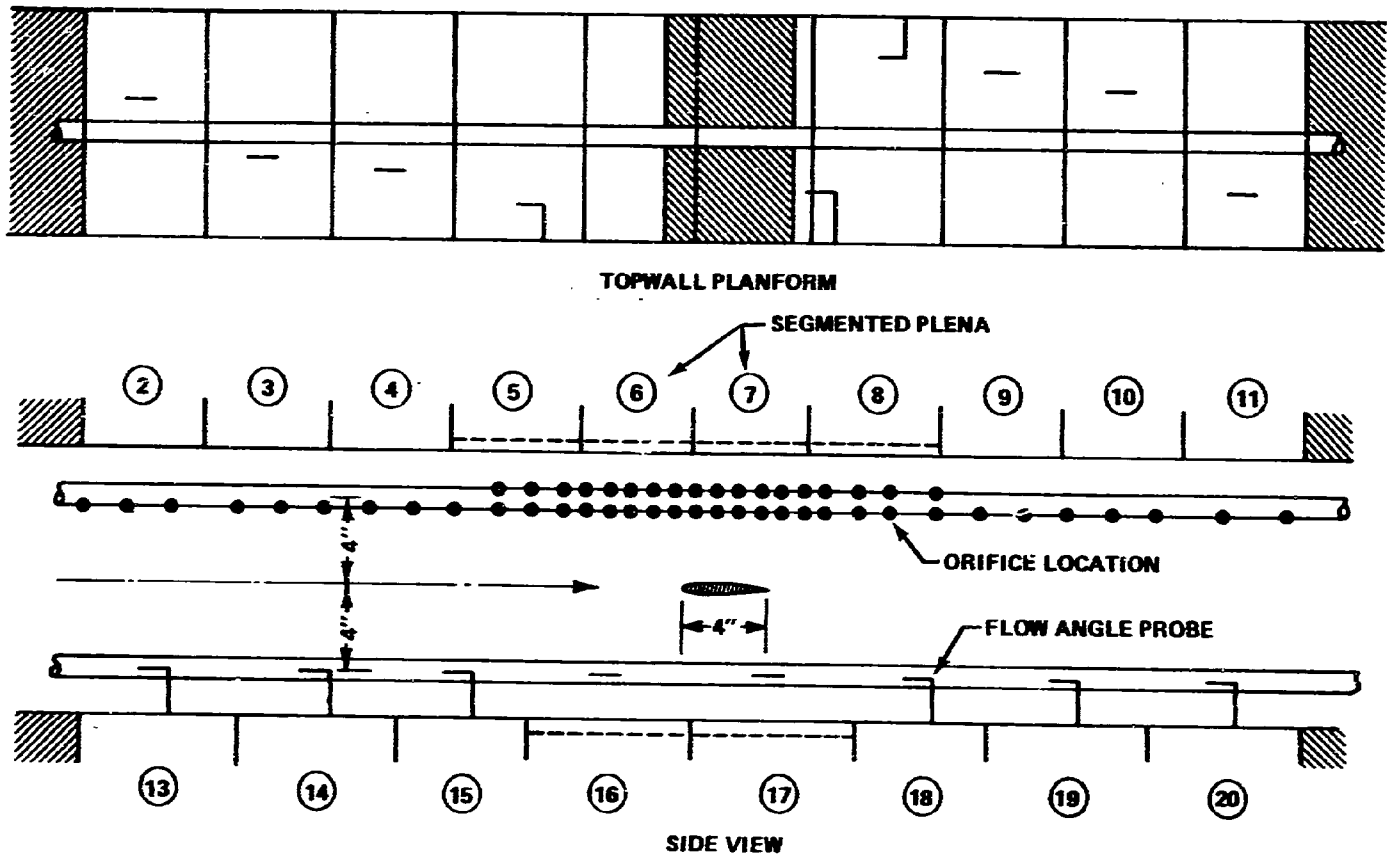

Figure 1 SCHEMATIC OF CALSPAN ONE-FOOT ADAPTIVE-WALL TUNNEL

Basically, the analysis consists of writing a pressure balance for the auxiliary suction system. The analysis includes the operating characteristics of the auxiliary compressor, the losses in the pipes, the recompression pressure loss arising from the compressor discharge into the diffuser, the pressure drop across the perforated walls, and the required unconfined-flow pressure at the wall locations due to the model. When suitable engineering approximations for these pressure terms were made, using, in part, data measured in the One-Foot Tunnel, the predicted limits on available control agreed reasonably well with experimental observations. One conclusion from this analysis was that the recompression penalty could be reduced considerably. This was accomplished by introducing an area change in the tunnel diffuser at the location where the flow from the auxiliary blower is vented into the tunnel circuit.

The analysis also illustrates the three major trade-offs available in the design and application of adaptive-wall test sections of this configuration; namely compression ratio, wall open-area ratio and model size. Tunnel performance could be improved by increasing the compression ratio, but the improvement would be available only at Mach numbers above about 0.75, because the wall perforations would be choked at Mach numbers below that value. That restriction could be relaxed considerably by using a larger open-area ratio, although the shock-wave reflection characteristics might not be as favorable. Decreasing the model size from 6% blockage to a smaller value would decrease the magnitude of the disturbance velocities at the walls and would improve the tunnel performance. Consequently, an NACA 0012 airfoil model with a 4-inch chord (4% solid blockage) was constructed. It has a row of pressure orifices along its centerline on the upper and lower surfaces, but there are no provisions for measuring the forces and pitching moment directly. This model was used in the experiments to be described below.

3.2 Initial Flow-Velocity Measurement Techniques

In the experiments prior to those of Ref. 9, local flow angle was measured by aerodynamic probes and the local static pressure by static pipes. These measurements were used, respectively, to determine v and u. The static pipes,[4,5] each with 52 static orifices along its length, were located with their centerlines nominally 4.0-inches above and below the tunnel centerline and had a 0.5-inch diameter. Eighteen flow-angle probes[4,5] were mounted nominally 4.5-inches above and below the centerline with each one opposite the center of a plenum chamber. Blockage and probe wake considerations limited the number of probes to this quantity, which made it difficult to obtain sufficient measurements to define adequately the v distributions in the vicinity of the model.

Operational procedures required that the distributions of the measured normal velocity component v be used as the boundary conditions on the external-flow calculations to provide the next approximation to u. It was difficult to carry out conventional interpolation procedures accurately based on the limited number of v measurements available. Fortunately, however, sufficient numbers of u measurements were available to provide a good definition of their distributions. Based on this situation, a procedure was devised to provide a better interpolation in the v data.

The first step in this interpolation procedure was to use the extensive u data, as interpolated by a cubic spline (smoothed or not, as desired), to calculate the corresponding unconfined-flow distribution $v[u]$. This calculation used a finite-difference solution of the transonic small-disturbance equations[8]. Next, the difference $v - v[u]$ was determined at each x location where v measurements were made. These differences were then interpolated linearly in x, so that the resultant interpolation in v was found by adding the interpolated difference, $v - v[u]$, to the calculated $v[u]$ distribution. Once the v interpolation had been found, the exterior-flow calculation of $u[v]$ was carried out to give the next approximation to u which was set in the tunnel. Again, transonic small-disturbance solutions were used.

This procedure thus used the shape of the v[u] distribution as a basis for interpolation since the distribution was well-defined experimentally. Clearly, as convergence of the tunnel iteration was approached, the differences v - v[u] approached zero and the interpolation improved. Limited use of this procedure in the experiments of Ref. 8 and a few subsequent ones indeed showed an improvement in the interpolation. However, questions still existed about the actual behavior of v between measuring points. Moreover, the probes have limited the research in other ways. The small probes used are very sensitive to contamination from oil present in the tunnel air stream and must be cleaned frequently. This cleaning can disturb them and render their calibrations for zero flow angle suspect, and thus require frequent re-calibration. Therefore, an alternative technique was sought.

3.3 Revised Flow-Velocity Measurement Techniques

The alternative technique selected for measuring v involves measuring the static pressures at one control surface and the difference between those pressures and the pressures at a second surface slightly farther away from the model. In effect, this can be regarded as measuring the local static pressure and its gradient, from which the streamwise derivative of the normal velocity, dv/dx, can be inferred. The advantage in this measurement technique is that static pressure is easy to measure with good precision and one can easily obtain good spatial resolution. The TSFOIL computer code[25] was used to calculate preliminary estimates of the pressure differences to be expected, and these differences are readily measurable in the immediate vicinity of the airfoil.

Development of a new static-pipe technique to achieve this was performed with AEDC sponsorship and is described in Ref. 9. Briefly, the new pipes, of 0.625-inch diameter, have diametrically opposed orifices on

---

[25] Murman, E.M., Bailey, F.R. and Johnson, M.L. "TSFOIL-A Computer Code for Two-Dimensional Transonic Calculations, Including Wind-Tunnel Wall Effects and Wave-Drag Evaluation" Paper No. 26 in Aerodynamic Analyses Requiring Advanced Computers, NASA-SP-347-Part 2, March 1975.

their top and bottom in the vicinity of the model. There are 18 pairs of these orifices extending 9 inches upstream and 11 inches downstream of the junction between plenum chambers 6 and 7, as shown in Figure 1. These dual orifices span the region where the static pressure differences are equal to, or greater than, the resolution capability of the pressure transducers being used. Upstream and downstream of this region, the static pipes have orifices which extend the full length of the test section along the side of the pipe facing the model. The most forward static pressure orifice on each pipe (which is located at the beginning of the test section) is connected to a manifold and the reading is taken to be the free-stream static pressure, p_{∞}. All remaining 33 pressures on the model sides of the pipes are measured relative to p_{∞}. In addition, the differential pressures between the 18 opposing pairs of orifices on each pipe are measured. The differential pressure transducers used have a probable error of 0.001 psi or less, and the read-out system has a resolution of 0.001 psi.

After fabrication, the new static pipes were mounted with their centerlines nominally 4.0 inches from the test-section centerline, as the original pipes were. However, in order to use the probe flow-angle data in conjunction with the differential pressure data, the probes were relocated to the plane of the static pipe centerlines from their original locations 4.5 inches from the test-section centerline. In the original configuration, four of the probes in the vicinity of the model were mounted through the test-section windows and their frames. It was not feasible to relocate or remove these probes, so they were retracted to lie against the side walls. However, two new flow-angle probes were fabricated and mounted in the vicinity of the model. The resulting locations of the flow-angle probes at the lower control surface are shown in the side view of Figure 1, while the upper probes are shown in the top planform view. The lateral staggering of the probes was chosen to avoid interference effects.

The flow about static pipes in the presence of model/wall-induced disturbances was analyzed[9] within the framework of conventional slender-body theory for subcritical, compressible flow and the theory of matched asymptotic expansions. This analysis relates the average of the pressure measurements across the pipe to u at the pipe centerline. In addition, the analysis relates the differential pressure measurements across the pipe to the streamwise derivative of the v at the pipe centerline. The derivative, dv/dx, can be integrated to obtain the distribution of v if at least one independent measurement of v is made. Based on experiences[9] with supercritical flows in which the shock wave from the model intersects the pipe, separate integrations of dv/dx are carried out upstream and downstream of the shock, thus requiring independent v measurements in each region.

As mentioned previously, it is necessary to calibrate the probes in the tunnel periodically to determine their apparent flow-angle readings for uniform flow parallel to the tunnel centerline. The procedure for this part of the overall probe calibration technique is to use the wall control to set a uniform static pressure along the entire length of both static pipes. The flow is assumed to be parallel to the tunnel centerline and the probe readings are taken to be those for zero flow inclination. An efficient independent measurement technique to assure that the flow is parallel to the centerline is not available. However, the procedure just described was verified independently early during this research effort by obtaining corresponding probe measurements in the test section after conversion to solid walls by the application of tape to the top and bottom walls.

While reviewing the empty-tunnel runs performed as part of the experiments in Ref. 9, however, it was observed that although the uniformity of the flow was comparable to that measured in earlier experiments, plenum pressure control valve settings to achieve uniform flow were quite different. In particular, at $M_{cn} = 0.8$ and 0.9, the first three upper plenum chambers were providing near-meximum suction, while the first two lower plenum

chambers were providing slight blowing. Therefore, it is suspected that the flow was inclined upwards at a constant angle along the length of the test section. This would cause probe calibration errors and could lead to observation of an apparent negative cross-flow bias in the experiments. Unfortunately, a uniform flow inclination along the length of the test section would not be apparent in the measurements of differential pressures across the static pipe since those measurements detect dv/dx, rather than v itself.

Accordingly, in the most recent empty-tunnel runs at $M_\infty = 0.8$, 0.9 and 0.94, extreme care has been taken to insure that the upper and lower valves were set to provide comparable amounts of suction at the upper and lower walls. The asymmetry of the test section, namely ten upper plenum chambers and eight lower ones, complicates the adjustment of comparable amounts of suction. However, it has been observed (see Fig. 6 of Ref. 9) that relatively large variations in pipe static pressure measurements occur near the upstream and downstream ends of the test section. Thus, by relaxing the requirements at the upstream end during the early stages of the adjustment process, uniform pressure could be set over most of the test section length with balanced amounts of suction. Further adjustments then could be made upstream and downstream to achieve uniform flow. The final valve settings do indicate that comparable suction is being applied at the upper and lower walls. The data obtained in this fashion provided revised probe calibrations for zero flow inclination and were incorporated into the data reduction procedure.

In the AEDC-sponsored experiments[9], the differential pressure measurements in uniform, parallel flow indicated an apparent gradient in normal velocity at the upper pipe for all Mach numbers tested. It was concluded that this gradient is an artifact of the pipe construction and installation. Accordingly, it was eliminated by treating the empty-tunnel gradient as a tare reading. In the most recent experiments, a slight revision of the empty-tunnel gradient tare was made for the upper pipe, and a small tare for the lower pipe was introduced as well.

Section 4

EXPERIMENTS WITH SUPERCRITICAL FLOW AT THE WALLS

4.1 Background

The major part of this investigation has been directed at flows which are supercritical at the control surfaces and walls. Experiments were performed which had the objective of demonstrating the segmented-plenum, perforated-wall implementation of the adaptive-wall tunnel concept for these practically important flow conditions. In the previous section, changes in the test section, auxiliary suction system, airfoil model and the instrumentation have been described. All of these were accomplished in order to provide the capability for completing these experiments successfully. Before summarizing briefly the early supercritical-wall experiments[7-9] and describing in detail the most recent experiments at $M_\infty = 0.9$, the rationale for the choice of supercritical-wall cases will be described.

The lift data for the 6-inch chord NACA 0012 airfoil, as tested[6] in the Calspan Eight-Foot Tunnel at a chord Reynolds number, Re_c, of 1.00×10^6, showed unusual characteristics at $M_\infty = 0.85$ and 0.9, see Fig. 2. In particular, the lift-curve slope is very small at small α and then has a gradual break between $\alpha = 2°$ and 3° to a larger slope. This behavior was not observed at $M_\infty = 0.8$ and below (see Fig. 5 of Ref. 6), or at $M_\infty = 0.925$ or 0.95, as shown in Fig. 2. The airfoil surface pressure data for these cases[6,8] show that both the upper and lower airfoil surfaces are supercritical over a fraction of the chord length. It might be expected that the shock-wave formations on the upper and lower surfaces would be sensitive to wall-interference effects, so these test conditions promised to be realistic tests of the Calspan adaptive-wall implementation. Accordingly, operation at $M_\infty = 0.85$ and 0.9 was originally selected for the supercritical-wall experiments.

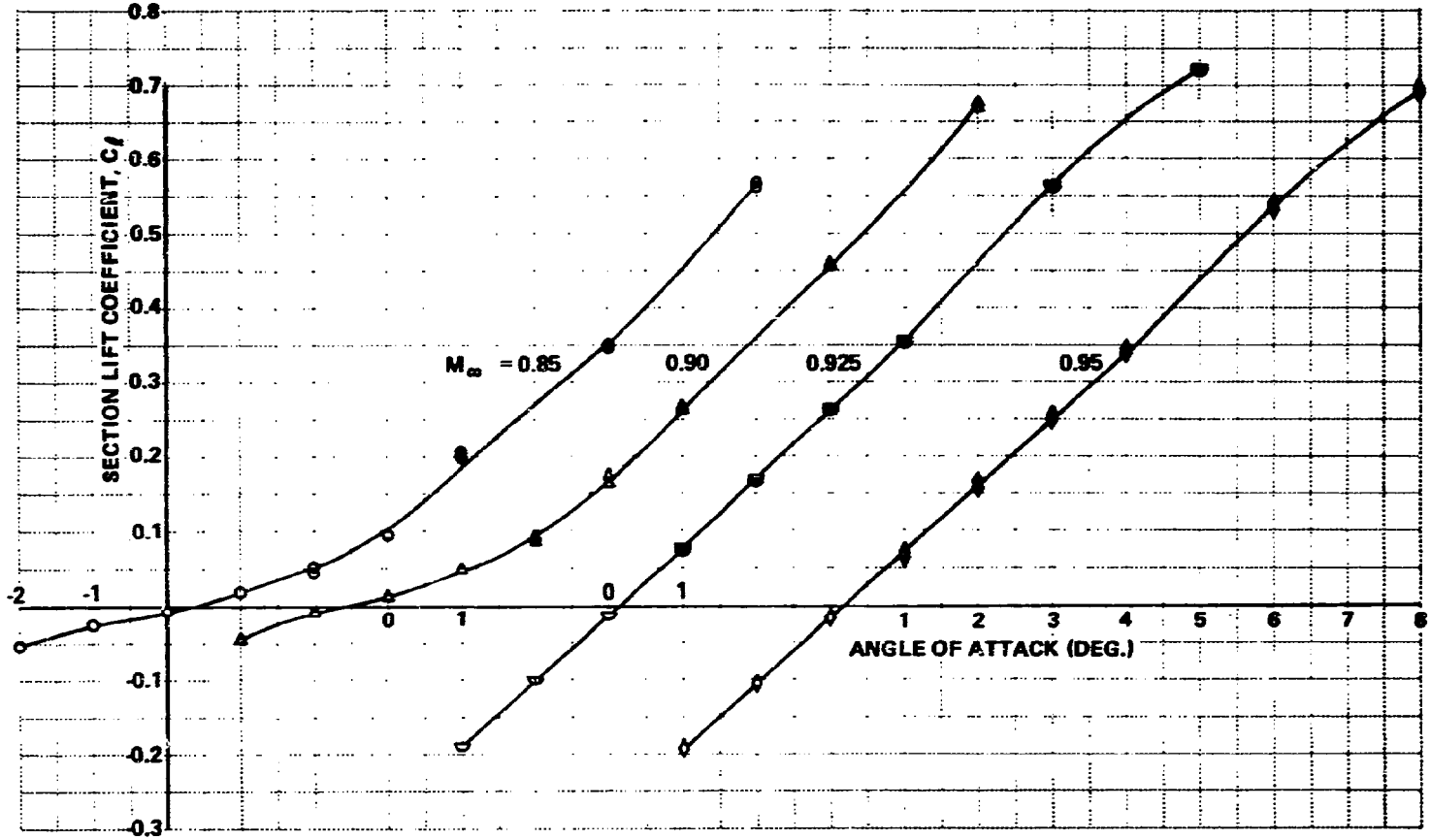

Figure 2 SECTION LIFT COEFFICIENT FOR A 6-INCH CHORD, NACA0012 AIRFOIL, $Re_c = 1.00 \times 10^6$, EIGHT-FOOT TUNNEL DATA

Later, while conducting supercritical-wall tests at $M_\infty = 0.9$, difficulties encountered in the iteration process prompted the reconsideration of the Eight-Foot Tunnel data. A close examination of the Eight-Foot Tunnel data at $M_\infty = 0.85$ and 0.9 for low α indicates considerable scatter. This apparently results from relatively large changes in the shock-wave locations on the airfoil due to small changes in α. Furthermore, the data in Fig. 2 and in Fig. 5 of Ref. 6 show that there was a small positive flow angularity in the Eight Foot Tunnel for all M_∞ except 0.9, where it was -0.62°. The intercept at $M_\infty = 0.9$ is suspect, however, because of the aforementioned scatter in the data. This intercept has been used in the experiments presented here, but the uncertainties associated with the Eight-Foot Tunnel data in this Mach number range might have unduly contributed to the difficulties encountered in providing definitive verification of interference-free flow. In principle, these uncertainties could be removed by operating at a higher Mach number. In these studies, however, this was prevented by the limitations in the One-Foot Tunnel capabilities.

One final aspect of the data concerns the Reynolds number. In the experiments with the 4%-blockage model in the One-Foot Tunnel, Re_c is limited to 0.67×10^6. This limitation arises because the tunnel cannot be run continuously at conditions which provide for $Re_c = 1.00 \times 10^6$ with the smaller model. Both these values are in a range where significant differences in the detailed and integrated flow characteristics can be expected as a function of Re_c. Therefore, a question remains about the pressure distributions, including shock-wave locations, that are to be expected in interference-free flow about the 4%-blockage model.

4.2 Initial Supercritical Wall Experiments

The first supercritical-wall experiments with the 4%-blockage NACA 0012 model were carried out[8] at $M_\infty = 0.85$ and $\alpha = 1°$. This case is in the range where the lift-curve slope is very small, see Fig. 2. These experiments were inconclusive because of flow-field unsteadiness. Wall control was used to obtain a first iterative step toward unconfined flow, but the shock wave on the lower surface fluctuated over about 15% of the chord. Subsequent attempts to iterate at this test condition did not

lead to a steady flow field, and it was concluded that this test condition was not suitable for iteration at this stage of the tunnel development.

Next, experiments were performed with the 4%-blockage model at $M_\infty = 0.8$ and $\alpha = 4°$, for which there is no shock wave on the lower airfoil surface and the upper shock extends almost to the static pipe. It was felt that this case should be a less severe test of the tunnel and could provide a basis for proceeding to higher M_∞. The iteration in this case exhibited steady flow at each step and convergence was approached as shown by comparisons between the measured data and evaluations of the functional relationships after three iterative steps. After the third step, the relationships were in good agreement with the worst discrepancies occurring in u at the lower control surface downstream of the model. A comparison of the airfoil pressure distributions also suggested that the flow field was approaching unconfined flow. A fourth iterative step was attempted at this test condition. The u components were set close to the desired values, but the resulting v components were in much worse agreement with the corresponding unconfined-flow distributions. This iterative step was attempted twice with similar results, which seemed to indicate a tunnel cross-flow condition. The airfoil pressure distribution confirmed that this was apparently a divergent step. The reasons for this behavior were not clear. It was clear, however, that an improved measurement technique for the v component was necessary.

Accordingly, the new static-pipe technique for determining the v component was developed and this case was investigated further[9]. Two converging steps in an experimental iteration were accomplished at $M_\infty = 0.8$ and $\alpha = 4°$. From runs made prior to beginning the actual iteration, it was concluded that undesired cross-flow conditions upstream of the model could be minimized in the first iterative step by initiating the wall-control adjustment with the upstream valves set at their tunnel-empty positions at that M_∞. These two iterative steps yielded sufficient

information to proceed to a flow with both walls supercritical. Accordingly, the same model was tested at the same α, but with M_∞ increased to 0.9.

Initial experiments at $M_\infty = 0.9$ and $\alpha = 4°$ were performed[9] with the upstream control valves at their tunnel-empty settings and the remaining valves at their $M_\infty = 0.8$ and $\alpha = 4°$ settings. The measured components at the control surfaces exhibited a reasonable distribution from the beginning of the test section to the vicinity of the airfoil trailing edge with these settings. Downstream of this point, however, the flow was choked and supersonic flow persisted to the end of the test section. The choking was relieved by increasing the suction at plenum chambers 6 and 16 just upstream of the model (see Fig. 1). Further control adjustments led to reasonable u distributions along the entire length of the control surfaces. Achievement of this flow[9] provided the starting point for the most recent experiments that are described in the next three subsections.

4.3 Experiments at $M_\infty = 0.9$ and $\alpha = 3°$

The angle of attack of the 4%-blockage NACA 0012 airfoil was readjusted to the nominal condition of $\alpha = 3°$, which corresponds to the geometric angle of 3.62° in the One-Foot Tunnel when the zero-lift offset in the Eight-Foot Tunnel (see Fig. 2) is taken into account. This case is in the region where the lift-curve slope is larger than it is at very small α and provided a steady case for which α could be reduced in later experiments. Adjustment of the flow at this condition was begun with the valves in plenum chambers 2, 3, 14 and 15 (see Fig. 1) at the new empty-tunnel settings obtained at $M_\infty = 0.9$, and with the remaining valves at their settings for the successful run at $M_\infty = 0.9$ and $\alpha = 4°$.

A first iterative step toward unconfined flow at this condition was performed by setting the pressures on the sides of the static pipes nearest the model approximately to the values predicted by the TSFOIL computer code.[25] Care was taken to insure that comparable amounts of

suction were used at the upper and lower walls upstream of the model. At the upper wall, blowing was required in plenum chambers 8, 9, 10 and 11 in this and all subsequent iterative steps at α = 3°, 2° and 1°. The normal velocity components, as measured by the new static-pipe technique, are presented in Figs. 3 and 4 at the upper and lower control surfaces, respectively. These measured v distributions were used as the boundary conditions at the control surfaces to evaluate the functional relationships which must be satisfied in unconfined flow according to solutions of the transonic small-disturbance equations. The measured streamwise disturbance velocity components, also found by using the new static-pipe technique, are presented in Figs. 5 and 6 at the upper and lower control surfaces, respectively, along with the results of the functional-relationship evaluations u[v]. Reasonable agreement is observed upstream of the shock, but the agreement is unsatisfactory downstream of the shock. In addition, the pressure distribution on the airfoil was in fair agreement with the Eight-Foot Tunnel data on both surfaces up to the shock wave. On the lower surface of the airfoil, the shock is at the trailing edge as it was in the Eight-Foot Tunnel tests. On the upper surface, however, the shock is too far forward of the Eight-Foot Tunnel position by about 25% of the chord (x/c = 0.45 instead of x/c = 0.70) and agreement with the Eight-Foot Tunnel data is very poor downstream of the shock.

A second iterative step was then taken based on the results of the first step. Small changes in the static pressure settings from the previous step were taken, corresponding to an iterative relaxation factor of 0.1. This small value of the relaxation factor had been found to be necessary in earlier experiments. The resulting functional-relationship evaluations, however, indicated that very little improvement had actually been accomplished. Accordingly, the relaxation factor was increased to 0.5 for the third iterative step.

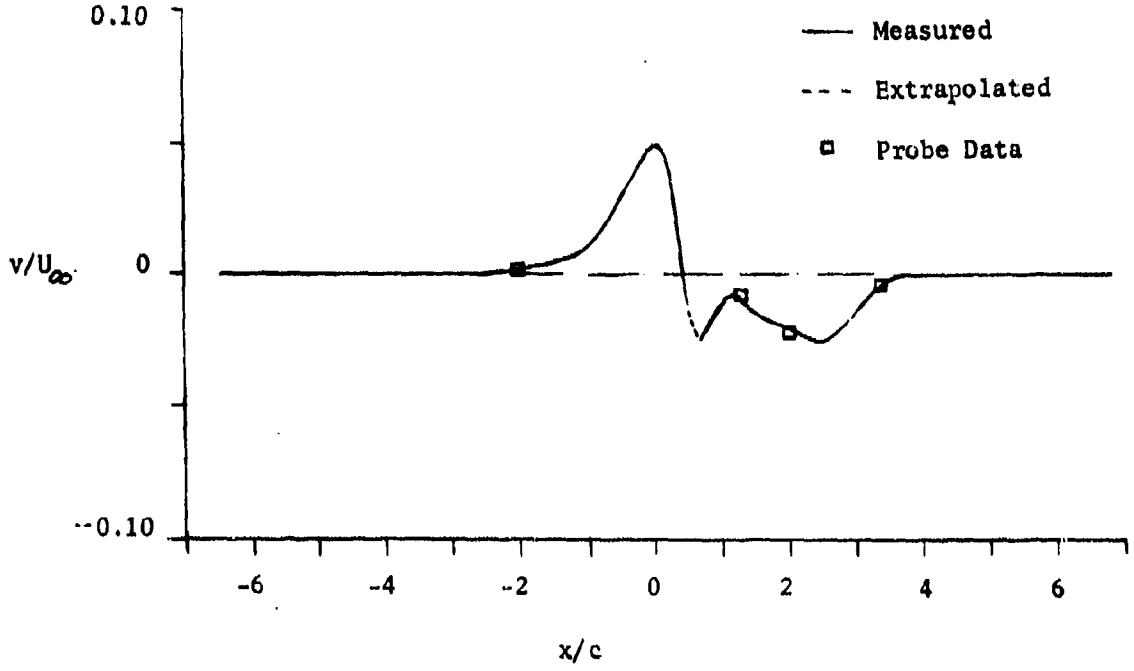

Figure 3. MEASURED NORMAL DISTURBANCE VELOCITY DISTRIBUTION, $M_\infty = 0.9$, $\alpha = 3°$, 4%-BLOCKAGE NACA 0012 AIRFOIL FIRST ITERATIVE STEP AT UPPER CONTROL SURFACE, $h/c = 1.0$.

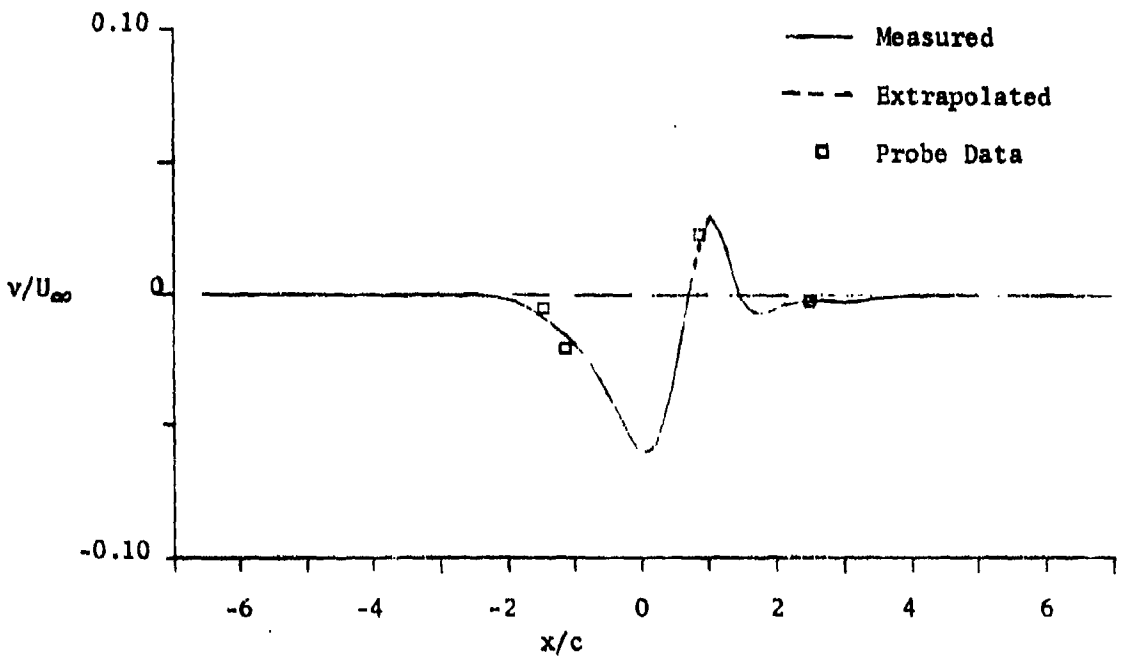

Figure 4. MEASURED NORMAL DISTURBANCE VELOCITY DISTRIBUTION, $M_\infty = 0.9$, $\alpha = 3°$, 4%-BLOCKAGE NACA 0012 AIRFOIL, FIRST ITERATIVE STEP AT LOWER CONTROL SURFACE, $h/c = -1.0$.

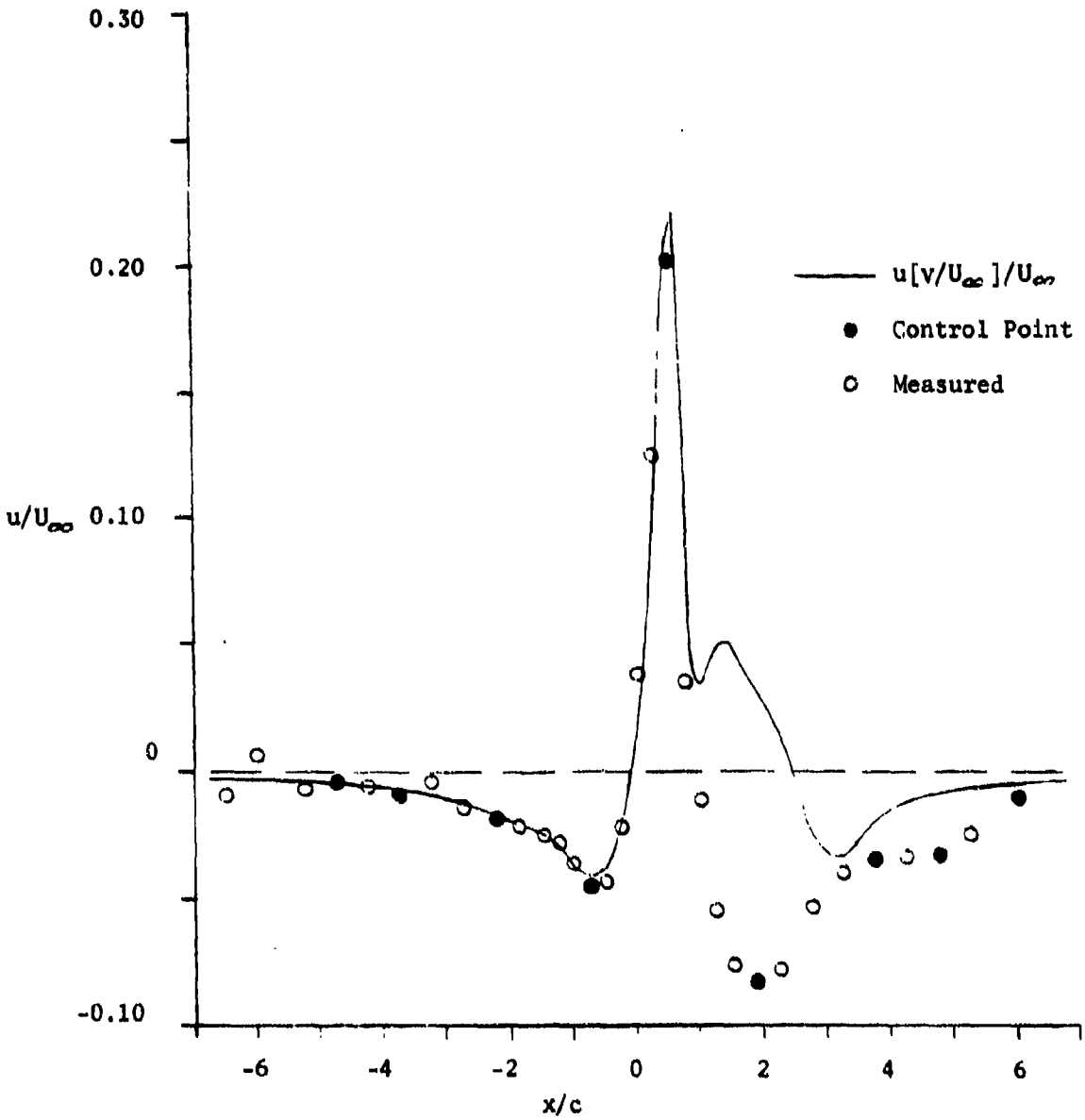

Figure 5. STREAMWISE DISTURBANCE VELOCITY DISTRIBUTIONS, $M_\infty = 0.9$, $\alpha = 3°$, 4%-BLOCKAGE NACA 0012 AIRFOIL, FIRST ITERATIVE STEP AT UPPER CONTROL SURFACE, $h/c = 1.0$

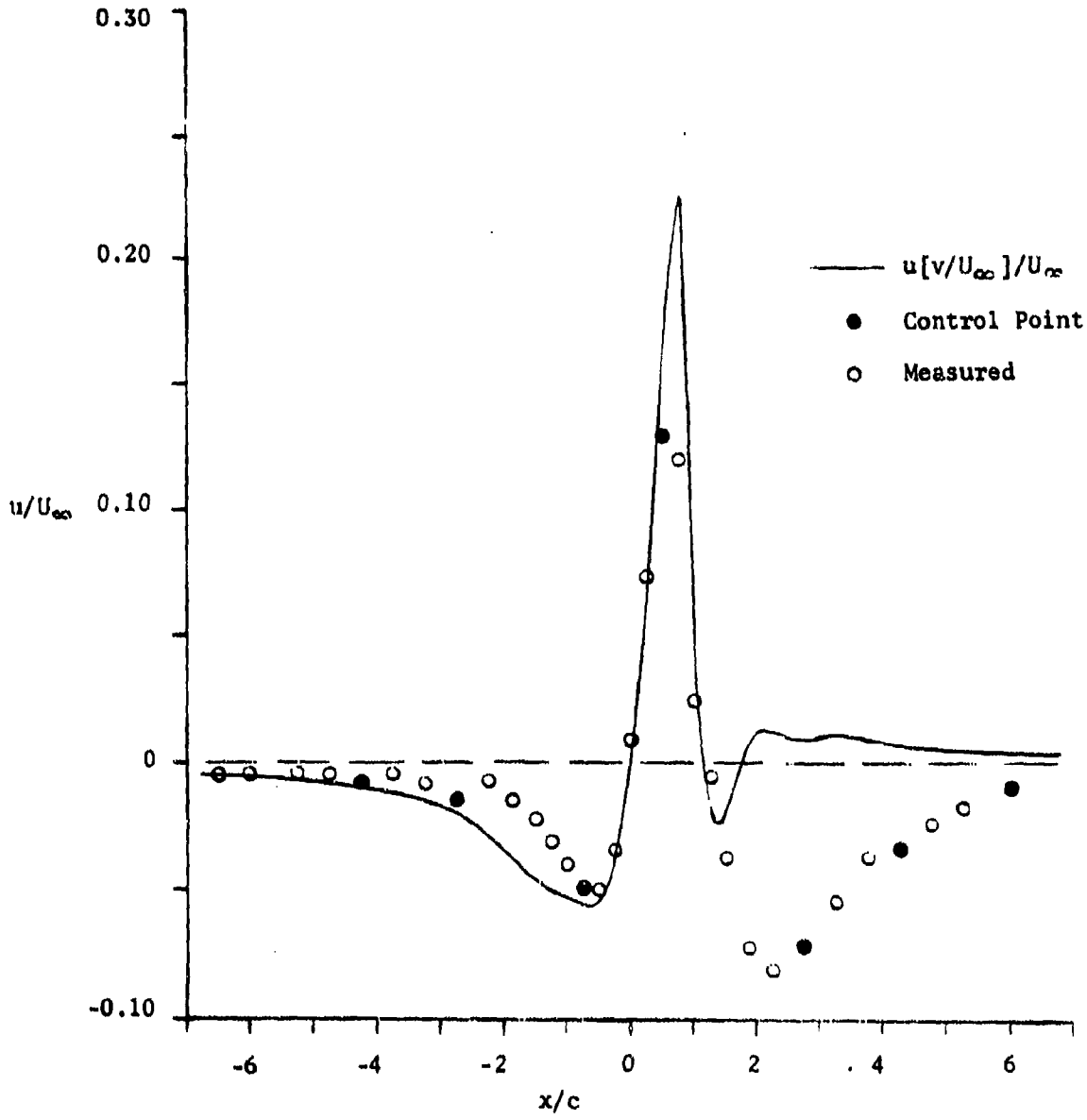

Figure 6. STREAMWISE DISTURBANCE VELOCITY DISTRIBUTIONS, $M_\infty = 0.9$, $\alpha = 3°$, 4%-BLOCKAGE NACA 0012 AIRFOIL, FIRST ITERATIVE STEP AT LOWER CONTROL SURFACE, $h/c = -1.0$

The agreement of the measured u distributions at the control surfaces in the third iterative step with the distributions u [v] from the functional-relationship evaluations improved significantly downstream of the model and remained good elsewhere as shown in Figs. 7 and 8. The shock wave moved rearward on the upper surface of the airfoil and is now too far forward by about 15% of the chord ($x/c = 0.55$ instead of $x/c = 0.70$).

Overall, the third iterative step was a significant improvement and showed that sufficient control was available to iterate toward unconfined flow. Moreover, the new static-pipe technique is a great improvement over the use of the flow-angle probes alone, especially with respect to ease and repeatability of the measurements. Nevertheless, certain limitations in the present implementation of the new technique were found to exist and certain fundamental questions about the pipe characteristics remain to be resolved. These will become clearer by discussing the representative results that are shown in Figs. 3 and 4.

The most obvious characteristic in the results of Figs. 3 and 4 is the dashed line representing the break in the curves in the vicinity of the shock wave. There are three problems near and downstream of the shock. First, the pipe orifices are spaced 1-inch apart, so that there is a gap of $\Delta(x/c) = 0.25$ between measurements. Second, the slender-body theory[9] relating pipe pressures to u and dv/dx is not strictly applicable when the disturbance causes formation of a supersonic pocket, followed by a shock such as occurs at both pipes in this case. Third, the response of the pipe boundary layer to the shock wave is not known. Proper assessment of the inviscid shock-pipe interaction and the possible effects on the pipe boundary layer were beyond the scope of this investigation, as was the development of a pipe traversing mechanism. In order to overcome these problems, it has been assumed that the slender-body analysis applies independently upstream and downstream of the shock. Then the curves on each side of the shock are extrapolated graphically as shown by the dashed lines.

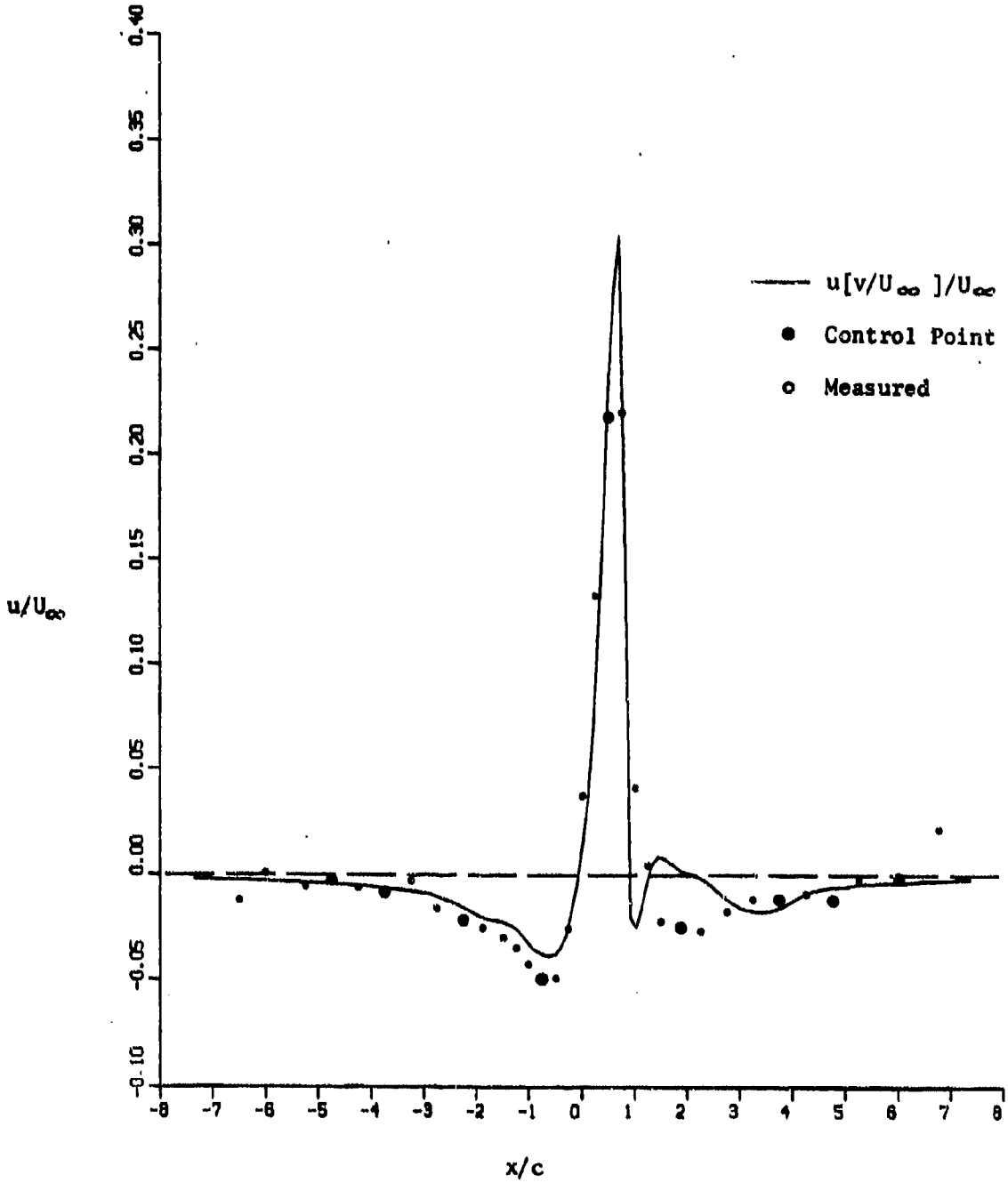

Figure 7. STREAMWISE DISTURBANCE VELOCITY DISTRIBUTIONS, $M_\infty = 0.9$, $\alpha = 3°$, 4%-BLOCKAGE NACA 0012 AIRFOIL, THIRD ITERATIVE STEP AT UPPER CONTROL SURFACE, $h/c = 1.0$.

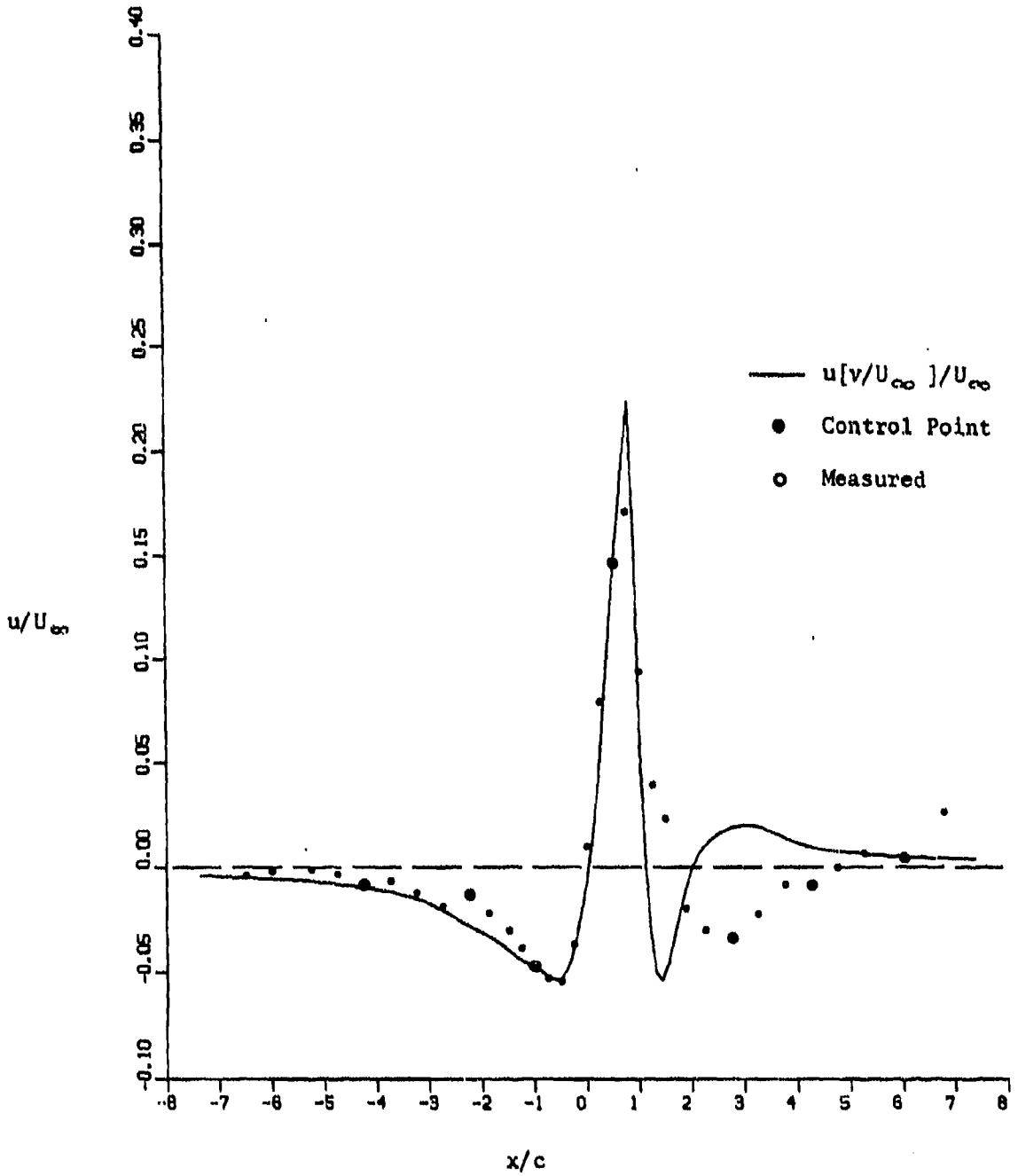

Figure 8. STREAMWISE DISTURBANCE VELOCITY DISTRIBUTIONS, $M_\infty = 0.9$, $\alpha = 3°$, 4%-BLOCKAGE NACA 0012 AIRFOIL, THIRD ITERATIVE STEP AT LOWER CONTROL SURFACE, $h/c = -1.0$.

In each of Figs. 3 and 4, the data for dv/dx up to the shock were fit by cubic splines and integrated up to the last data point before the shock with the constant of integration found by a least-squares fit to the probe data over that interval. Figures 3 and 4 are typical of all the results upstream of the shock in that the generally smooth v distributions are similar to those expected from theoretical considerations. Downstream of the shock, a similar spline fit and integration were performed. At the lower pipe, the probe measurement at x/c = 0.8275 was not considered in the fit to determine the constant of integration because its location with respect to the shock was not known precisely, nor was its accuracy.

The results in Figs. 3 and 4 downstream of the shock are typical of most of the experiments to be described below, especially with regard to the variations in v downstream of the shocks. These unusual variations give rise, of course, to the variations in u[v] shown in Figs. 5 to 8. In particular, the asymptotic approach to v = 0 far downstream was not always from negative values of v at the upper pipe as it is in Fig. 3, while in most cases, the approach at the lower pipe was from the negative side as shown in Fig. 4. Global considerations for the disturbances generated by the model in unconfined flow indicate that v = 0 should be approached from the negative side for the upper pipe and from the positive side for the lower pipe. There are several possible reasons for deviations from this expected behavior. First, the applicability of the subsonic, shock-free theory relating the pipe pressures to u and dv/dx is in doubt near the shock. Second, the flow control during early steps in the adaptive-wall iterative scheme may be such that the flow is so far from interference-free conditions that the measurements are actually correct despite their unexpected behavior. Finally, the probe measurements used to fix the constant of integration may be in error, especially at the lower pipe, where only the single measurement at x/c = 2.515 is available.

These lingering uncertainties about the interpretation of the static-pipe measurements led to the conclusion that the third iterative step was probably at the limits of measurement accuracy, so far as further iterations were concerned. Therefore, it was decided instead to reduce α successively to 2° and 1°, so that an investigation could be made of these cases where the lift-curve slope is smaller. It was in this range at $M_\infty = 0.85$ that steady flow could not be achieved.

Before these lower α cases were investigated, however, several runs were made at $M_\infty = 0.9$ and $\alpha = 3°$ to examine the effects of increased Reynolds number. In order to achieve these conditions, the tunnel pressure conditions were changed. However, no valve setting changes were made in the auxiliary suction and pressure systems. The power requirements and heating behavior of the tunnel were such that run time was limited to about 20 minutes at the higher Re_c. This time did permit acquisition of pressure data on the upper surface of the airfoil.

As Re_c was increased from 0.67×10^6 to 0.83×10^6, C_p on the upper airfoil surface decreased by about 30% (acceleration of the flow) everywhere upstream of the shock wave, which moved rearward by about 2.5% of the chord. As Re_c was increased further to 1.00×10^6, C_p decreased by an additional 30% ahead of the shock, which moved forward by about 7.5% of the chord so that it was 5% ahead of its location at $Re_c = 0.67 \times 10^6$. The shock became stronger as Re_c increased. This behavior apparently results from the interaction of the revised pressure levels in the tunnel with those in the auxiliary suction and pressure systems. That is, wall-interference effects are introduced by the mismatch in pressures. Complete readjustment of the wall control at each flow condition would be necessary to assess the effect of Re_c on the model properly. This was not feasible with the limited run time. These tests definitely established the sensitivity of the flow to Reynolds number and indicated the necessity to repeat the iteration procedure whenever M_∞, α or Re_c are changed.

4.4 Experiments at $M_\infty = 0.9$ and $\alpha = 2°$

The airfoil angle of attack was reduced to the nominal value (Fig. 2) of $\alpha = 2°$, which corresponds to the geometric angle of $\alpha = 2.62°$ in the One-Foot Tunnel. The first step in the iterative procedure was made by retaining the plenum pressure control valves at their final settings for the $\alpha = 3°$ iterations and simply acquiring a full set of static-pipe and probe data. The agreement at both control surfaces between the measured u distributions and the u[v] obtained from the functional-relationship evaluations is generally comparable to that shown in Figs. 5 and 6 for the first iterative step at $\alpha = 3°$. The largest differences still are downstream of the shock waves. The shock on the upper surface of the airfoil is at x/c = 0.55, as compared to x/c = 0.75 in the Eight-Foot Tunnel data. On the lower surface, the shock is at x/c = 0.95 instead of 0.975 as in the Eight-Foot Tunnel data.

A second iterative step was made with a relaxation factor of 0.5, as had proved better at $\alpha = 3°$. This choice was satisfactory here, too, inasmuch as the agreement at this step is comparable to that shown in Figs. 7 and 8 for the third step at $\alpha = 3°$. The shock on the upper surface of the airfoil moved rearward to x/c = 0.65, while the lower surface shock moved slightly rearward.

Overall, then, these results at $\alpha = 2°$ reflected the behavior at $\alpha = 3°$. The flow was again steady, without evidence of shock-wave fluctuations. At the lower control surface, the measured v distributions at both iterative steps were very similar to those at $\alpha = 3°$, (see Fig. 4). The asymptotic approach to zero downstream was still contrary to that expected for interference-free flow. At the upper control surface in both iterative steps, however, there was a departure from the behavior shown in Fig. 3; that is, the asymptotic approach to zero downstream was from the positive side. Despite these questions, the iterations for this case were terminated at the second step so that the $\alpha = 1°$ case could be investigated more thoroughly.

4.5 Experiments at $M_\infty = 0.9$ and $\alpha = 1°$

The angle of attack was reduced to the nominal setting of $\alpha = 1°$, which corresponds to the geometrical angle of 1.62° in the One-Foot Tunnel. The first and second iterative steps were carried out as they had been for $\alpha = 2°$. That is, the first step was made with the plenum control valves at their final settings for $\alpha = 2°$ and the second step was taken with an iterative relaxation factor of 0.5. The basic trend of the results for the distributions is similar to the first and second steps at $\alpha = 2°$ and the first and third steps at $\alpha = 3°$. However, the shock wave on the upper surface of the airfoil moved from x/c = 0.65 at the first step to x/c = 0.85 at the second. This is aft of its location at x/c = 0.725 in the Eight-Foot Tunnel tests. At the lower surface of the airfoil, the shock was slightly forward of its Eight-Foot Tunnel location at the first step, but subsequently moved aft. The flow was steady at each step and there was no exceptional difficulty in setting the second step.

A third iterative step was taken, again with a relaxation factor of 0.5. The resulting measured v components at the control surfaces are given in Figs. 9 and 10. These are used, in turn, as the boundary conditions for the functional-relationship evaluations u[v], results of which are compared with the measured u data in Figs. 11 and 12. The agreement in the u distributions at both control surfaces is far superior to that observed for any of the previous cases. However, there are still some important differences downstream of the shocks. The chordwise distributions of the airfoil surface pressures for the third iterative step, presented in terms of βC_p, are compared with the corresponding Eight-Foot Tunnel data in Fig. 13. The shock waves on both surfaces are nearly coincident for the two flows. However, there is an appreciable deviation of the pressures on the upper surface ahead of the shock and the One-Foot Tunnel data appear to have a smoother variation than the Eight-Foot Tunnel data. The reason for these differences is not known.

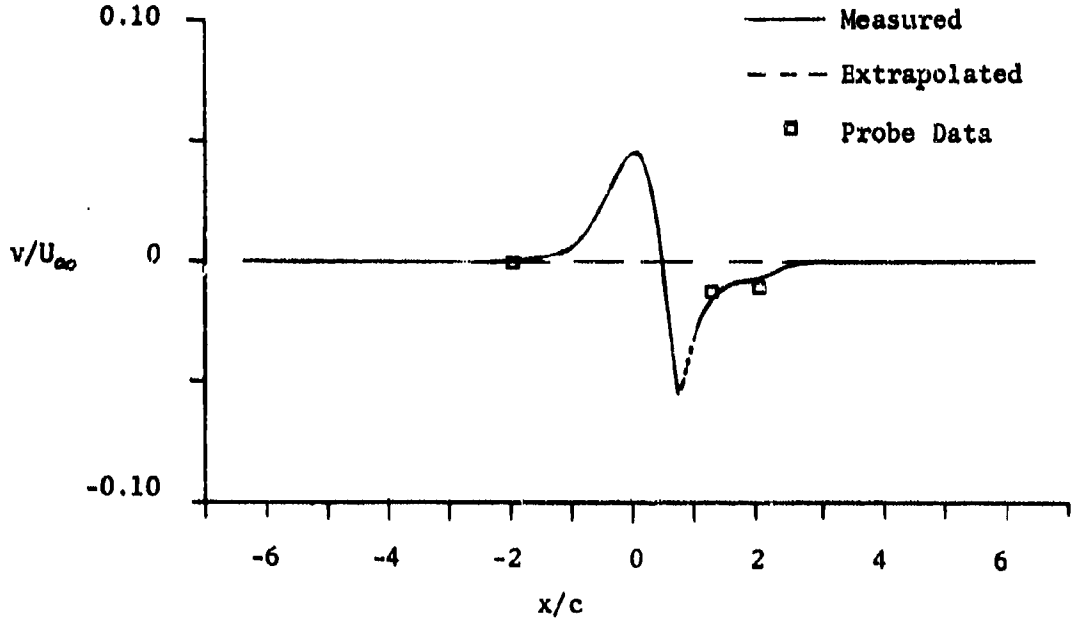

Figure 9. MEASURED NORMAL DISTURBANCE VELOCITY DISTRIBUTION, $M_\infty = 0.9$, $\alpha = 3°$, 4%-BLOCKAGE NACA 0012 AIRFOIL, THIRD ITERATIVE STEP AT UPPER CONTROL SURFACE, $h/c = 1.0$.

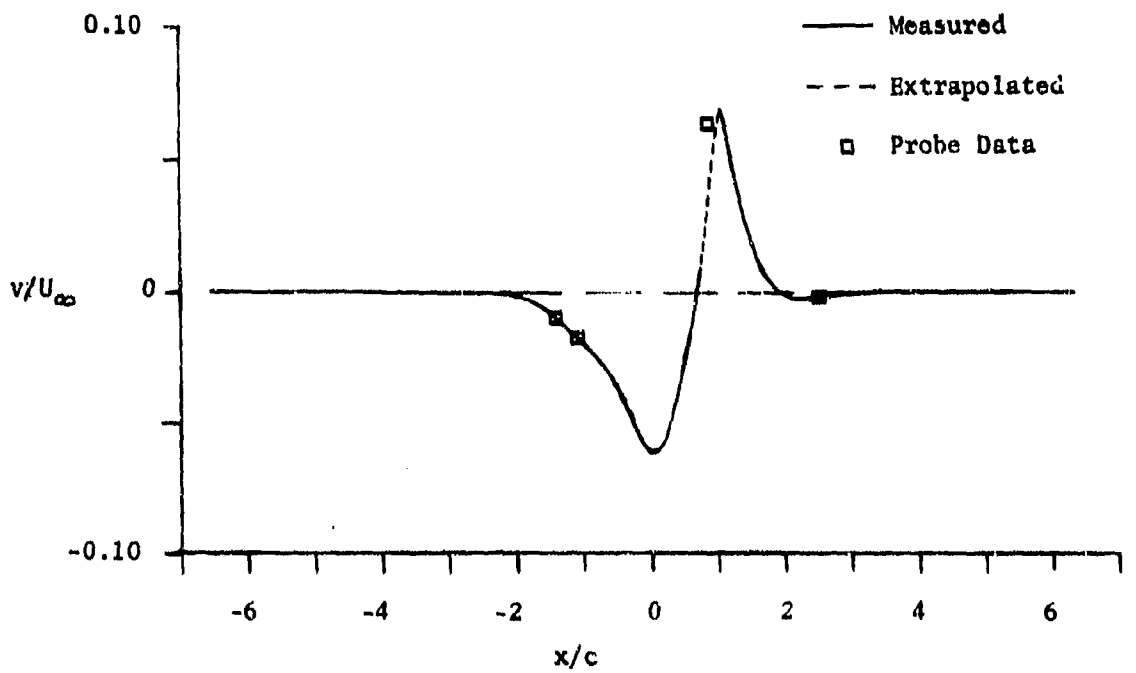

Figure 10. MEASURED NORMAL DISTURBANCE VELOCITY DISTRIBUTION, $M_\infty = 0.9$, $\alpha = 1°$, 4%-BLOCKAGE NACA 0012 AIRFOIL THIRD ITERATIVE STEP AT LOWER CONTROL SURFACE, $h/c = -1.0$.

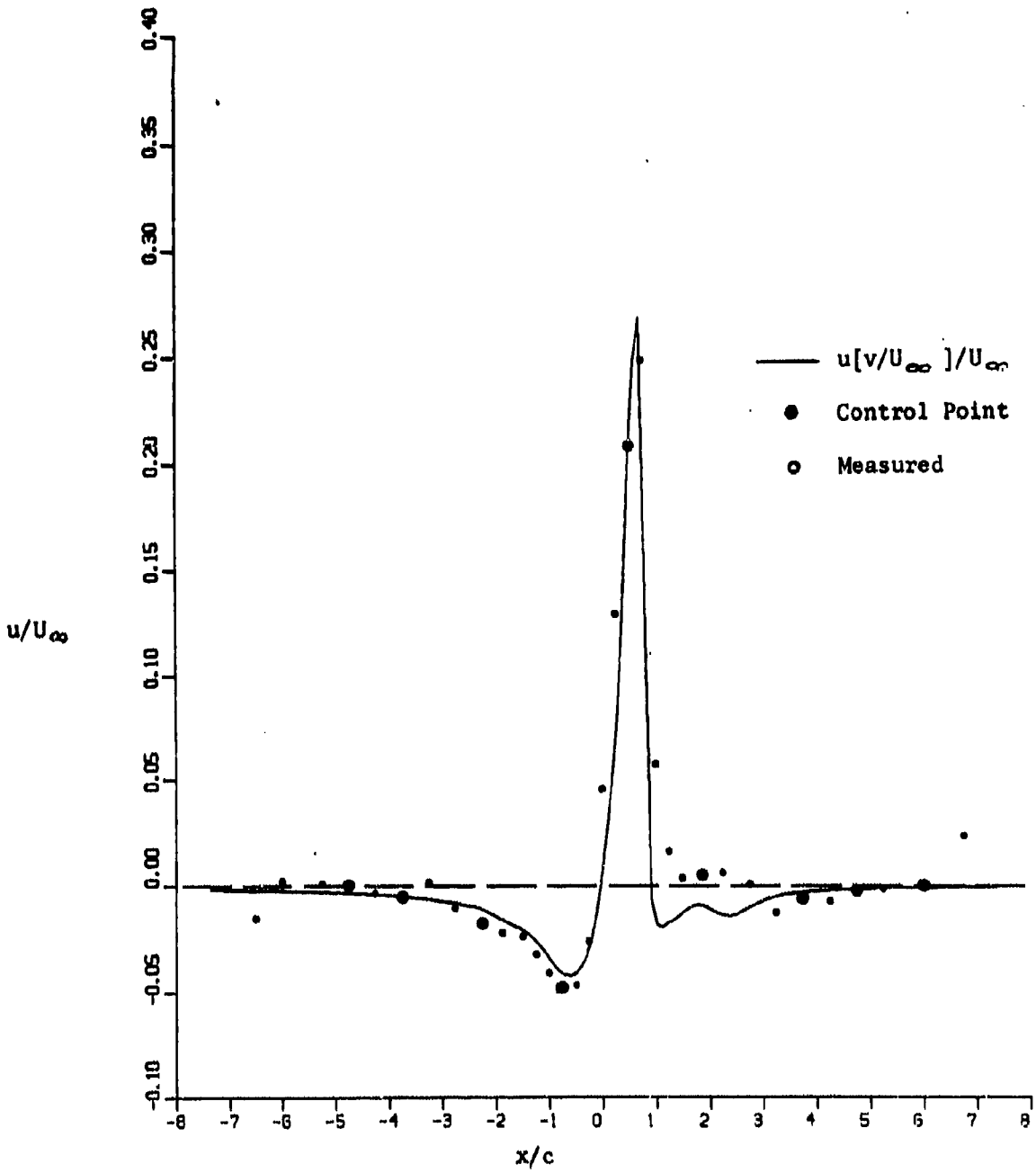

Figure 11. STREAMWISE DISTURBANCE VELOCITY DISTRIBUTIONS, $M_\infty = 0.9$, $\alpha = 1°$, 4%-BLOCKAGE NACA 0012 AIRFOIL, THIRD ITERATIVE STEP AT UPPER CONTROL SURFACE, $h/c = 1.0$.

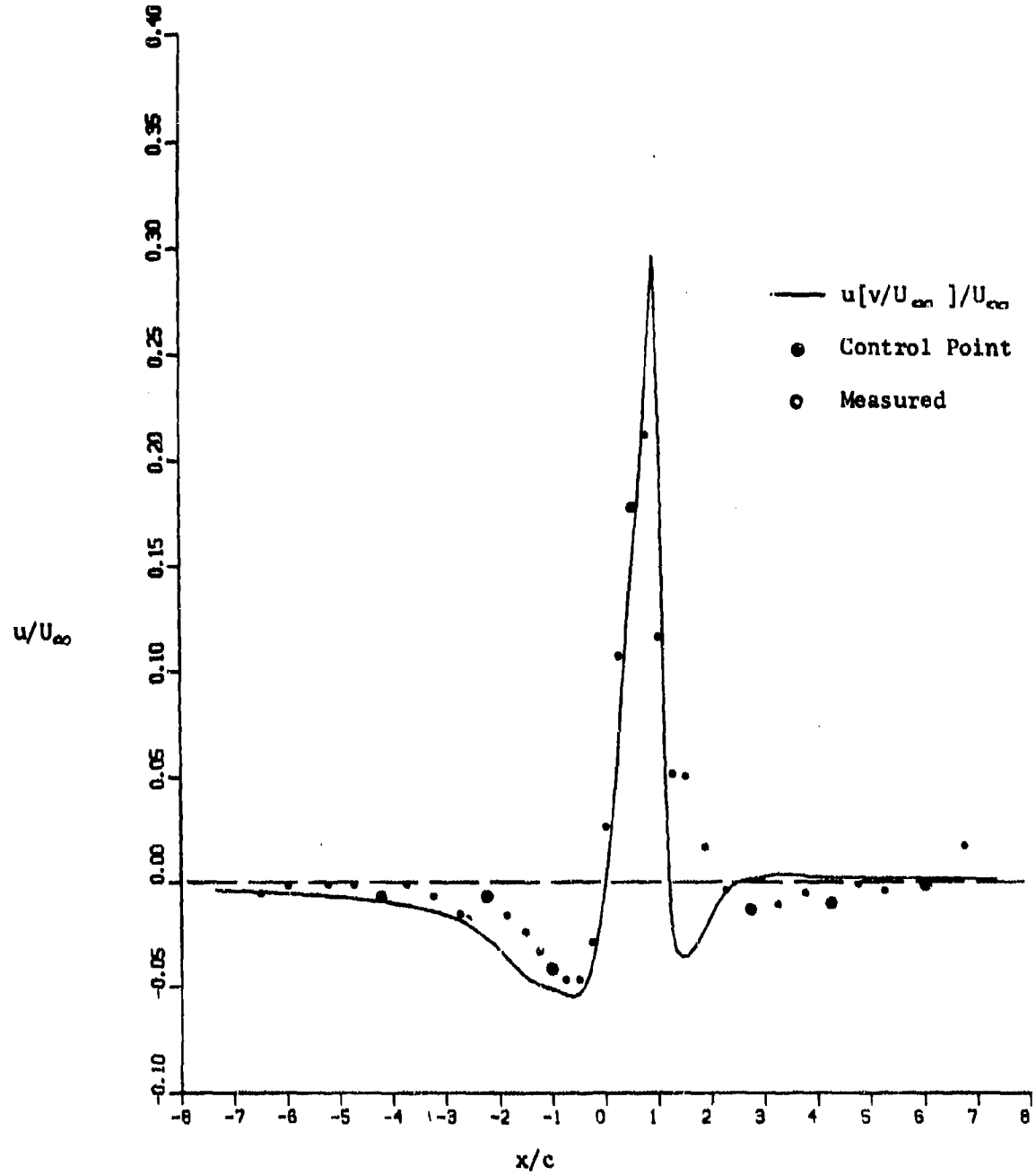

Figure 12. STREAMWISE DISTURBANCE VELOCITY DISTRIBUTIONS, $M_\infty = 0.9$, $\alpha = 1°$, 4%-BLOCKAGE NACA 0012 AIRFOIL, THIRD ITERATIVE STEP AT LOWER CONTROL SURFACE, $h/c = -1.0$.

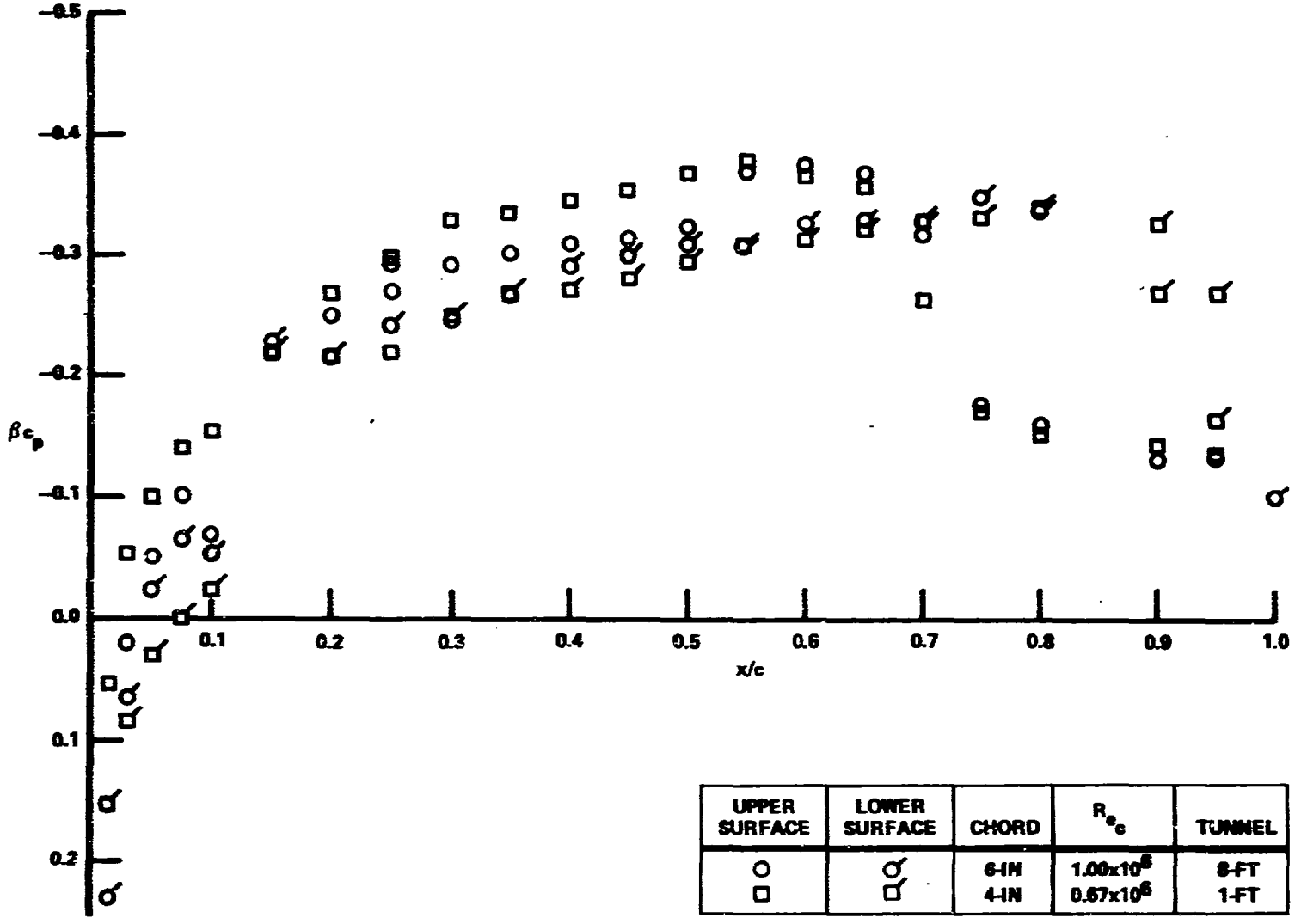

Figure 13. COMPARISON OF MEASURED AIRFOIL PRESSURE DISTRIBUTIONS, $M_\infty = 0.9$, $\alpha = 1°$, THIRD ITERATIVE STEP.

The v distributions measured at the third iterative step follow the trend expected from theoretical predictions for unconfined flow. That is, the nonuniform variation in the distribution downstream of the shock at the upper control surface (Fig. 9) is not as severe as it was for the first iterative step at $\alpha = 3^{\circ}$ (Fig. 3) and for most of the intervening cases. Also, the asymptotic approach to $v = 0$ is satisfactory. At the lower control surface (Fig. 10), too, the v distribution is more reasonable with only a small overshoot in the asymptotic behavior downstream. This overshoot may result from uncertainty in the probe measurement at $x/c = 2.515$.

Overall, the trend of the iterations for all three angles of attack at $M_{\infty} = 0.9$ is towards convergence. Improvements were made in the agreement between the measured u distributions and the u[v] computed by the functional-relationship evaluations at each iterative step. Thus, it would appear that the entire angle-of-attack range can be iterated to a reasonable approximation of interference-free flow conditions. Further refinement of the results achieved here should be possible after resolution of the outstanding questions about the static-pipe data and the Reynolds number effects.

Section 5

CONCLUDING REMARKS

The new static-pipe technique[9] for determining the streamwise and normal disturbance velocity components provided significant improvements in the ease and reliability of the normal component measurements. The extensive use of the technique that has been accomplished herein, however, has led to uncertainties about the interpretation of the pipe measurements in some regions of the flow field. In particular, results in the vicinity of the interaction of a shock wave from the model with the pipe has raised several questions which must be answered before additional use of the technique is undertaken. Although the new static pipes have greatly improved the definition of the normal velocity distribution near the model, an even more refined definition is needed in regions of rapid gradients, especially near a shock. A translation mechanism for the static pipes could provide this capability. The subsonic slender-body theory developed in Ref. 9 should be replaced by a transonic theory, particularly in the vicinity of the shock, in order to provide an accurate relationship between the pressure measurements on the pipe and the two velocity components. Furthermore, an analysis of the effects of the pipe boundary-layer on the relationship between the pressures and velocity components should be performed. Finally, experiments should be made in which the results of the static-pipe measurements can be compared with independent measurements of the two velocity components. Successful resolution of these questions could lead to use of the new static-pipe technique for measurements in flow fields other than those in adaptive-wall wind tunnels.

Successful experimental iterations toward interference-free flow have been achieved at a free-stream Mach number of 0.9 and angles of attack of 3°, 2° and 1°. As the iterations proceeded, significant improvements were observed in the agreement between the measured streamwise disturbance velocity distributions and the corresponding distributions resulting from the exterior-flow functional-relationship evaluations. These evaluations

used the measured normal velocity distributions as boundary conditions for transonic small-disturbance calculations. Therefore, we conclude that the existing perforated-wall, segmented-plenum implementation of the adaptive-wall concept can provide sufficient control to iterate when locally-supersonic flow and shock waves extend to both tunnel walls. In the wall-control adjustment procedure, care must be exercised to balance the amount of suction in the upper and lower plenum chambers upstream of the model. This is necessary to avoid introducing unwanted flow inclination upstream of the model. Furthermore, positive pressure was necessary in the upper plenum chambers downstream of the model in order to provide the blowing velocity through the wall from the plenum chambers into the tunnel that was required to achieve control of the flow.

We believe that an improved two-dimensional test section with the same perforated-wall, segmented-plenum, wall-control technique is possible. These improvements, which are described in Appendix II, should provide more refined control in the near vicinity of the model for supercritical-wall cases. The refinements would be accomplished by changing plenum-chamber size, particularly by reducing the length of those chambers near the model where the gradients in the disturbance velocity components are greatest. Also, walls with different open-area ratios for smaller losses in the auxiliary suction system might be possible away from the immediate vicinity of the shock waves. Finally, symmetrical plenum segmentation on the upper and lower walls would provide greater flexibility of operation, particularly for calibration and routine checks of the instrumentation, both without a model present and with a symmetrical model at zero angle of attack.

The numerical simulation investigation is presented in detail in the AIAA paper that is attached to this report, and extensive concluding remarks are given there. However, it is worthwhile to summarize them here. The low-speed numerical-simulation methodology gives a realistic description of the behavior of a perforated-wall, segmented-plenum test section, as

demonstrated by baseline numerical simulations of a representative case. Influence functions calculated for changes in the velocity components at the control surfaces due to a change in the pressure in one plenum chamber at a time, while holding the other chamber pressures constant, can be approximated reasonably well by universal curves based on linearized theory. Extension of the numerical simulation technology to flows which are supercritical at the walls could be used as a basis for wide-ranging studies of test-section design and operational procedures. In particular, simulations would enable the development of procedures for automated wall adjustment, which is crucial to the ultimate practical application of the adaptive-wall concept. This is clearly apparent in light of the great care that was necessary in the manual adjustments required during the iteration experiments described in this report.

As a result of our entire experience with the two-dimensional test section, through both experiment and numerical simulation, and the preliminary design studies described in Appendix II, we believe that the perforated-wall, segmented-plenum implementation is viable for a fully three-dimensional test section. This would be especially so if additional design studies were to show that adequate control would be possible with even a smaller number of plenum chambers than the 64 discussed in Appendix II. Appropriate adaptations of the numerical simulation methodology could be used to perform these design studies. The new static-pipe technique has been shown theoretically[9] to be applicable to the measurement of three-dimensional disturbance velocity fields when suitably modified. This technique is an attractive possibility for use in a three-dimensional adaptive-wall test section.

REFERENCES

1. Ferri, A. and Baronti, P. "A Method for Transonic Wind Tunnel Corrections" AIAA Journal, Vol. 11, No. 1, pp. 63-66, January 1973.

2. Sears, W.R. "Self-Correcting Wind Tunnels" (The Sixteenth Lanchester Memorial Lecture) Calspan Report No. RK-5070-A-2, July 1973; also the Aeronautical Journal, Vol. 78, No. 758/759, pp. 80-89, February/March 1974.

3. Erickson, J.C., Jr. and Nenni, J.P. "A Numerical Demonstration of the Establishment of Unconfined-Flow Conditions in a Self-Correcting Wind Tunnel" Calspan Report RK-5070-A-1, November 1973.

4. Vidal, R.J., Erickson, J.C., Jr. and Catlin, P.A. "Experiments with a Self-Correcting Wind Tunnel" AGARD-CP-174, October 1975; also Calspan Report No. RK-5070-A-4, October 1975.

5. Sears, W.R., Vidal, R.J., Erickson, J.C., Jr. and Ritter, A. "Interference-Free Wind-Tunnel Flows by Adaptive-Wall Technology" ICAS Paper No. 76-02, 10th Congress of the International Council of the Aeronautical Sciences, Ottawa, Canada, 3-8 October 1976; also Journal of Aircraft, Vol. 14, No. 11, pp. 1042-1050, November 1977.

6. Vidal, R.J., Catlin, P.A. and Chudyk, D.W. "Two-Dimensional Subsonic Experiments with an NACA 0012 Airfoil" Calspan Report No. RK-5070-A-3, December 1973.

7. Vidal, R.J. and Erickson, J.C., Jr. "Experiments on Supercritical Flows in a Self-Correcting Wind Tunnel" AIAA Paper No. 78-788, AIAA 10th Aerodynamic Testing Conference, San Diego, California, 19-21 April 1978.

8. Vidal, R.J. and Erickson, J.C., Jr. "Research on Adaptive-Wall Wind Tunnels" AEDC Report No. AEDC-TR-78-36, November 1978.

9. Erickson, J.C., Jr., Wittliff, C.E. and Daughtry, D.C. "Further Investigations of Adaptive-Wall Wind Tunnels" AEDC Report No. AEDC-TR-80-34, October 1980.

10. Chevallier, J.P. "Soufflerie Transsonique a Parois-Adaptables" AGARD-CP-174, October 1975; also translated into English as European Space Agency Report ESA-TT-326, October 1976, available as NASA Accession No. N77-13085.

REFERENCES (Cont'd.)

11. Poisson-Quinton, P. "Some New Approaches for Wind-Tunnel Testing Through the Use of Computers" AIAA Paper No. 79-0707, First Intersociety Atlantic Aeronautical Conference, Williamsburg, Virginia 26-28 March 1979; also ONERA TP No. 1979-24.

12. Goodyer, M.J. "A Low-Speed Self Streamlining Wind Tunnel" AGARD-CP-174, October 1975.

13. Goodyer, M.J. and Wolf, S.W.D. "The Development of a Self-Streamlining Flexible Walled Transonic Test Section" AIAA Paper No. 80-0440, AIAA 11th Aerodynamic Testing Conference, Colorado Springs, Colorado, 18-20 March 1980.

14. Ladson, C.L. "A New Airfoil Research Capability" in Advanced Technology Airfoil Research, Vol. 1, NASA CP-2045, Part 1, March 1979.

15. Ganzer, U. "Windkanale mit Adaptiven Wanden zur Beseitigung von Wandinterferenzen" Zeitschrift fur Flugwissenschaften und Weltraumforschung, Vol. 3, No. 2, pp. 129-133, 1979; also translated into English as NASA TM-75501, August 1979.

16. Ganzer, U. "Adaptable Wind Tunnel Walls for 2-D and 3-D Model Tests" ICAS Paper No. 23-3, 12th Congress of the International Council of the Aeronautical Sciences, Munich, Germany, 12-17 October 1980.

17. Kemp, W.B., Jr. "Toward the Correctable-Interference Transonic Wind Tunnel" AIAA Paper No. 76-1794, AIAA 9th Aerodynamic Testing Conference, Arlington, Texas, 7-9 June 1976.

18. Kemp, W.B., Jr. "TWINTAN: A Program for Transonic Wall Interference Assessment in Two-Dimensional Wind Tunnels" NASA TM-81819, May 1980.

19. Capelier, C., Chevallier, J-P. and Bouniol, F. "A New Method for Correcting Wall Interference" La Recherche Aerospatiale, 1978, No. 1, January-February 1978, pp. 1-11; also translated into English as European Space Agency Report ESA-TT-491, August 1978, available as NASA Accession No. N79-11997.

20. Murman, E.M. "A Correction Method for Transonic Wind Tunnel Wall Interference" AIAA Paper No. 79-1533, AIAA 12th Fluid and Plasma Dynamics Conference, Williamsburg, Virginia, 24-26 July 1979.

REFERENCES (Cont'd.)

21. Weeks, T.M. "Reduction of Transonic Slotted Wall Interference by Means of Slat Contouring: Air Force AFFDL-TR-74-139, March 1975.

22. Kraft, E.M. and Parker, R.L., Jr. "Experiments for the Reduction of Wind Tunnel Wall Interference by Adaptive-Wall Technology" AEDC Report No. AEDC-TR-79-51, October 1979.

23. Parker, R.L., Jr. and Sickles, W.L. "Application of Adaptive Wall Techniques in a Three-Dimensional Wind Tunnel with Variable Wall Porosity" AIAA Paper No. 80-0157, AIAA 18th Aerospace Sciences Meeting, Pasadena, California, 14-16 January 1980.

24. Bodapati, S., Schairer, E. and Davis, S. "Adaptive-Wall Wind-Tunnel Development for Transonic Testing" AIAA Paper No. 80-0441, AIAA 11th Aerodynamic Testing Conference, Colorado Springs, Colorado, 18-20 March 1980.

25. Murman, E.M., Bailey, F.R. and Johnson, M.L. "TSFOIL-A Computer Code for Two-Dimensional Transonic Calculations, Including Wind-Tunnel Wall Effects and Wave-Drag Evaluation" Paper No. 26 in Aerodynamic Analyses Requiring Advanced Computers, NASA-SP-347-Part 2, March 1975.

26. Bailey, F.R. and Ballhaus, W.F. "Comparison of Computed and Experimental Pressures for Transonic Flows About Isolated Wings and Wing-Fuselage Configurations" NASA-SP-347-Part 2, March 1975.

APPENDIX I

PAPERS, REPORTS AND PRESENTATIONS

The following is a list of all papers, reports and presentations prepared under this contract.

Sears, W.R., Vidal, R.J., Erickson, J.C., Jr. and Ritter, A. "Interference-Free Wind Tunnel Flows by Adaptive-Wall Technology," ICAS Paper No. 76-02, Tenth Congress of the International Council of the Aeronautical Sciences, Ottawa, Canada, 3-8 October 1976; also Calspan Report No. RK-6040-A-1, January 1977; also Journal of Aircraft, Vol. 14, No. 11, pp 1042-1050, November 1977.

Erickson, J.C., Jr. "The Calspan Self-Correcting Wind Tunnel," 13th Annual Meeting of the Subsonic Aerodynamic Testing Association, held at AEDC, Arnold Air Force Station, Tennessee, 4-5 May 1977.

Vidal, R.J. "Recent Experiments in the Calspan Self-Correcting Wind Tunnel," Workshop on New Developments in Transonic Wind Tunnel Wall Interference, held at AEDC, Arnold Air Force Station, Tennessee, 16-17 August 1977.

Vidal, R.J. and Erickson, J.C., Jr. "Research on Self-Correcting Wind Tunnels," Conference on Advanced Technology Airfoil Research, held at NASA/Langley Research Center, 7-9 March 1978; published as Advanced Technology Airfoil Research, Vol. 1, NASA CP-2045, Part 2, March 1979.

Vidal, R.J. and Erickson, J.C., Jr. "Experiments on Supercritical Flows in a Self-Correcting Wind Tunnel," AIAA Paper No. 78-788, AIAA 10th Aerodynamic Testing Conference, San Diego, California, 19-21 April 1978.

Erickson, J.C., Jr. "Adaptive-Wall Technology for V/STOL Testing," Workshop on V/STOL Aircraft Aerodynamics Sponsored by Naval Air Development Center, held at Naval Postgraduate School, Monterey, California, 16-18 May 1979; published in Workshop Proceedings, Vol. 1, pp 444-461.

Erickson, J.C., Jr. and Wittliff, C.E. "Intelligent Wall Wind Tunnels," AFOSR/AFFDL Program Review of Research in External Aerodynamics, Dayton, Ohio, 6-8 June 1979.

Erickson, J.C., Jr. and Homicz, G.F. "Numerical Simulations of a Segmented-Plenum, Perforated, Adaptive-Wall Wind Tunnel" AIAA Paper No. 81-0160, AIAA 19th Aerospace Sciences Meeting, St. Louis, MO 12-15 January 1981.

In addition, Calspan personnel participated in Adaptive Transonic Wall Meetings held at AEDC on 19 January 1978, 10 August 1978, 19 January 1979, 12 July 1979, 26 February 1980 and 16 January 1981. Research performed under this contract was presented at these meetings.

APPENDIX II

THREE-DIMENSIONAL ADAPTIVE-WALL DESIGN STUDIES

The objectives of these studies were to establish requirements for three-dimensional adaptive-wall test sections and then to examine the adaptability of the Calspan One-Foot Tunnel to meet these requirements. The test section requirements were investigated by calculating the unconfined flow about a few representative configurations. Estimates were based on both Prandtl-Glauert theory and finite-difference solutions of the transonic small-disturbance equations, using the Bailey-Ballhaus code.[26] The emphasis in the adaptation study was on working toward the design of a suitable test section, as well as a corresponding model configuration with which to carry out a demonstration of the concept.

Choice of a suitable model configuration for demonstration testing is very important. The model should not only be representative of practical configurations, but should also have a large amount of interference in a passive-wall tunnel so that a clear-cut demonstration can be made. A wing-body-horizontal tail model is a minimum requirement so that the contribution of the horizontal tail to the pitching moment can be assessed. This contribution should be sensitive to the capability of the chosen adaptive-wall implementation for assuring that the trailing vortex system from the wing retains its unconfined-flow characteristics and location. The most suitable existing model is the AEDC Wall-Interference Model[23], which has a slender axisymmetric body with a swept, untapered, constant-thickness wing and horizontal tail. This model is attractive for a three-dimensional demonstration because the wall interference should be relatively large.

---

[26] Bailey, F.R. and Ballhaus, W.F. "Comparison of Computed and Experimental Pressures for Transonic Flows About Isolated Wings and Wing-Fuselage Configurations" NASA-SP-347-Part 2, March 1975.

Before the above model was considered, initial calculations of the unconfined flows about two different wing configurations were made with the Bailey-Ballhaus code. One wing was swept, tapered and untwisted while the other was rectangular in planform and untwisted. Thus, their flowfields, which were calculated for a single angle of attack, each at a Mach number of 0.9, were quite distinctive. A computer program was written to evaluate the disturbance velocity components at walls or control surfaces of rectangular cross section. This program reads the velocity potential for unconfined flow throughout the field, as saved on tape in the Bailey-Ballhaus program, and differentiates and interpolates numerically to get the desired flowfield velocities. It also estimates the separate effects of thickness and lift so that superposition can be used to approximate the velocity field for other values of these parameters. Superposition is not strictly valid for nonlinear supercritical flows. However, it does provide useful estimates of the velocity magnitudes and distributions, especially when the flow at the field location is subcritical.

Prandtl-Glauert calculations based on line distributions of thickness and lift for rectangular planforms were useful for estimating the effects of free-stream Mach number on the disturbance velocity distributions. In both two and three dimensions, an increase in Mach number shifts closer together the maxima and minima of the normal and streamwise velocity distributions on the upper and lower walls. For bodies, slender-body theory was used to obtain an axial source distribution for a given axisymmetric body-cross-section distribution. The source distribution is then approximated by discrete source elements, which are used in conjunction with Prandtl-Glauert theory to calculate the velocity components at the control surface and wall locations.

Once these three-dimensional unconfined flow fields had been obtained, we began to consider test section designs so that we could define more fully the outstanding problems which require resolution before a definitive design can be achieved. Early in the investigation, we examined the prospects for a reflection-plane test section with control on only three

walls. This is attractive, principally, because a larger model can be accommodated for a given tunnel cross-sectional area, thus providing more uncontrolled wall interference to be eliminated in the demonstration. However, a convincing demonstration would require that the same model also be tested in a larger tunnel to obtain substantially interference-free data for comparisons. It would be very difficult to account properly for the differences in the reflection-plane boundary layers on tests in two, very different tunnel sizes. Moreover, for model configurations that are symmetrical laterally, we believe that it is important to demonstrate that the walls can be adjusted so as to insure the same symmetry in the flow field. Also, demonstrations should be made for moderately non-symmetrical model attitudes. Therefore, we concluded that a fully three-dimensional test section should be built with active control on all four walls.

We decided that an extension of our two-dimensional design principles would be used as a base line. That is, the test section would have perforated walls, behind which would be segmented plenum chambers with individual pressure control. Accordingly, the next step in the design process was to reconsider the present two-dimensional design in light of our operational experience. It appears that smaller plenum chambers near the model would be advantageous to accommodate the rapid variations that occur in the velocity components along and normal to the walls at high Mach numbers. The original design was based on distributions calculated at low speeds. As mentioned above, at higher Mach numbers, the maxima and minima are closer together so that the distributions of the velocity components are no longer approximately linear over the plena near the model. On the other hand, farther away from the model, it appears that larger plenum chambers might be possible. In addition, the use of walls with a larger open-area ratio is attractive for reducing the suction requirements in regions where no shock waves are expected. Where shocks are expected, the present 22.5% open-area ratio probably should be retained because of its superior shock-cancellation properties. Although these features appear attractive, based on our experience in two dimensions, more evidence of their effectiveness is required and consequently, further work should be carried out to resolve these matters.

An important decision on the test section configuration is the cross-section shape. Most modern tunnels are square for maximum flexibility in testing a wide variety of configurations, including vehicles at very large angles of attack. For the purposes of an adaptive-wall demonstration, we initially considered rectangular cross sections with height-to-width ratios from about 1/2 to 1. A ratio of 0.7 gives a good balance between the peak magnitudes of the unconfined-flow velocity components on the side, top and bottom walls for as large a model span as is practical to test in a given tunnel width. This still permits configurations to be tested at moderate angles of attack. This ratio is also compatible with the existing contraction section of the Calspan One-Foot Tunnel.

A preliminary layout was made of the plenum segmentation required in the streamwise direction, using the features set forth above, based on our two-dimensional experience. It was found that both the rectangular and swept wings, which we considered, could be accommodated by the same basic segmentation, provided that each model could be mounted in a different location with respect to the plenum chambers. We believe that we can achieve wall control using the same number of streamwise plenum chambers as in two dimensions, including provisions for the fuselage-induced disturbance velocities. In the resulting streamwise breakdown, the velocity components vary approximately linearly over the extent of each plenum. A corresponding segmentation of the side, top and bottom walls was also chosen on the same basis of approximately linear variations. Overall, this initial design had 64 individual plenum chambers, with 8 laterally at each of 8 streamwise segments.

After completion of the preliminary layout, alternative tunnel cross-section shapes were considered. For rectangular cross sections at a given axial station, the induced normal velocity for unconfined flow over representative wings varies considerably over the walls and becomes small in

the corners. If the corners are modified by wall segments that make the cross section octagonal, it was found that the normal velocity is nearly constant over these additional segments, if the segments are proportioned suitably. Also, the streamwise variation of the normal velocity is essentially the same for both the octagonal and rectangular shapes. Consideration of flow control requirements then indicates that the octagonal section does not require any more plenum chambers than the rectangular. Consequently, octagonal cross sections offer promise of more effective flow control, along with model span maximization for a given tunnel mass flow.

Finally, a conceptual design for a new plenum chamber and header configuration for providing both suction and blowing capability was developed. This design promises a considerable reduction in the complexity of the auxiliary pressure and suction circuits, compared to our two-dimensional design. However, it is regarded only as part of a first step toward a three-dimensional design. Overall, the conceptual design holds considerable promise for a three-dimensional demonstration experiment. Further research would be required to refine the requirements and to prepare a final detailed design.

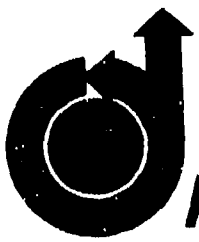

AIAA-81-0160

Numerical Simulations of a Segmented-Plenum, Perforated, Adaptive-Wall Wind Tunnel

J.C. Erickson, Jr. and G.F. Homicz, Calspan Corp., Buffalo, N.Y.

AIAA 19th AEROSPACE SCIENCES MEETING

January 12-15, 1981/St. Louis, Missouri

NUMERICAL SIMULATIONS OF A SEGMENTED-PLENUM, PERFORATED, ADAPTIVE-WALL WIND TUNNEL

J. C. Erickson, Jr.* and G. F. Homicz*
Aerodynamic Research Department
Calspan Advanced Technology Center
Buffalo, New York 14225

Abstract

Flow within the tunnel is simulated by modeling the incompressible interaction of the transpired turbulent boundary layers on the walls with the flow over the airfoil. Despite the fact that a finite number of plenum chambers can exert only imperfect control over the flow, it is demonstrated that one can still achieve what is for all practical purposes unconfined flow about the airfoil. Velocity differences produced at control surfaces outside the boundary layers by changing the pressure in one plenum chamber at a time, holding the other chamber pressures constant, are presented as influence functions. Implications of the analysis on tunnel design and automation are described.

Nomenclature

C_f, C_{f_o}	friction coefficients with and without transpiration, respectively
C_p	pressure coefficient on airfoil surface, $(p - p_\infty)/q_\infty$
C_{p_n}	pressure coefficient in plenum n, $(p_e - p_n)/q_\infty$, Eq. (2)
c	airfoil chord, Fig. 1
H	boundary-layer shape factor, δ^*/θ
h	distance from model to tunnel walls, Fig. 1
I_u, I_v	influence functions for u and v determined from simulations, defined in Eqs. (5) and (6)
$\hat{I}_u, \hat{I}_v$	idealized influence functions, defined in Eqs. (B-19) and (B-20)
l_n	length of plenum chamber n
M	Mach number
p	static pressure
q	dynamic pressure
U	total velocity component in x direction
u, v	perturbation velocity components in x, y directions
$\Delta u, \Delta v$	change in u, v after changing pressure in one plenum
δu	$\Delta u(\infty) - \Delta u(-\infty)$
v_δ	effective inviscid normal velocity at wall due to boundary-layer displacement (positive out of the wall), Eq. (4)
v_w	transpiration velocity at wall (positive out of the wall)
x, y	coordinate system with origin at airfoil quarter chord, Fig. 1
x_n	streamwise location of center of plenum chamber n
$\bar{x}$	$(x - x_n)/l_n$
y_c	distance from tunnel center line to control surfaces, Fig. 1
$\bar{y}$	y/h
α	airfoil angle of attack
β	$(1 - M_\infty^2)^{1/2}$
δ	boundary-layer thickness
δ^*	boundary-layer displacement thickness
θ	boundary-layer momentum thickness
ξ, η	coordinate system with origin at the center of plenum chamber n midway between the walls
ϕ	disturbance velocity potential in Appendix B

Subscripts

a	evaluated at control surface adjacent to plenum chamber n
e	condition at edge of boundary layer
n	condition in plenum n
o	evaluated at control surface opposite to plenum chamber n
∞	free-stream condition

1. Introduction

The concept of an adaptive-wall wind tunnel has attracted much attention recently[1-14] because of its promise for significant reductions in tunnel-wall interference, particularly in the transonic flight regime. An adaptive-wall wind tunnel[1-3] provides for active control of the flow in the vicinity of the test-section walls in order to minimize or eliminate the interference on the model. The distributions of the disturbance velocity components are measured at discrete points along control surfaces, or interfaces, in the flow field near the walls, but away from the model and outside the boundary layers on the walls. A theoretical representation for the flow exterior to these control surfaces, including the desired unconfined-flow boundary condition that all disturbances vanish at infinity, is used to establish the functional relationships which must be satisfied at the control surfaces by the measured disturbance velocities. If the measured velocities do not satisfy these relationships, an iterative procedure provides a new approximation for the flow field at the surfaces, and the wall control is readjusted until the measured quantities satisfy the functional relationships for unconfined flow.

Although the ultimate application is to fully three-dimensional flows, most of the adaptive-wall work to date has been carried out in two dimensions. Several different adaptive-wall implementations have been investigated experimentally in two dimensions, namely: impermeable, flexible walls,[9-11] perforated walls with constant plenum pressure but a porosity distribution that varies in the streamwise direction,[1-8] perforated walls with constant plenum pressure and a porosity which is uniform along each wall, but can vary from one wall to another[12] (including a three-dimensional application[13]), slotted walls with segmented plenum chambers,[14] and perforated walls with segmented

*Principal Engineer, AIAA Member

plenum chambers.[2-8] In the latter two ventilated-wall implementations, the pressure in each of the approximately twenty segmented plenum chambers can be controlled individually.

Simulations of adaptive-wall tunnels, including theoretical representations of the flow within the tunnel, played an important role in the early development of the concept. Simulations were carried out by several investigators for incompressible flows,[4,15] compressible, subcritical flows[16-19] and flows which are supercritical at the tunnel walls.[4,17-18] Not only did these studies demonstrate, numerically, that the overall procedure converged to unconfined flow, even for supercritical walls, but they also cast a great deal of light on the nature of the iterative process, especially the necessity for underrelaxation of the iterations. Furthermore, the accuracy required in the satisfaction of the functional relationships for unconfined flow was examined. These simulations were highly idealized, however. No attempt was made to model the flow in the vicinity of actual wall configurations. Instead, it was assumed that perfect control of either the streamwise, u, or normal, v, disturbance velocity component was available everywhere along the control surfaces, even at shock waves. The only exception was a study by Sears,[19] who considered an approximate representation of imperfect wall control and examined the errors in the converged solutions.

A two-dimensional perforated-wall, segmented-plenum configuration has been investigated extensively at Calspan in the One-Foot Wind Tunnel and the experimental configuration has been described previously.[2-8] It was not absolutely necessary to know the details of the flow in the vicinity of the walls in order to achieve unconfined-flow conditions. That is, if the desired disturbance velocities at the control surfaces could be set experimentally at each step of the iterative procedure, the details of the flow at the walls were of little interest. However, as the experimental investigation proceeded,[2-8] it was concluded that operational procedures for exercising wall control, including its eventual automation, could be enhanced by the development of more realistic simulations. These simulations would model the flow through the walls, the influence of that flow on the wall boundary layers and, consequently, the interaction with the flow within the control surfaces.

The simulation methodology developed for two-dimensional incompressible flows is described in Section II with some details given in Appendix A. Results for the incompressible-flow approximation should be representative of subsonic, subcritical flows in general. Results for the base-line simulation of a 6%-blockage NACA 0012 airfoil section at an angle of attack, α, of 4° are presented in Section III. Influence functions for the velocity perturbations introduced in the test section by changing the pressure in one plenum chamber at a time, while holding the pressure in the other chambers constant, are presented in Section IV and are compared with idealized influence functions which are derived in Appendix B. Finally, major conclusions drawn from the simulations are presented.

II. Methodology

Tunnel Configuration

The Calspan One-Foot Wind Tunnel[3-4] is a continuous-flow, closed-circuit facility that operates at Mach numbers from about 0.5 to 0.95 at a unit Reynolds number of 2×10^6 per foot. The adaptive-wall test section is two dimensional, with perforated top and bottom walls of 22.5% open-area ratio. The plenum chambers behind the perforated walls have been divided into 18 segments, 10 on the top and 8 on the bottom, and each segment is connected to a pressure and a suction source through individual control valves. The pressure source is the tunnel stilling chamber, and the suction source is an auxiliary compressor discharging into the tunnel circuit in the diffuser.

The model and test section are shown schematically in Fig. 1. The model is an NACA 0012 airfoil section with a 6-inch chord, c, (6% solid blockage) and is situated midway between walls that are located at $y = \pm h = \pm 6.00$ inches. The test-section instrumentation at the control surfaces consists of flow-angle probes and static-pressure pipes. The control surfaces are located outside the wall boundary layers, namely at $y_c = \pm 3.93$ in. The u and v disturbance velocity components are determined from measurements made with this instrumentation.[7]

The simulation procedure that is developed here does not provide directly for the simulation of the iterative process used in running the Calspan tunnel. That is, it does not simulate the plenum-pressure adjustment technique that is used[3-4] to set desired $u(x, \pm y_c)$ distributions in the tunnel. Such simulations could be developed later, if desired, on the basis of the model described here.

Calculation Method

Simulation of the flow within this adaptive-wall test section requires solutions for the flow over the airfoil in the presence of the viscous effects at the perforated, segmented, plenum-pressure-controlled walls. Outside of the wall boundary layers, the flow is assumed to be inviscid. For the inviscid flow, a procedure is required for calculating the flow over a model with prescribed distributions of the normal velocity components as boundary conditions at the walls. Two tools are needed to treat the wall boundary layers. First, a relationship is required between the transpiration velocity at the wall and the pressure drop across the wall. Second, a method is needed for calculating the characteristics of turbulent boundary layers with a transpiration velocity (either into or out of the walls) which is continuous over each plenum segment, but is likely to be discontinuous at junctions between segments.

Inviscid-Flow Model

A computer program developed originally to predict the two-dimensional flow over airfoils in a solid-wall wind tunnel with nonuniformly-sheared free streams[20-21] had been modified[15] to simulate the inviscid flow within an adaptive-wall wind tunnel and was adapted further for this investigation. The computer program can accommodate airfoils with arbitrary thickness and camber. In the program, the airfoil is represented by a vortex

distribution along its actual surface while the walls are represented by surface source distributions. These vortex and source distributions are broken up into small segments, each of which has a constant strength. Beyond a specified distance from the airfoil, both upstream and downstream, the source distributions at the walls are assumed to decay inversely with x as x approaches $\pm\infty$ because the source strength is closely related to the normal velocity there. The velocity components induced at any field point by each segment are given by closed-form algebraic expressions. Total velocity components due to the walls and the airfoil are then found by summing the contributions of all segments. The strength of each small segment is found by satisfying simultaneously the normal-flow boundary conditions $v(x, \pm h)$ at the walls, and the condition of no normal flow through the airfoil surface. The normal-flow boundary conditions are applied at the center of each segment. For N vortex and source segments, N algebraic equations result from the boundary conditions, but only $N-1$ of them are linearly independent, as shown by von Mises.[22] Addition of the Kutta-Joukowski condition completes the set of equations, which is solved using a smoothing technique.[23-24]

Transpired-Wall Characteristics

The relationship between the transpiration velocity at the wall, v_w, (taken as positive out of the wall) and the pressure drop across the wall was determined empirically. Data were obtained by Chew[25] for the same 22.5% open-area ratio walls (1/16 in. thick plate with 1/16 in. diameter holes on 1/8 in. centers). These data, which are only for suction, were measured at Mach numbers from 0.75 to 1.175. Although these data were an averaged v_w over a long run of plate with constant plenum pressure, p_n, and uniform pressure, p_e, in the test section, it was assumed that they could be applied in the present analysis on a point-by-point basis. The data of Ref. 25 are correlated reasonably well by

$$(p_e - p_n)/M_\infty q_\infty = 0.005 + 220.0\,(v_w/U_\infty)^2 \qquad (1)$$

where q_∞ and M_∞ are the free-stream dynamic pressure and Mach number. This result had to be extended to lower values of M_∞ and to include blowing. For blowing, Fig. 6.2 of Ref. 26 indicates that the data could reasonably be assumed to be anti-symmetric about $v_w = 0$. Ref. 26 also indicates that at lower Mach numbers, a Prandtl-Glauert behavior is expected. Therefore, a Prandtl-Glauert scaling was matched to the empirical variation of Eq. (1) and the anti-symmetric character was accounted for to obtain

$$C_{p_n} = (p_e - p_n)/q_\infty = f(M)\left[0.005 - 220.0\left|\frac{v_w}{U_\infty}\right|\left(\frac{v_w}{U_\infty}\right)\right] \qquad (2)$$

where

$$f(M) = \begin{cases} 0.5\,(1-M^2)^{-1/2}, & M \le (2)^{-1/2} \\ M, & M \ge (2)^{-1/2} \end{cases} \qquad (3)$$

For the incompressible-flow calculations of this study, $f(M) = 0.5$ was used.

Boundary-Layer Model

The most important characteristic of the boundary layer for the present application is its interaction with the inviscid flow. Lighthill[27] has described several ways of interpreting the displacement thickness and its effect on the inviscid flow. The interpretation chosen here is an extension to transpired walls of what Lighthill calls the method of "equivalent sources." In this procedure, the original wall surface is retained and the effect of the boundary layer on the inviscid flow is represented by a distribution of sources on this surface. This procedure has been used with success in calculations of the effect of the boundary layer on the flow over airfoils by several authors, as in Refs. 28 and 29, for example. In the present analysis then, the effect of the boundary layer on the inviscid flow is written as an inviscid velocity distribution $v_e(x)$ (taken as positive out of the wall) which, when applied at the actual wall surface, gives the proper displacement effect. For transpired boundary layers, v_e is given by

$$v_e(x) = v_w(x) + d\left[U_e(x)\,\delta^*(x)\right]/dx \qquad (4)$$

where δ^* is the boundary-layer displacement thickness, and U_e is the total inviscid streamwise velocity component outside the boundary layer. In general, $\delta^*(x)$ in Eq. (4) depends on $v_w(x)$, $U_e(x)$ and the initial conditions for the boundary-layer calculation.

Since the details of the boundary-layer profile are of less concern for this application, Head's well-known integral method[30] was adopted for the boundary-layer calculations. An outline of the method and representative results are given in Appendix A. The resulting boundary-layer equations are integrated for arbitrarily-prescribed distributions of $U_e(x)$ and $v_w(x)$ and appropriate initial conditions.

Simulation Logic

The establishment of the inviscid-flow calculation method, the wall-characteristic model, and the boundary-layer calculation method thus set the stage for development of a simulation procedure for approximating unconfined flow in the tunnel while accounting for the perforated walls with segmented plenum chambers. First, however, ideal point-by-point wall control was examined from the standpoint of transpired turbulent boundary-layer behavior.

Both ideal and segmented-plenum wall control simulations require use of the inviscid-flow program to calculate the unconfined flow about the model at a given angle of attack. This provides the unconfined-flow distributions $u(x, \pm h)$ and $v(x, \pm h)$ at the walls so that $U_e(x) = U_\infty + u(x, \pm h)$ and hence $p_e(x)$ at each wall are known.

Ideal Wall Control

Investigation of ideal wall control was initiated in order to shed light on how the wall boundary-layer and transpiration velocity characteristics must interact to provide perfect point-by-point control of the flow within the tunnel. Calculations with this procedure then serve as guidelines for simulations of the imperfect wall control that exists in the segmented-plenum configuration.

The unconfined-flow distributions $u(x, \pm h)$ and $v(x, \pm h)$ at the walls, in the form of $U_e(x)$ and $v_e(x)$, are specified on a point-by-point basis in order to calculate the ideal, continuous wall transpiration velocity distribution $v_w(x)$ which would reproduce exactly the unconfined flow. The boundary-layer problem posed by this ideal wall control is an inverse one because U_e and v_e are prescribed and v_w must be found. Because of the implicit nature of their dependence on v_w, the governing equations cannot be integrated directly in this case, and an iterative solution becomes necessary. This is carried out at each step of the integration as follows. A value of v_w constant over the length of the step is assumed, and the equations are integrated for the step. Eq. (4) is evaluated next to determine the calculated v_e which is compared with the desired value. If they do not agree to a specified accuracy, the value of v_w is readjusted and the process is repeated iteratively until the calculated v_e agrees with the prescribed value. The $v_w(x)$ distributions which result from this calculation provide a useful reference for beginning more realistic segmented-plenum calculations, as shown next.

Segmented-Plenum Wall Control

The modeling of segmented-plenum wall control also relies on the unconfined-flow distributions $p_e(x)$ and $v_e(x)$. The heart of the procedure is then the determination of p_n, the plenum pressure in the n^{th} plenum chamber. This is accomplished iteratively as follows. At the center of each plenum chamber, x_n, the inviscid-flow pressure, $p_e(x_n)$, is known, and since an initial estimate for $v_w(x_n)$ can be obtained from the ideal-wall calculation, an initial guess for p_n can be found from Eqs. (2) and (3). With p_n and $p_e(x)$ then known, the corresponding initial approximation to $v_w(x)$ is found over the length of each plenum chamber by Eqs. (2) and (3). In general, this procedure leads to discontinuities in $v_w(x)$ at the boundaries between plenum chambers. The boundary-layer calculation is then made over each plenum chamber in turn on the basis of the prescribed input $p_e(x)$, $v_w(x)$, and the initial conditions. The effective inviscid velocity distribution at the walls, $v_e(x)$, is found from the computed results and Eq. (4). The integral of $v_e(x)$ over each plenum chamber is then compared with the integral of the unconfined-flow distribution $v(x, \pm h)$ over the same plenum. (It should be noted that in the different coordinate systems used for the inviscid-flow and boundary-layer calculations, $v(x, h) = -v_e(x)$ and $v(x, -h) = v_e(x)$.) The p_n are then revised and the boundary-layer calculation is repeated until the integrals of $v_e(x)$ and $v(x, \pm h)$ over each plenum agree. Satisfaction of this condition, locally at each plenum, insures that the integral of the source elements over each wall is zero as is the case for fully unconfined flow. This is equivalent to the fact that the drag on the airfoil is zero in unconfined, inviscid flow.

Once the $v_e(x)$ distributions at both walls have been found in this way, they are used as boundary conditions in the inviscid-flow program to calculate the flow over the airfoil in the presence of the segmented-plenum, perforated-wall constraints. Results found by such a procedure can be used to investigate the magnitude of the errors introduced by having segmented-plenum, imperfect wall control instead of ideal, perfect wall control; this is discussed in the next section.

III. Base-Line Simulation Results

The example chosen for the base-line simulation is the NACA 0012 airfoil of the experiments at an angle-of-attack, α, of 4°. This choice gives a good balance between the lift and thickness effects on the disturbance velocity field at the control surfaces and walls. Wall and control-surface locations at 1.0 and 0.655 chords above and below the model correspond to the experimental configuration. Within this geometrical input, both ideal and segmented-plenum wall control were examined.

For ideal wall control, the calculated distribution of $v_w(x)$ and the prescribed, unconfined-flow distribution $v_e(x)$ are presented in Fig. 2 for the upper wall. Note that upstream of the origin there is suction and a favorable pressure gradient so $v_e(x)$ follows $v_w(x)$ closely. Downstream of the origin there is blowing and an adverse pressure gradient, which give rise to a ratio of v_e to v_w of two or greater, i.e., an amplification of the wall velocity when blowing is present. Such behavior is typical, and the reasons for it are described at greater length in Appendix A.

The results of Fig. 2 were used to initiate the iterative calculation of the streamwise distributions of $v_w(x)$ for the segmented-plenum model, as described in Section II. The result for the upper wall is shown as the solid curve in Fig. 3; results for the lower wall display a similar behavior. The tick marks on the abscissa of Fig. 3 correspond to the junctions between plenum chambers as shown in Fig. 1. For comparison, the ideal point-by-point distribution of $v_w(x)$ from Fig. 2 is shown as the dashed curve on Fig. 3. The additional curves and data points on this and the next few figures will be discussed in Section IV. The streamwise distributions of $v_w(x)$ that result from the matching procedure have very large variations over each plenum chamber, with discontinuities at the junctions between plenum chambers.

The discontinuous $v_w(x)$ distributions yield correspondingly large variations in $v_e(x)$ from the boundary-layer calculations, particularly as amplified when blowing is present. The distribution of $v_e(x)$ for the upper wall is given as the solid curve in Fig. 4, along with the dashed curve, which is the unconfined-flow distribution $v(x, h)$ from Fig. 2. The large variations in $v_e(x)$ and the associated discontinuities at the plenum junctions are certainly not realistic physically. The response of the boundary layers at the junctions would not have such an extreme character. Nevertheless, these details do not have a significant influence on the resultant flow conditions at the control surfaces or model, as will be seen below, so this representation was retained.

The segmented-plenum $v_e(x)$ distribution of Fig. 4, and its counterpart at the lower wall, were used as boundary conditions in the calculation of the inviscid flow about the airfoil. Results for the streamwise and normal velocity components at the upper and lower control surfaces are presented in Figs. 5 and 6 by the crosses. The unconfined-flow distributions are given by the dashed curve while the results given by the circles will be discussed in Section IV.

Examination of Figs. 5 and 6 indicates that the agreement between the segmented-plenum and unconfined-flow distributions is generally excellent where suction is present at the walls, namely upstream of the origin at the upper control surface and downstream of the origin at the lower control surface. The discrepancies observed in u at the upstream and downstream limits of the test section result from the truncation of $v_e(x)$ from the distributions shown in Fig. 4 to zero upstream and downstream of the controlled part of the test-section walls. Repeating the inviscid flow calculation with $v_e(x)$ equal to the unconfined-flow distributions beyond the controlled sections resulted in excellent agreement of u at the upstream and downstream limits of the test section.

Overall, the results indicate that the finite size of the plenum chambers and the attendant large variations in $v_e(x)$ from modeling the flow at the walls do not prevent the realization of a good approximation to the unconfined-flow distributions for these low-speed flow conditions. This is consistent with the earlier experimental demonstrations of the adaptive-wall concept for flows which are supercritical at the model, but subcritical at the control surfaces and walls.[3,4] In those cases, the desired flows could be set up experimentally without large fluctuations in the measured streamwise velocity components from point to point.

The distributions of the pressure coefficient, C_p, on the airfoil surface are given in Fig. 7, with the dashed lines indicating unconfined flow and the crosses the results of the segmented-plenum model. The excellent agreement shown is confirmed by integrating the C_p distributions to obtain normal force coefficients of 0.490 for unconfined flow and 0.482 for the segmented-plenum model, a difference of only 1.6%. The remarkable agreement in both the airfoil C_p distributions and the disturbance velocity distributions at the control surfaces, despite the unrealistic nature of the $v_e(x)$ distributions, results from the elliptic nature of the governing equations of motion for the flow within the tunnel. Furthermore, this behavior is representative of the actual tunnel flow.

We believe that these simulations, despite the exaggerations in the variations of $v_w(x)$ and $v_e(x)$ over the individual plenum chambers, especially at the plenum junctions, model the essential features of the flow near the walls. We believe further that the qualitative features of these base-line simulations, although they are strictly for incompressible flow only, can be generalized to compressible, subcritical flow because there are no fundamental differences in the flow phenomena involved. However, once the flow becomes supercritical at the walls, different phenomena are involved and modeling of the shock-wave/boundary-layer interaction becomes necessary.

The existing simulation methodology can serve as the basis for further investigations of the behavior of adaptive-wall wind tunnels with this wall configuration. For example, it can be used to examine the effects of plenum chamber number and size and of the porosity distribution of the perforated walls. Also, it forms a framework for the development of more systematic procedures for adjusting the tunnel flows that are required at each step of the overall adaptive-wall iterative process.[3-4] These adjustment procedures would provide the logic for the ultimate automation of adaptive-wall wind tunnels. A first step toward logical procedures for tunnel adjustment is described in the next section.

IV. Influence Functions Due to Plenum Pressure Change

As a first step toward the development of automated wall-adjustment procedures, a study was made of the effect on the flow produced by changing the pressure, p_n, in one plenum chamber at a time, while holding the pressure in the other chambers constant. The example described in Section III was chosen for these calculations. Numerous cases were investigated, including plenum chambers at various streamwise locations in the tunnel with suction and with blowing.

In one pair of examples, the pressure in plenum 6 (see Fig. 1) was changed by amounts such that $v_w(x_6)/U_\infty$ was changed by ± 0.0100 (and so C_{p_6} by -0.031 and 0.053, respectively), where x_n is the x-coordinate of the center of plenum n. The overall changes in $v_w(x)$ over plenum 6 are shown in Fig. 3. The $v_e(x)$ distributions which result from the boundary-layer calculation are shown on Fig. 4. It is remarkable that these resulting $v_e(x)$ distributions are changed significantly along the length of that plenum chamber, but negligibly at all other chambers, even those immediately downstream. This behavior occurs for all examples considered, whether the basic condition is suction or blowing at the plenum chamber where the pressure change is made. This does not imply that the boundary layer is unaffected downstream. Many of its properties, e.g., δ^* and θ, change appreciably downstream; however, $d(U_e\delta^*)/dx$ and hence $v_e(x)$ from Eq. (4) are not affected significantly there.

Results from the inviscid-flow calculation for the increased suction example of Fig. 4 ($\Delta v_w(x_6)/U_\infty = -0.0100$ or $\Delta C_{p_6} = 0.053$) are shown as the circles in Figs. 5 and 6. When compared with the base-line simulation represented by the crosses, it is observed in Fig. 5 that u has increased upstream and decreased downstream of plenum 6 at both control surfaces with a crossover at plenum 6 itself. This behavior is consistent with the presence of a sink at the wall of a confined channel, such as exists here. An increase in suction (or a decrease in blowing) at one plenum chamber gives rise to an increased sink strength at that wall location. Conversely, other results not presented here show that a decrease in suction (or an increase in blowing) gives rise to an increased source strength and the differences in the u distributions will be of opposite sign. This source (or sink) effect in an otherwise confined channel is felt even to large distances upstream and downstream, as observed in Fig. 5.

The sink effect described here was observed in an experiment performed in the Calspan One-Foot Adaptive-Wall Tunnel before this analysis was undertaken. The suction was increased simultaneously at both plenum chambers 5 and 15. The increased suction increased the flow velocity at that station far upstream where M_∞ is measured and set. In order to maintain the desired M_∞, compensating adjustments were made in the tunnel drive, effectively removing the upstream perturbation.

Therefore, during experimental iterations at a constant M_∞, one can expect the primary changes in u to occur at, and downstream of, the plenum being adjusted.

On the other hand, the changes in the v distributions at the control surfaces, as shown in Fig. 6, occur only locally in the immediate vicinity of the plenum chamber at which the control is changed. There is only a slight effect at the same streamwise position on the opposite control surface and negligible effect upstream and downstream at both control surfaces. This localized behavior also was observed in the One-Foot Tunnel experiments.

The results of all the calculations in which the pressure in a single plenum chamber was changed, while holding the remainder at their original pressures, were analyzed and cast in terms of influence functions. The notation $\Delta u(x)$ will refer to the difference given by the streamwise velocity perturbation after a plenum adjustment has been made minus its value in the base-line simulation; an analogous definition is made for $\Delta v(x)$. If $\delta u \equiv \Delta u(\infty) - \Delta u(-\infty)$ is the difference in this calculated perturbation over the length of the test section, then a natural form for expressing the influence functions is

$$I_u(\bar{x}) = \left[\Delta u(\bar{x}) - \Delta u(-\infty)\right] / \delta u \qquad (5)$$

$$I_v(\bar{x}) = -\left|\Delta v(\bar{x}) / \delta u\right| \qquad (6)$$

where $\bar{x} = (x - x_n)/l_n$ is a coordinate normalized by l_n, the length of plenum n. The normalization in Eqs. (5) and (6) reflects the experimental situation in which the tunnel operator removes any Δu that is introduced far upstream so as to maintain a constant M_∞; hence $I_u(-\infty) = 0$ and $I_u(\infty) = 1$. The form of I_v, including the sign, is chosen so that pressure changes at both upper and lower plenum chambers are consistent with the results of Appendix B. (See the discussion leading up to Eqs. (B-19) and (B-20).)

The influence functions I_{u_a} and I_{v_a}, where the subscript a denotes the control surface adjacent to plenum n, are presented in Figs. 8 to 11 as functions of $\bar{x}$, where the lines at $\bar{x} = \pm 0.5$ demarcate the ends of plenum n. In Figs. 8 and 9, the data from all the plenum chambers considered in the calculations are plotted, namely plenum chambers 2, 3 and 6 with increased suction, plenum 6 with decreased suction, and plenum chambers 11, 15 and 16 with increased blowing. For comparison, idealized influence functions, $\hat{I}_{u_a}$ and $\hat{I}_{v_a}$, are plotted as solid curves. These idealizations are derived in Appendix B using linearized theory without a model present and assume a uniform $\Delta v_e(x)$ between $\bar{x} = \pm 0.5$. Figs. 10 and 11 are plotted to an enlarged $\bar{x}$ scale to illustrate how the details of the changes in the v_e distribution in Fig. 4 affect the influence functions in the immediate vicinity of plenum 6. Since the increments in v_e in that vicinity are larger at the downstream end of the plenum than at the upstream end, I_{u_a} and I_{v_a} in Figs. 10 and 11 are skewed as shown. Farther away from the plenum the idealized influence functions, which assume a constant Δv_e along the plenum, provide a satisfactory approach to the asymptotic conditions.

The influence functions I_{u_o} and I_{v_o}, where the subscript o denotes the control surface at the opposite side of the tunnel from plenum n, are presented in Figs. 12 and 13. Again, the details of the boundary-layer behavior at plenum n primarily affect the distribution only in the immediate vicinity of that plenum while the behavior away from this region is approximated reasonably well by the idealized representation, $\hat{I}_{u_o}$ and $\hat{I}_{v_o}$.

The fact that the idealized distributions $\hat{I}_u$ and $\hat{I}_v$ derived for linearized, empty-tunnel flows are such a good representation of the distributions computed with the model present, I_u and I_v, is quite remarkable. As can be seen from the derivation of the linearized model, the general behavior is a function of plenum length and the distance of the control surfaces from the walls. It is expected that other segmented-plenum configurations, e.g., those with slotted walls or those with perforated walls of different open-area ratios or slanted holes, should exhibit the same general characteristics.

The relationship between the change in pressure, Δc_{p_n}, say, in plenum n and the total change in the u component, δu, will depend on the wall geometry, of course. This relationship depends on the details of the boundary layer and the wall characteristics and for the Calspan One-Foot Tunnel walls is implicitly represented by the form of Eqs. (1) to (4). For example, in the cases presented in Figs. 3 and 4, the increment $\Delta c_{p_6} = -0.0310$ results in $\delta u/U_\infty = 0.0069$ and the increment $\Delta c_{p_6} = 0.0530$ results in $\delta u/U_\infty = -0.0037$, where these cases represent increments in $\Delta v_w(x_6)/U_\infty$ of 0.0100 and -0.0100, respectively.

There are two important next steps in the development of this simulation and influence-function technique. The first would be the extension of the analysis to compressible flows. As mentioned in Section III, no significant differences are expected until supercritical-flow conditions are reached. Then it is expected that I_u and I_v would depart significantly from the idealized subsonic behavior. The other step would be the experimental verification of the influence-function behavior by measuring the appropriate quantities. This would be straightforward but was beyond the scope of the experimental programs performed thus far. Bodapati, et al.[14] have measured I_{v_a} and I_{v_o} for empty-tunnel conditions in their segmented-plenum, slotted-wall test section. Their results are generally of the form predicted here.

Once the validity of the predicted influence-function behavior has been established explicitly, the procedures could be used to investigate automated control procedures. For example, in the Calspan experiments, the u component is set along the control surfaces so that I_{u_a} and I_{u_o} are of principal importance. In order to effect a change in u at each control point, the sum of the changes induced at that point due to pressure changes Δc_{p_n} in each of the n plenum chambers must be found. Since similar changes are desired at all the control points, a system of equations can be derived relating the prescribed changes in u to the plenum pressure changes. This system of equations must be solved for the Δc_{p_n} that are necessary to achieve the desired flow. Since the influence functions of Eqs. (5) and (6) are defined

in terms of δ_w, this quantity must be related to the pressure change ΔC_{p_n} for each plenum. As discussed, this relationship is a highly nonlinear one. Use of both the idealized and the more exact relationships could be investigated by simulations to establish the accuracy to which the influence functions must be represented in the vicinity of each control plenum to iterate automatically and quickly to unconfined flow.

V. Concluding Remarks

The following are viewed as the principal results and conclusions drawn from the present investigation.

To the authors' knowledge, the base-line simulation represents the first realistic numerical demonstration that an adaptive-wall wind tunnel with imperfect wall control can nevertheless achieve what is, for most practical purposes, unconfined flow about the model (see Fig. 7). This is accomplished in spite of the fact that the modeling of the wall transpiration characteristics and boundary layers was relatively crude, and if anything exacerbated the effects of imperfect control.

The local boundary-layer displacement effect, as embodied by $v_e(x)$ in Eq. (4), is influenced primarily by pressure changes in the plenum chambers in the immediate vicinity, and is somewhat dependent on the detailed distributions of transpiration velocity through the walls (see Fig. 4).

When appropriately defined, the influence functions, I_u and I_v, appear to fall on a more or less universal curve independent of plenum location and whether suction or blowing is being applied (see Figs. 8-13). However, the relationship between ΔC_{p_n} and the normalization factor (Eqs. (5) and (6)) will depend on the particular tunnel configuration.

The influence functions well away from the immediate vicinity of a given plenum appear to depend only on the integrated normal velocity and may be predicted adequately by a simplified theory.

Though the present simulations are confined to low-speed flow for simplicity, the extension to compressible subsonic speeds is not expected to alter these conclusions qualitatively, provided the flow remains subcritical. For supercritical wall conditions, which may prove of great practical significance, a model of shock-wave/boundary-layer interaction would have to be added; the attendant possibility of separated flow at the wall and the sensitivity of shock-wave position to details of the flow at the walls may lead to qualitatively new phenomena. Once this question is answered, the application of the model to simulating the actual iterative wall-control process[3-4] at high subsonic speeds should be possible.

Acknowledgments

This investigation was sponsored jointly by the Office of Naval Research and the Air Force Office of Scientific Research. The authors wish to thank the technical monitors, Mr. M. Cooper of ONR and Dr. J. D. Wilson of AFOSR, as well as their Calspan colleagues Dr. J. P. Nenni and Mr. C. E. Wittliff and Calspan consultant Prof. W. R. Sears of the University of Arizona for their useful discussions of this research.

References

1. Ferri, A. and Baronti, P. "A Method for Transonic Wind Tunnel Corrections" AIAA Journal, Vol. 11, No. 1, January 1973, pp. 63-66
2. Sears, W.R. "Self-Correcting Wind Tunnels" (The Sixteenth Lanchester Memorial Lecture) Aeronautical Journal, Vol. 78, No. 758/759, February/March 1974, pp. 80-89
3. Sears, W.R., Vidal, R.J., Erickson, J.C., Jr. and Ritter A. "Interference-Free Wind-Tunnel Flows by Adaptive-Wall Technology" ICAS Paper No. 76-02, Tenth Congress of the International Council of the Aeronautical Sciences, Ottawa, Canada, 3-8 October 1976; also Journal of Aircraft, Vol. 14, No. 11, November 1977, pp. 1042-1050
4. Vidal, R.J., Erickson, J.C., Jr. and Catlin, P.A. "Experiments with a Self-Correcting Wind Tunnel" AGARD-CP-174, October 1975
5. Vidal, R.J. and Erickson, J.C., Jr. "Experiments on Supercritical Flows in a Self-Correcting Wind Tunnel" AIAA Paper No. 78-788, AIAA 10th Aerodynamic Testing Conference, San Diego, CA, 19-21 April 1978
6. Vidal, R.J. and Erickson, J.C., Jr. "Research on Adaptive Wall Wind Tunnels" AEDC Report No. AEDC-TR-78-36, November 1978
7. Erickson, J.C, Jr. Wittliff, C.E. and Daughtry, D.C. "Further Investigations of Adaptive-Wall Wind Tunnels" AEDC Report No. AEDC-TR-80-34, October 1980
8. Erickson, J.C., Jr., Wittliff, C.E. and Padova, C. "Adaptive-Wall Wind-Tunnel Experiments with Supercritical Flow at the Walls" Calspan Report No. RK-6040-A-2 (to be published)
9. Chevallier, J.P. "Soufflerie Transonique a Parois-Adaptables" AGARD-CP-174, October 1975; also translated into English as European Space Agency Report ESA-TT-326, October 1976, available as NASA Accession No. N77-13085
10. Goodyer, M.J. and Wolf, S.W.D. "The Development of a Self-Streamlining Flexible Walled Transonic Test Section" AIAA Paper No. 80-0440, AIAA 11th Aerodynamic Testing Conference, Colorado Springs, CO, 18-20 March 1980
11. Ganzer, U. "Adaptable Wind Tunnel Walls for 2-D and 3-D Model Tests" ICAS Paper No. 23.3, 12th Congress of the International Council of the Aeronautical Sciences, Munich, Germany, 13-17 October 1980
12. Kraft, E.M. and Parker, R.L., Jr. "Experiments for the Reduction of Wind Tunnel Wall Interference by Adaptive-Wall Technology" AEDC Report No. AEDC-TR-79-51, October 1979
13. Parker, R.L., Jr. and Sickles, W.L. "Application of Adaptive Wall Techniques in a Three-Dimensional Wind Tunnel with Variable Wall Porosity" AIAA Paper No. 80-0157, 14-16 January 1980

14. Bodapati, S., Schairer, E. and Davis, S. "Adaptive-Wall Wind-Tunnel Development for Transonic Testing" AIAA Paper No. 80-0441, AIAA 11th Aerodynamic Testing Conference, Colorado Springs, CO, 18-20 March 1980
15. Erickson, J.C, Jr. and Nenni, J.P. "A Numerical Demonstration of the Establishment of Unconfined-Flow Conditions in a Self-Correcting Wind Tunnel" Calspan Report No. RK-5070-A-1, November 1973
16. Sears, W.R. "A Note on Adaptive-Wall Wind Tunnels" Zeitschrift fur angewandte Mathematik und Physik, Vol. 28, 1977, pp. 915-927
17. Lo, C.F. and Kraft, E.M. "Convergence of the Adaptive-Wall Wind Tunnel" AIAA Journal, Vol. 16, No. 1, January 1978, pp. 67-72
18. Lo, C.F. and Sickles, W.L. "Analytical and Numerical Investigation of the Convergence of the Adaptive-Wall Concept" AEDC Report No. AEDC-TR-79-55, November 1979
19. Sears, W.R. "Adaptive Wind Tunnels with Imperfect Control" Journal of Aircraft, Vol. 16, No. 5, May 1979, pp. 344-348
20. Brady, W.G. and Ludwig, G.R. "Theoretical and Experimental Investigation of the Aerodynamic Properties of Airfoils Near Stall in Two-Dimensional Nonuniformly Sheared Flow" U.S. Army AVLABS TR 66-36, June 1966
21. Ludwig, G.R. and Erickson, J.C., Jr. "Airfoils in Two-Dimensional Nonuniformly Sheared Slipstreams" Journal of Aircraft, Vol. 8, No. 11, November 1971, pp. 874-880
22. von Mises, R. Theory of Flight McGraw-Hill, New York, 1945, pp. 188-198
23. Phillips, B.L. "A Technique for the Numerical Solution of Certain Integral Equations of the First Kind" Journal of the Association for Computing Machinery, Vol. 9, No. 1, January 1962, pp. 84-97
24. Twomey, S. "On the Numerical Solution of Fredholm Integral Equations of the First Kind by the Inversion of the Linear System by Quadrature" Journal of the Association of Computing Machinery, Vol. 10, No. 1, January 1963, pp. 97-101
25. Chew, W.L. "Cross-Flow Calibration at Transonic Speeds of Fourteen Perforated Plates With Round Holes and Airflow Parallel to the Plates" AEDC Report No. AEDC-TR-54-65, July 1955
26. Goethert, B.H. Transonic Wind Tunnel Testing Pergamon Press, New York, 1961, Chapter 11
27. Lighthill, M.J. "On Displacement Thickness" Journal of Fluid Mechanics, Vol. 4, No. 4, August 1958, pp. 383-392
28. Hess, J.L. "Review of Integral-Equation Techniques for Solving Potential-Flow Problems With Emphasis on the Surface Source Method" Computer Methods in Applied Mechanics and Engineering, Vol. 5, 1975, pp. 145-196
29. McInik, R.E. "Wake Curvature and Trailing Edge Interaction Effects in Viscous Flow Over Airfoils" NASA CP-2045, Part 1, Vol. I, March 1979, pp. 255-270
30. Head, M.R. "Entrainment in the Turbulent Boundary Layer" Aeronautical Research Council, R & M No. 3152, September 1958
31. Thompson, B.G.J. "The Calculation of Shape-Factor Development in Incompressible Turbulent Boundary Layers With or Without Transpiration" in Part I of "Recent Developments in Boundary Layer Research" AGARDograph 97, May 1965
32. McQuaid, J. "The Calculation of Turbulent Boundary Layers With Injection" R & M No. 3542, January 1967
33. Ludwieg, H. and Tillmann, W. "Investigations of the Wall-Shearing Stress in Turbulent Boundary Layers" NACA TM 1285, May 1950
34. Simpson, R.L., Moffat, R.J. and Kays, W.M. "The Turbulent Boundary Layer on a Porous Plate: Experimental Skin Friction With Variable Injection and Suction" International Journal of Heat and Mass Transfer, Vol. 12, 1969, pp. 771-789
35. Schlichting, H. Boundary Layer Theory McGraw-Hill, New York, 1955, pp. 229-236
36. Jacocks, J.L. "An Investigation of the Aerodynamic Characteristics of Ventilated Test Section Walls for Transonic Wind Tunnels" Ph.D. Thesis, University of Tennessee, Knoxville, TN, December 1976 (University Microfilms No. 77-10777)
37. Erdelyi, A., Magnus, W., Oberhettinger, F. and Tricomi, F.G., Editors of Tables of Integral Transforms, Vol. 1, Bateman Manuscript Project, McGraw-Hill, New York, 1954, p. 88, Eq. 7
38. Glauert, H. "Theoretical Relationships for an Airfoil With Hinged Flap" Aeronautical Research Council, R & M No. 1095, April 1927
39. Spence, D.A. "The Lift on a Thin Aerofoil With a Jet-Augmented Flap" The Aeronautical Quarterly, Vol. 9, August 1958, pp. 287-299

Appendix A

Boundary-Layer Model and Amplification Effect

For the purpose of studying the effects of the boundary layer on the inviscid interior flow, it is the integral properties of the layer, as opposed to the detailed profiles across it, which are of primary interest. Accordingly, an integral (as opposed to finite-difference) method was chosen as the most efficient means to model the boundary layer. The particular method used is that first proposed by Head,[30] which had been applied successfully by others in predicting the behavior of transpired turbulent layers.[31-32]

Basically, Head's method consists of simultaneously solving three equations. The first is his so-called entrainment equation,

$$\frac{1}{U_e}\frac{d}{dx}(U_e\,\theta\,H_1) = F(H_1)+\frac{v_w}{U_e} \qquad \text{(A-1)}$$

where H_1 is a modified shape factor defined by $H_1 = (\delta-\delta^*)/\theta$, and U_e is the local streamwise velocity at the layer's edge. Here δ, δ^*, and θ refer respectively to the boundary-layer, displacement, and momentum thicknesses. H_1 is related to the more conventional shape factor, $H = \delta^*/\theta$, by $H_1 = G(H)$. The functions $F(H_1)$ and $G(H)$ were empirically derived from existing data. The rationale behind Eq. (A-1) can be found in Refs. 30-32.

The second equation is:

$$\frac{d\theta}{dx}+\frac{\theta}{U_e}(H+2)\frac{dU_e}{dx}-\frac{v_w}{U_e} = \frac{C_f}{2} \qquad \text{(A-2)}$$

which is simply the well known von Karman integral momentum equation derived in most boundary layer texts. The only new quantity introduced is C_f, the local skin-friction coefficient.

Head's original applications were to solid-wall boundary layers, for which he used the Ludwieg-Tillmann correlation[33] to predict C_f. For the present application this procedure was modified as follows: first, the Ludwieg-Tillmann correlation was used to compute C_{f_o}, the skin-friction coefficient that would obtain if no transpiration were present,

$$C_{f_o} = (0.246)\,10^{-0.678H}\,Re_\theta^{-0.268} \qquad \text{(A-3)}$$

where Re_θ is the local momentum-thickness Reynolds number. This value was then corrected for the effects of blowing or suction via the empirical correction suggested by Simpson, Moffat, and Kays:[34]

$$\frac{C_f}{C_{f_o}} = \left[\frac{\ln|1+B|}{B}\right]^{0.7} \qquad \text{(A-4)}$$

where $B = 2v_w/C_f U_e$. Due to the implicit dependence of B on C_f and the transcendental nature of Eq. (A-4), it had to be solved using Newton-Raphson iteration, but the convergence is quite rapid.

The above system of three equations (two differential, one algebraic) was solved for the three unknowns θ, H and C_f using a Runge-Kutta procedure. Required inputs are the distributions $U_e(x)$ and $v_w(x)$, and initial conditions on θ and H at the starting point.

To validate the boundary-layer program, its predictions were compared with experimental data of other investigators for several representative flows, including various streamwise pressure gradients with and without transpiration. An example which is of particular interest to the present application is an experimental configuration investigated by McQuaid.[32] In this case, there was uniform blowing of constant strength up to $x = 17.5$ in.; downstream of this point v_w was nominally zero. The equations were integrated up to $x = 17.5$ in. using the experimental values of θ and H at $x = 11.5$ in. as initial conditions and $v_w/U_\infty = 0.0035$. The calculated values of θ and H at $x = 17.5$ in. were then used as initial conditions for further integration downstream with $v_w/U_\infty = 0$. Results of the calculation are shown in Fig. 14. The predicted development of δ^*, θ and H from their initial values agrees well with the data. In particular, the calculated distributions display discontinuities in their slopes at the discontinuity in blowing velocity, and this behavior reflects the observed variation there reasonably well. This and other comparisons gave confidence in the ability of the model to predict the integral properties of the boundary layer adequately.

The first application of the boundary-layer model specifically to the Calspan One-Foot Tunnel configuration shown in Fig. 1 was done to see whether it confirmed a so-called "boundary-layer amplification" effect that had been noted in adjusting the plena to achieve a desired flow condition. In early experiments with the model present in the tunnel,[4] it was observed in many cases that the normal velocity measured by a probe 1.5 in. from the wall was considerably greater in magnitude than v_w, the velocity at the wall itself. Although part of this amplification was due to the increase over that distance in the inviscid velocity induced by the model, there was still a marked increase in the magnitude of the amplification as more blowing was applied. Accordingly, the present boundary-layer computational method was used to examine the relationship between v_e and v_w; i.e., to cast light on the amplification of the normal velocity across the boundary layer. For these calculations, flow without the model present was represented by assuming uniform flow over a flat surface with zero streamwise pressure gradient. With the assumption of constant transpiration velocity along the controlled section, calculations were made to cover the range $-0.0275 \le v_w/U_\infty \le 0.0150$. A plot of v_e/U_∞ vs v_w/U_∞ over part of this range is given Fig. 15 for locations corresponding to the upstream and downstream limits of the controlled test section length and shows only a weak dependence on x. When $v_w/U_\infty < -0.0050$, there appears to be an asymptotic suction behavior of the same nature that exists in laminar flow.[35] That is, the boundary layer ceases to grow, and its integral properties, particularly δ^*, become independent of x. Eq. (4) then predicts that $v_e = v_w$, so that the slope of the curve in this region is just unity, and there is no amplification by the boundary layer. However, as v_w/U_∞ increases above -0.0050, the slope of the curve in Fig. 15 increases significantly, and in the region of blowing, v_e greatly exceeds v_w. Not only has the first term on the right-hand side of Eq. (4) increased, but this in turn has greatly magnified the boundary-layer growth represented by the second term; since these terms are additive, amplification of the normal velocity across the layer results. Jacocks[36] has performed calculations with a finite-difference boundary-layer code and experimentally-determined wall-pressure data with a model present. The envelope which he determined for his calculated results is quite similar to that exhibited in Fig. 15.

In addition to helping in an understanding of the simulation results discussed in the main text, Fig. 15 carries a very practical lesson for the users of such adaptive-wall tunnels; viz., control of the inviscid flow via plenum adjustments is linear and well-behaved for suction, but likely to be highly nonlinear when blowing is needed.

Appendix B

Idealized Influence Functions

In this appendix, an idealized form of the influence functions of Section IV is found. A linear approximation for the flow in a tunnel without the model present has been chosen. Thus, the idealized analysis here will be related to the differences found in the results of the simulations of Section IV when the pressure is changed in one plenum, while holding the pressure constant in the other chambers. These relationships will be pointed out as the analysis proceeds.

The ξ-η coordinate system used here is the same as the x-y system in Fig. 1 except that the origin of ξ is located in line with the center of the plenum chamber being adjusted, which has length ℓ_n, whereas the origin of x is at the quarter chord of the model. In the ξ-η system, the flow investigated is induced by a uniform normal velocity, v_1, imposed at the upper wall over the interval $-\ell_n/2 \le \xi \le \ell_n/2$ with $v = 0$ prescribed everywhere else on the upper wall as well as on the entire lower wall. The free-stream

velocity is U_∞ and the streamwise disturbances, u, are assumed to be zero far upstream, just as in the experiments. The magnitude of v_1 is related to the differences in the integral of $v_e(x)$ over the length of plenum n as carried out before and after changing the pressure in that plenum.

The linearized compressible-flow analysis is carried out in the Prandtl-Glauert approximation, so that a disturbance velocity potential, ϕ, exists and satisfies

$$\beta^2 \phi_{\xi\xi}(\xi,\eta) + \phi_{\eta\eta}(\xi,\eta) = 0 \qquad \text{(B-1)}$$

where $\beta^2 = 1 - M_\infty^2$ and the subscripts ξ and η denote partial differentiation with respect to those variables. The boundary conditions that the u disturbance-velocity component must be zero at infinity upstream and that v at the walls must be as described above are expressed as

$$\phi_\xi(-\infty,\eta) = 0 \qquad \text{(B-2)}$$

$$\phi_\eta(\xi,-h) = 0 \qquad \text{(B-3)}$$

$$\phi_\eta(\xi,h) = \begin{cases} v_1, & -l_n/2 < \xi < l_n/2 \\ 0, & |\xi| > l_n/2 \end{cases} \qquad \text{(B-4)}$$

The problem is solved by means of Fourier transforms, which are defined as

$$\bar{\phi}(\eta;s) = \frac{1}{\sqrt{2\pi}} \int_{-\infty}^{\infty} \phi(\xi,\eta)\, e^{is\xi}\, d\xi \qquad \text{(B-5)}$$

$$\phi(\xi,\eta) = \frac{1}{\sqrt{2\pi}} \int_{-\infty}^{\infty} \bar{\phi}(\eta;s)\, e^{-is\xi}\, ds \qquad \text{(B-6)}$$

Upon transformation, Eq. (B-1) becomes

$$-\beta^2 s^2 \bar{\phi}(\eta;s) + \bar{\phi}_{\eta\eta}(\eta;s) = 0 \qquad \text{(B-7)}$$

which is an ordinary differential equation with the solution

$$\bar{\phi}(\eta;s) = A_1 e^{\beta s \eta} + A_2 e^{-\beta s \eta} + A_3 \qquad \text{(B-8)}$$

where A_1 to A_3 are constants. Since the constant A_3 transforms back to the ξ-η coordinates as a delta function, which has no physical significance in this problem, A_3 is taken to be zero. The boundary condition of Eq. (B-2) will be satisfied later after transformation back to the ξ coordinate. The boundary conditions of Eqs. (B-3) and (B-4) transform to

$$\bar{\phi}_\eta(-h;s) = 0 \qquad \text{(B-9)}$$

$$\bar{\phi}_\eta(h;s) = 2 v_1 \sin(s l_n/2)/\sqrt{2\pi}\, s \qquad \text{(B-10)}$$

Performing the appropriate operations on Eqs. (B-8), (B-9) and (B-10) yields

$$\bar{\phi}(\eta;s) = \frac{2 v_1 \sin(s l_n/2)\cosh[\beta s(\eta+h)]}{\sqrt{2\pi}\,\beta s^2 \sinh(2\beta s h)} \qquad \text{(B-11)}$$

The potential itself is then found by substituting in Eq. (B-6). Since the right-hand side of Eq. (B-11) is an even function of s, this result can be simplified to

$$\phi(\xi,\eta) = \frac{2 v_1}{\pi\beta} \cdot \int_0^\infty \frac{\cosh[\beta(\eta+h)s]\cosh(2\beta h s)\sin(l_n s/2)\cos\xi s}{s^2}\, ds \qquad \text{(B-12)}$$

Differentiating this twice with respect to ξ gives

$$\phi_{\xi\xi}(\xi,\eta) = -\frac{v_1}{\pi\beta} \int_0^\infty \cosh[\beta(\eta+h)s]\cosh(2\beta h s) \cdot \left\{ \sin[(\xi + l_n/2)s] - \sin[(\xi - l_n/2)s] \right\} ds \qquad \text{(B-13)}$$

which can be integrated[37] to give

$$\phi_{\xi\xi}(\xi,\eta) = -\frac{v_1}{4\beta^2 h} \left\{ \frac{\sinh\left[\frac{\pi(\xi + l_n/2)}{2\beta h}\right]}{\cosh\left[\frac{\pi(\xi + l_n/2)}{2\beta h}\right] + \cos\left[\frac{\pi(\eta+h)}{2h}\right]} - \frac{\sinh\left[\frac{\pi(\xi - l_n/2)}{2\beta h}\right]}{\cosh\left[\frac{\pi(\xi - l_n/2)}{2\beta h}\right] + \cos\left[\frac{\pi(\eta+h)}{2h}\right]} \right\} \qquad \text{(B-14)}$$

The desired u component is found by integrating Eq. (B-14) with respect to ξ, namely

$$\phi_\xi(\xi,\eta) = -\frac{v_1}{2\pi\beta} \cdot \ln\left\{ \frac{\cosh\left[\frac{\pi(\xi + l_n/2)}{2\beta h}\right] + \cos\left[\frac{\pi(\eta+h)}{2h}\right]}{\cosh\left[\frac{\pi(\xi - l_n/2)}{2\beta h}\right] + \cos\left[\frac{\pi(\eta+h)}{2h}\right]} \right\} + A_4 \qquad \text{(B-15)}$$

where A_4 is a constant of integration. This is evaluated by satisfying the boundary condition in Eq. (B-2), which gives

$$A_4 = -v_1 l_n / 4\beta^2 h \qquad \text{(B-16)}$$

so that

$$\phi_\xi(\xi,\eta) = -\frac{v_1 l_n}{2\beta^2 h} \cdot \left\{ \frac{1}{2} + \frac{\beta h}{\pi l_n} \ln\left[\frac{\cosh\left[\frac{\pi(\xi + l_n/2)}{2\beta h}\right] + \cos\left[\frac{\pi(\eta+h)}{2h}\right]}{\cosh\left[\frac{\pi(\xi - l_n/2)}{2\beta h}\right] + \cos\left[\frac{\pi(\eta+h)}{2h}\right]} \right] \right\} \qquad \text{(B-17)}$$

The desired v component is found in a similar fashion. Using Eq. (B-14) in conjunction with Eq. (B-1) gives an equation for $\phi_{\eta\eta}(\xi,\eta)$ which can be integrated with respect to η to yield

$$\phi_\eta(\xi,\eta) = \frac{\nu_1}{\pi}\left\{\operatorname{sgn}(\xi+\ell_n/2)\tan^{-1}\left\{\tanh\left[\frac{\pi|\xi+\ell_n/2|}{4\beta h}\right]\cdot\tan\left[\frac{\pi(\eta+h)}{4h}\right]\right\} - \operatorname{sgn}(\xi-\ell_n/2)\cdot\tan^{-1}\left\{\tanh\left[\frac{\pi|\xi-\ell_n/2|}{4\beta h}\right]\tan\left[\frac{\pi(\eta+h)}{4h}\right]\right\}\right\} \tag{B-18}$$

where the constant of integration is zero by Eq. (B-3) and $\operatorname{sgn}(\xi)$ is ± 1 according to whether $\xi \gtrless 0$.

The results are now cast in terms of the variables $\bar{x}$ and $\bar{y}$, where $\bar{x} = \xi/\ell_n$ and $\bar{y} = \eta/h$. In particular, the idealized influence functions, denoted by $\hat{I}_u$ and $\hat{I}_v$ to distinguish them from those calculated in the simulations, are found from Eqs. (B-17) and (B-18). From Eq. (B-17), it follows that $\phi_\xi(-\infty,\eta) = 0$ and $\phi_\xi(\infty,\eta) = -\nu_1\ell_n/2h$, so that in terms of Eqs. (5) and (6), $\delta_u = \phi_\xi(\infty,\eta) - \phi_\xi(-\infty,\eta) = -\nu_1\ell_n/2h$. Thus both ϕ_ξ and ϕ_η must be divided by this factor to get $\hat{I}_u$ and $\hat{I}_v$, which for incompressible flow ($\beta = 1$) are

$$\hat{I}_u(\bar{x},\bar{y}) = \frac{1}{2} + \frac{h}{\pi\ell_n}\cdot\ln\left\{\frac{\cosh\left[\frac{\pi\ell_n(\bar{x}+1/2)}{2h}\right]+\cos\left[\frac{\pi(\bar{y}+1)}{2}\right]}{\cosh\left[\frac{\pi\ell_n(\bar{x}-1/2)}{2h}\right]+\cos\left[\frac{\pi(\bar{y}+1)}{2}\right]}\right\} \tag{B-19}$$

$$\hat{I}_v(\bar{x},\bar{y}) = -\frac{2h}{\pi\ell_n}\left\{\operatorname{sgn}(\bar{x}+1/2)\cdot\tan^{-1}\left\{\tanh\left[\frac{\pi\ell_n|\bar{x}+1/2|}{4h}\right]\tan\left[\frac{\pi(\bar{y}+1)}{4}\right]\right\} - \operatorname{sgn}(\bar{x}-1/2)\tan^{-1}\left\{\tanh\left[\frac{\pi\ell_n|\bar{x}-1/2|}{4h}\right]\tan\left[\frac{\pi(\bar{y}+1)}{4}\right]\right\}\right\} \tag{B-20}$$

The $\hat{I}_{u_a}$, $\hat{I}_{v_a}$, $\hat{I}_{u_c}$ and $\hat{I}_{v_c}$ curves of Figs. 8 to 13 were evaluated from Eqs. (B-19) and (B-20) for $\ell_n/h = 1$ and $\bar{y} = y_c/h = \pm 2/3$. The expression for $\hat{I}_u(\bar{x},\bar{y})$ in Eq. (B-19) is valid everywhere except at the two points $\bar{y} = 1$, $\bar{x} = \pm 1/2$, where there are singularities introduced by the discontinuities in ν at these points. As is well known in linearized thin-airfoil theory, such a discontinuity leads to a logarithmic singularity in u there. (See Refs. 38 and 39 for the singularity at the kink in a bent flat plate.) In the calculated values of $\hat{I}_u$ shown in Figs. 8 and 10, there are no singularities because $\bar{y} = 2/3$, but the overshoot observed near $\bar{x} = \pm 1/2$ has its origin in that singular behavior.

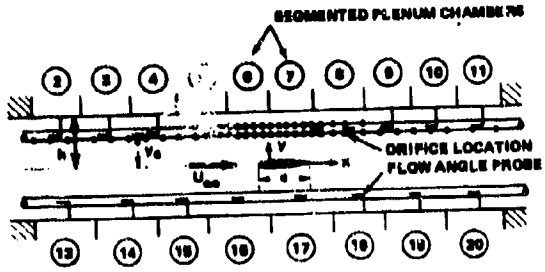

Figure 1 SCHEMATIC OF CALSPAN ONE-FOOT ADAPTIVE-WALL WIND TUNNEL.

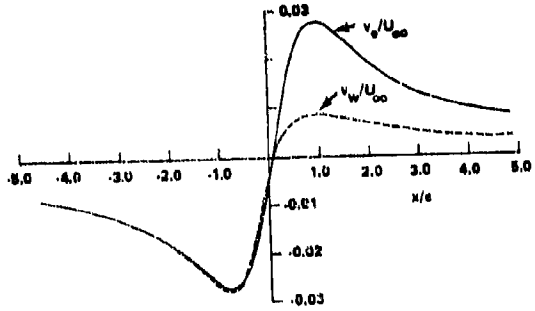

Figure 2 COMPARISON OF DISTRIBUTIONS OF PRESCRIBED INVISCID NORMAL VELOCITY v_e/U_∞ AND CALCULATED WALL NORMAL VELOCITY v_w/U_∞ FOR IDEAL WALL CONTROL. NACA 0012 AIRFOIL, $M_\infty = 0$, $\alpha = 4^0$, UPPER TUNNEL WALL AT $y/c = 1.0$.

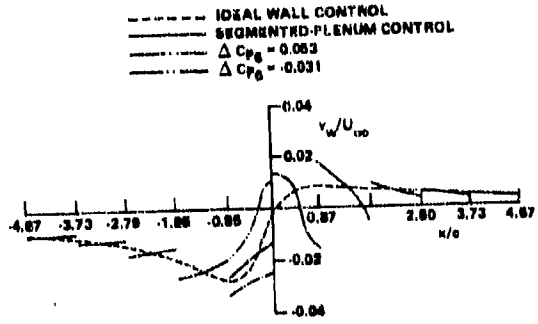

Figure 3 TRANSPIRATION VELOCITY AT UPPER TUNNEL WALL FOR SEGMENTED-PLENUM CONTROL. NACA 0012 AIRFOIL, $M_\infty = 0$, $\alpha = 4^0$, $y/c = 1.0$.

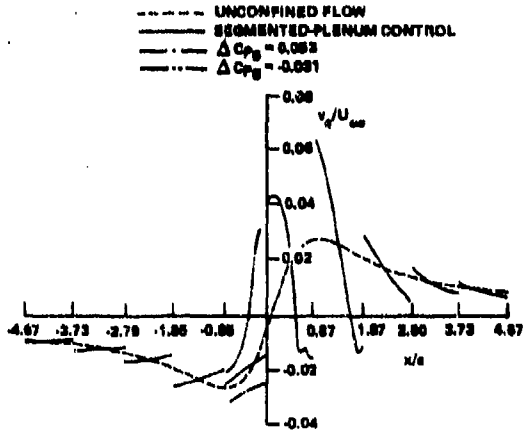

Figure 4 EFFECTIVE INVISCID NORMAL VELOCITY AT UPPER TUNNEL WALL DUE TO BOUNDARY-LAYER DISPLACEMENT EFFECT FOR SEGMENTED-PLENUM CONTROL. NACA 0012 AIRFOIL, $M_\infty = 0$, $\alpha = 4^0$, $y/c = 1.0$.

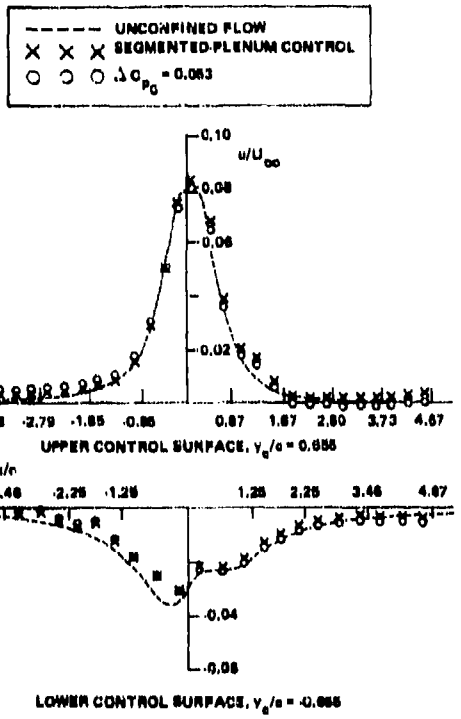

Figure 5 COMPARISON OF STREAMWISE DISTURBANCE VELOCITY AT CONTROL SURFACES FOR UNCONFINED FLOW AND SEGMENTED-PLENUM CONTROL. NACA 0012 AIRFOIL, $M_\infty = 0$, $\alpha = 4^0$.

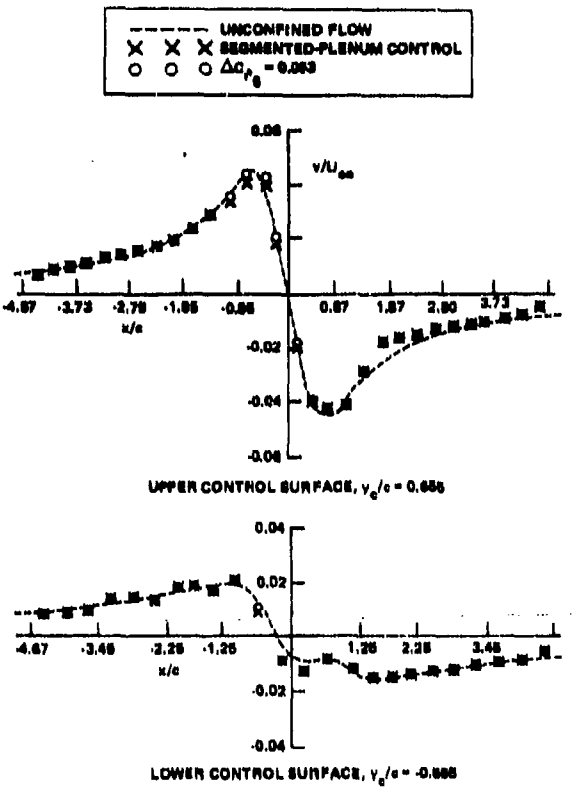

Figure 6 COMPARISON OF NORMAL VELOCITY AT CONTROL SURFACES FOR UNCONFINED FLOW AND SEGMENTED-PLENUM CONTROL. NACA 0012 AIRFOIL, $M_\infty = 0$, $\alpha = 4^0$.

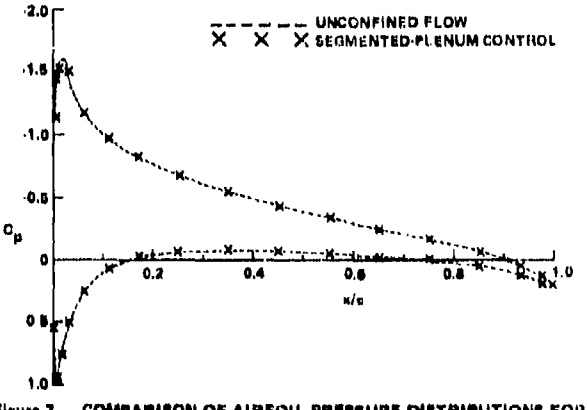

Figure 7 COMPARISON OF AIRFOIL PRESSURE DISTRIBUTIONS FOR UNCONFINED FLOW AND SEGMENTED-PLENUM CONTROL. NACA 0012 AIRFOIL, $M_\infty = 0$, $\alpha = 4^0$.

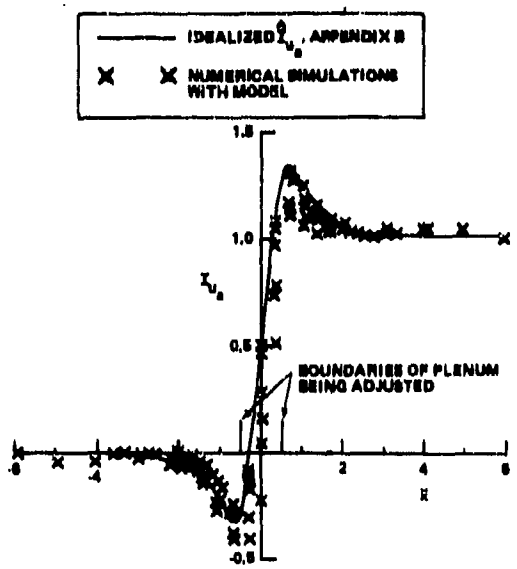

Figure 8 INFLUENCE FUNCTIONS FOR STREAMWISE VELOCITY COMPONENT AT CONTROL SURFACE ADJACENT TO PLENUM BEING ADJUSTED.

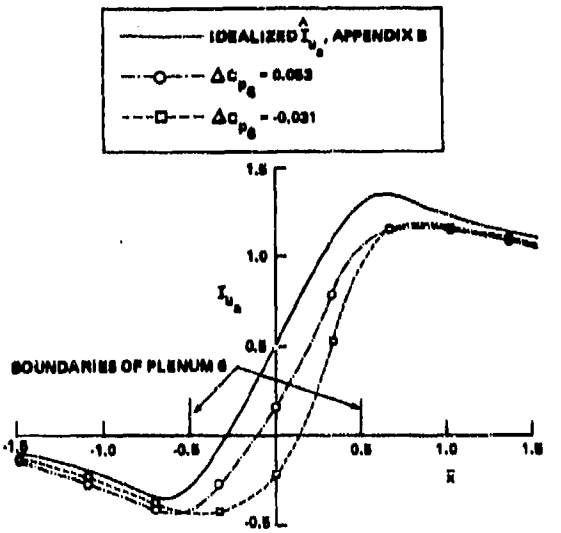

Figure 10 AMPLIFIED DISTRIBUTIONS OF INFLUENCE FUNCTIONS FOR STREAMWISE VELOCITY COMPONENT AT CONTROL SURFACE ADJACENT TO PLENUM 6.

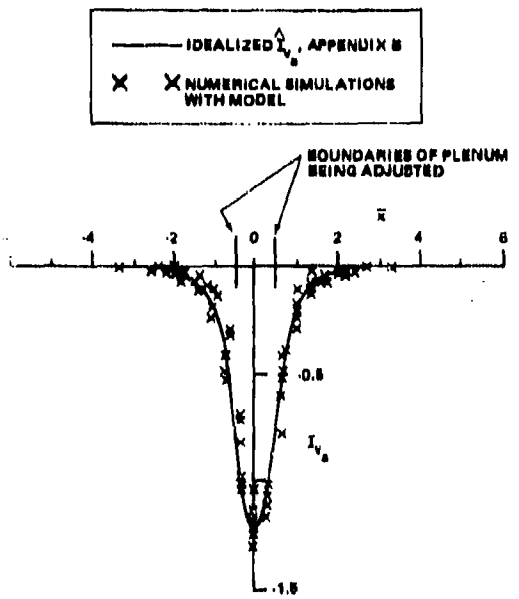

Figure 9 INFLUENCE FUNCTIONS FOR NORMAL VELOCITY COMPONENT AT CONTROL SURFACE ADJACENT TO PLENUM BEING ADJUSTED.

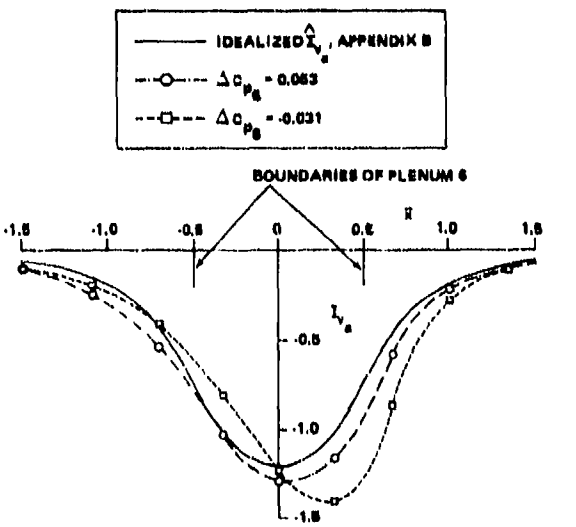

Figure 11 AMPLIFIED DISTRIBUTIONS OF INFLUENCE FUNCTIONS FOR NORMAL VELOCITY COMPONENT AT CONTROL SURFACE ADJACENT TO PLENUM 6.

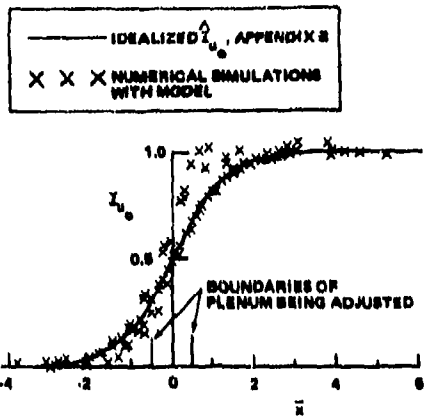

Figure 12 INFLUENCE FUNCTIONS FOR STREAMWISE VELOCITY COMPONENT AT CONTROL SURFACE OPPOSITE TO PLENUM BEING ADJUSTED.

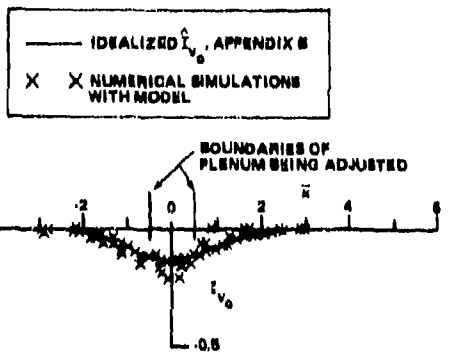

Figure 13 INFLUENCE FUNCTIONS FOR NORMAL VELOCITY COMPONENT AT CONTROL SURFACE OPPOSITE TO PLENUM BEING ADJUSTED.

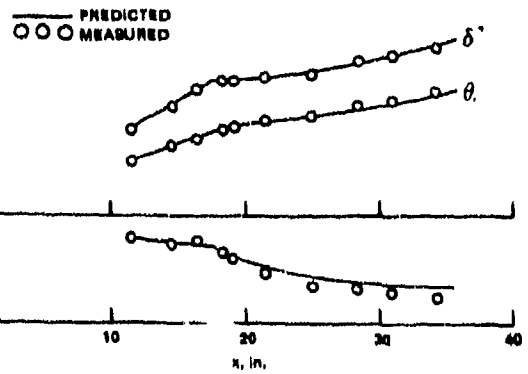

Figure 14 COMPARISON OF PREDICTED AND MEASURED BOUNDARY-LAYER CHARACTERISTICS. DISCONTINUOUS BLOWING EXPERIMENT OF McQUAID (REF. 22), $v_w/U_\infty = 0.0035$ FOR $x < 17.5$ IN., $v_w/U_\infty = 0.0000$ FOR $x > 17.5$ IN.

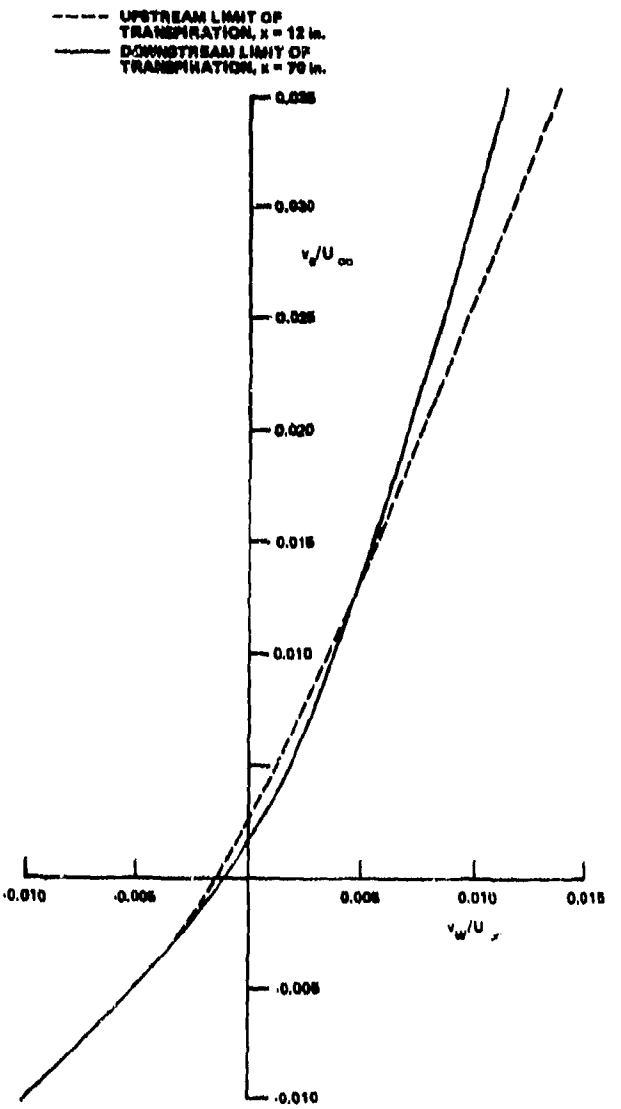

Figure 15 CALCULATED INVISCID NORMAL VELOCITY v_e/U_∞ DUE TO BOUNDARY-LAYER DISPLACEMENT ON FLAT WALL WITH TRANSPIRATION VELOCITY v_w/U_∞ AND ZERO PRESSURE GRADIENT.

DISTRIBUTION LIST FOR UNCLASSIFIED
TECHNICAL REPORTS AND REPRINTS ISSUED UNDER
CONTRACT N00014-77-C-0452 TASK 061-199

All addresses receive one copy unless otherwise specified

Technical Library
Building 313
Ballistic Research Laboratories
Aberdeen Proving Ground, MD 21005

Mr. Aviars Celmins
Ballistic Research Laboratory
Ballistic Modelling Division
Aberdeen Proving Ground, MD 21005

Dr. P. J. Roache
Ecodynamics Research Associates, Inc.
P. O. Box 8172
Albuquerque, NM 87108

Defense Technical Information Center
Cameron Station, Building 5
Alexandria, VA 22314 12 copies

Library
Naval Academy
Annapolis, MD 21402

Director, Tactical Technology Office
Defense Advanced Research Projects
Agency
1400 Wilson Boulevard
Arlington, VA 22209

Code 211
Office of Naval Research
800 N. Quincy Street
Arlington, VA 22217

Code 438
Office of Naval Research
800 N. Quincy Street
Arlington, VA 22217 2 copies

Dr. J. L. Potter
Deputy Director, Technology
von Karman Gas Dynamics Facility
Arnold Air Force Station, TN 37389

Professor J. C. Wu
School of Aerospace Engineering
Georgia Institute of Technology
Atlanta GA 30332

Library
Aerojet-General Corporation
6352 North Irwindale Avenue
Azusa, CA 91702

NASA Scientific and Technical
Information Facility
P. O. Box 8757
Baltimore/Washington International
Airport, MD 21240

Dr. K. C. Wang
Martin Marietta Corporation
Martin Marietta Laboratories
1450 South Rolling Road
Baltimore, MD 21227

Professor A. J. Chorin
Department Mathematics
University of California
Berkeley, CA 94720

Professor M. Holt
Department of Mechanical Engineering
University of California
Berkeley, CA 94720

Dr. H. R. Chaplin
Code 1600
David W. Taylor Naval Ship Research
and Development Center
Bethesda, MD 20084

Dr. Hans Lugt
Code 1802
David W. Taylor Naval Ship Research
and Development Center
Bethesda, MD 20084

Dr. Francois Frenkiel
Code 1802
David W. Taylor Naval Ship Research
and Development Center
Bethesda, MD 20084

Dr. G. R. Inger
Department of Aerospace Engineering
Virginia Polytechnic Institute and
State University
Blacksburg, VA 24061

Professor C. H. Lewis
Department of Aerospace and Ocean
Engineering
Virginia Polytechnic Institute and
State University
Blacksburg, VA 24061

Professor A. H. Nayfeh
Department of Engineering Science
Virginia Polytechnic Institute and
State University
Blacksburg, VA 24061

Dr. A. Rubel
Research Department
Grumman Aerospace Corporation
Bethpage, NY 11714

Commanding Officer
Office of Naval Research Eastern/
Central Regional Office (Boston)
666 Summer Street, Bldg. 114, Section D
Boston, MA 02210

Dr. J. C. Erickson, Jr.
CALSPAN Corporation
Advanced Technology Center
P. O. Box 400
Buffalo, NY 14225

Mr. C. E. Wittliff
CALSPAN Corporation
Advanced Technology Center
P. O. Box 400
Buffalo, NY 14225

Professor R. F. Probstein
Department of Mechanical Engineering
Massachusetts Institute of Technology
Cambridge, MA 02139

Commanding Officer
Office of Naval Research Branch Office
536 South Clark Street
Chicago, IL 60605

Code 753
Naval Weapons Center
China Lake, CA 93555

Mr. J. Marshall
Code 4063
Naval Weapons Center
China Lake, CA 93555

Professor R. T. Davis
Department of Aerospace Engineering
University of Cincinnati
Cincinnati, OH 45221

Professor S. G. Rubin
Department of Aerospace Engineering
and Applied Mechanics
University of Cincinnati
Cincinnati, OH 45221

Library MS 60-3
NASA Lewis Research Center
21000 Brookpark Road
Cleveland, OH 44135

Dr. J. D. Anderson, Jr.
Chairman, Department of Aerospace
Engineering
College of Engineering
University of Maryland
College Park MD 20742

Professor O. Burggraf
Department of Aeronautical and
Astronautical Engineering
Ohio State University
1314 Kinnear Road
Columbus, OH 43212

Technical Library
Naval Surface Weapons Center
Dahlgren Laboratory
Dahlgren, VA 22448

Dr. F. Moore
Naval Surface Weapons Center
Dahlgren Laboratory
Dahlgren, VA 22448

Technical Library 2-51131
LTV Aerospace Corporation
P. O. Box 5907
Dallas, TX 75222

Library, United Aircraft Corporation
Research Laboratories
Silver Lane
East Hartford, CT 06108

Professor G. Moretti
Polytechnic Institute of New York Long
Island Center
Department of Aerospace Engineering and
Applied Mechanics
Route 110
Framingdale, NY 11735

Dr. W. R. Briley
Scientific Research Associates, Inc.
P. O. Box 498
Glastonbury, CT 06033

Professor P. Gordon
Calumet Campus
Department of Mathematics
Purdue University
Hammond, IN 46323

Library (MS 185)
NASA Langley Research Center
Langley Station
Hampton, VA 23665

Professor A. Chapmann
Chairman, Mechanical Engineering
Department
William M. Rice Institute
Box 1892
Houston, TX 77001

Technical Library
Naval Ordnance Station
Indian Head, MD 20640

Professor D. A. Caughey
Sibley School of Mechanical and
Aerospace Engineering
Cornell University
Ithaca, NY 14850

Professor E. L. Resler
Sibley School of Mechanical and
Aerospace Engineering
Cornell University
Ithaca, NY 14850

Professor S. F. Shen
Sibley School of Mechanical and
Aerospace Engineering
Cornell University
Ithaca, NY 14850

Library
Midwest Research Institute
425 Volker Boulevard
Kansas City, MO 64110

Dr. M. M. Hafez
Flow Research, Inc.
P. O. Box 5040
Kent, WA 98031

Dr. E. M. Murman
Flow Research, Inc.
P. O. Box 5040
Kent, WA 98031

Dr. J. J. Riley
Flow Research, Inc.
P. O. Box 5040
Kent, WA 98031

Dr. S. A. Orszag
Cambridge Hydrodynamics, Inc.
54 Baskin Road
Lexington, MA 02173

Dr. P. Bradshaw
Imperial College of Science and
Technology
Department of Aeronautics
Prince Consort Road
London SW7 2BY, England

Professor T. Cebeci
Mechanical Engineering Department
California State University, Long
Beach
Long Beach , CA 90840

Dr. H. K. Cheng
University of Southern California,
Department of Aerospace Engineering
University Park
Los Angeles, CA 90007

Professor J. D. Cole
Mechanics and Structures Department
School of Engineering and Applied Science
University of California
Los Angeles, CA 90024

Engineering Library
University of Southern California
Box 77929
Los Angeles, CA 90007

Dr. C. -M. Ho
Department of Aerospace Engineering
University of Southern California
University Park
Los Angeles, CA 90007

Dr. T. D. Taylor
The Aerospace Corporation
P. O. Box 92957
Los Angeles, CA 90009

Commanding Officer
Naval Ordnance Station
Louisville, KY 40214

Mr. B. H. Little, Jr.
Lockheed-Georgia Company
Department 72-74, Zone 369
Marietta, GA 30061

Professor E. R. G. Eckert
University of Minnesota
241 Mechanical Engineering Building
Minneapolis, MN 55455

Dr. Gary Chapman
Mail Stop 227-4
Ames Research Center
Moffett Field, CA 94035

Library
Naval Postgraduate School
Monterey, CA 93940

Dr. J. L. Steger
Flow Simulations, Inc.
735 Alice Avenue
Mountain View, CA 94041

Dr. S. S. Stahara
Nielsen Engineering and Research Inc.
510 Clyde Avenue
Mountain View, CA 94043

Engineering Societies Library
345 East 47th Street
New York, NY 10017

Professor A. Jameson
Courant Institute of Mathematical Sciences
New York University
251 Mercer Street
New York, NY 10012

Professor G. Miller
Department of Applied Science
New York University
26-36 Stuyvesant Street
New York, NY 10003

Office of Naval Research
New York Area Office
715 Broadway - 5th Floor
New York, NY 10003

Dr. R. Vaglio-Laurin
Department of Applied Science
New York University
26-36 Stuyvesant Street
New York, NY 10003

Mr. D. Farmer
Naval Ocean Research and Development Activity
Code 332
NSTL Station, MS 39522

Librarian, Aeronautical Library
National Research Council
Montreal Road
Ottawa 7, Canada

Lockheed Missiles and Space Company
Technical Information Center
3251 Hanover Street
Palo Alto, CA 94304

Commanding Officer
Office of Naval Research Western Regional Office (Pasadena)
1030 East Green Street
Pasadena, CA 91106

Engineering Division
California Institute of Technology
Pasadena, CA 91109

Library
Jet Propulsion Laboratory
4800 Oak Grove Drive
Pasadena, CA 91103

Professor H. Liepmann
Department of Aeronautics
California Institute of Technology
Pasadena, CA 91109

Mr. L. I. Chasen, MGR-MSD Lib.
General Electric Company
Missile and Space Division
P. O. Box 8555
Philadelphia, PA 19101

Technical Library
Naval Missile Center
Point Mugu, CA 93042

Professor S. Bogdonoff
Gas Dynamics Laboratory
Department of Aerospace and
Mechanical Sciences
Princeton University
Princeton, NJ 08540

Professor S. I. Cheng
Department of Aerospace and
Mechanical Sciences
Princeton University
Princeton, NJ 08540

Dr. J. E. Yates
Aeronautical Research Associates
of Princeton, Inc.
50 Washington Road
Princeton, NJ 08540

Professor L. Sirovich
Division of Applied Mathematics
Brown University
Providence, RI 02912

Redstone Scientific Information Center
Chief, Document Section
Army Missile Command
Redstone Arsenal, AL 35809

U.S. Army Research Office
P. O. Box 12211
Research Triangle, NC 27709

Editor, Applied Mechanics Review
Southwest Research Institute
8500 Culebra Road
San Antonio, TX 78228

Library and Information Services
General Dynamics-CONVAIR
P. O. Box 1128
San Diego, CA 92112

Dr. R. Magnus
General Dynamics-CONVAIR
Kearny Mesa Plant
P. O. Box 80847
San Diego, CA 92138

Office of Naval Research
San Francisco Area Office
One Hallidie Plaza, Suite 601
San Francisco, CA 94102

Library
The RAND Corporation
1700 Main Street
Santa Monica, CA 90401

Dr. P. E. Rubbert
Boeing Aerospace Company
Boeing Military Airplane Development
Organization
P. O. Box 3707
Seattle, WA 98124

Dr. H. Yoshihara
Boeing Aerospace Company
P. O. Box 3999
Mail Stop 41-18
Seattle, WA 98124

Librarian
Naval Surface Weapons Center
White Oak Laboratory
Silver Spring, MD 20910

Dr. J. M. Solomon
Naval Surface Weapons Center
White Oak Laboratory
Silver Spring, MD 20910

Professor J. H. Ferziger
Department of Mechanical Engineering
Stanford University
Stanford, CA 94305

Professor K. Karamcheti
Department of Aeronautics and
Astronautics
Stanford University
Stanford, CA 94305

Professor O. Buneman
Institute for Plasma Research
Stanford University
Stanford, CA 94305

Engineering Library
McDonnell Douglas Corporation
Department 218, Building 101
P. O. Box 516
St. Louis, MO 63166

Dr. R. J. Hakkinen
McDonnell Douglas Corporation
Department 222
P. O. Box 516
St. Louis, MO 63166

Dr. N. Malmuth
Rockwell International Science Center
1049 Camino Dos Rios
P. O. Box 1085
Thousand Oaks, CA 91360

Library
Institute of Aerospace Studies
University of Toronto
Toronto 5, Canada

Professor W. R. Sears
Aerospace and Mechanical Engineering
University of Arizona
Tucson, AZ 85721

Professor A. R. Seebass
Department of Aerospace and
Mechanical Engineering
University of Arizona
Tucson, AZ 85721

Dr. K. T. Yen
Code 3015
Naval Air Development Center
Warminster, PA 18974

Air Force Office of Scientific
Research (SREM)
Building 1410, Bolling AFB
Washington, DC 20332

Chief of Research and Development
Office of Chief of Staff
Department of the Army
Washington, DC 20310

Library of Congress
Science and Technology Division
Washington, DC 20540

Director of Research (Code RR)
National Aeronautics and Space
Administration
600 Independence Avenue, SW
Washington, DC 20546

Library
National Bureau of Standards
Washington, DC 20234

National Science Foundation
Engineering Division
1800 G Street, NW
Washington, DC 20550

AIR 320D
Naval Air Systems Command
Washington, DC 20361

AIR 950D
Naval Air Systems Command
Washington, DC 20375

Code 2627
Naval Research Laboratory
Washington, DC 20375

SEA 03512
Naval Sea Systems Command
Washington, DC 20362

SEA 09G3
Naval Sea Systems Command
Washington, DC 20362

Dr. A. L. Slafkosky
Scientific Advisor
Commandant of the Marine Corps
(Code AX)
Washington, DC 20380

Director
Weapons Systems Evaluation Group
Washington, DC 20350

Research Library
AVCO Corporation
Missile Systems Division
201 Lowell Street
Wilmington, MA 01887

AFAPL (AFRC)
AB
Wright Patterson, AFB, OH 45433

Dr. Donald J. Harney
AFFDL/FX
Wright Patterson AFB, OH 45433

Dr. D. R. Kotansky
Department 341
P. O. Box 516
St. Louis, MO 63166